

CHAPTER 4

OPERATIONAL APPLICATIONS

4.1 Introduction. This chapter discusses potential operational uses of the WSR-88D products as well as the structure of certain meteorological phenomena. It provides information on observing and forecasting meteorological phenomena using WSR-88D products. Also included in the early sections is a discussion of operationally troublesome radar returns due to such things as ground clutter and sidelobes. Pictorial representations of some applications have been included.

Basic meteorological skills should be applied to determine the best products to use under different meteorological situations. The phenomena discussed within this chapter are not all-inclusive and by no means is the forecaster limited to products talked about in certain situations in the chapter. As more information continues to become available it will be incorporated in or result in changes to this chapter.

While the obvious emphasis of this Handbook is the WSR-88D application and use, it is important to recognize that the WSR-88D is but one tool available to the meteorological practitioner or scientist. Other tools and data sets include, but are not limited to, atmospheric soundings, surface and upper air conventional observations and their derived fields, numerical models, satellites, lightning detection systems, and visual observations. In order to gain the most complete understanding of the state and evolution of the atmosphere, a synthesis of all observations is necessary. Thus, while not specifically stated in the following sections, it is assumed that the reader and radar user recognizes this fundamental concept.

4.2 Non-Meteorological Radar Echoes. This section briefly describes methods of identifying and assessing the impacts of ground clutter, anomalous propagation (AP), sidelobes, and sunrise and sunset effects. In addition, recognition methods for and impacts of range folded and incorrectly dealiased velocity data are discussed.

4.2.1 Ground Clutter. Prior to calculation of reflectivity, velocity, or spectrum width, return signals from ranges within the radar's normal ground clutter pattern are processed to remove most of the signal returned from targets that are stationary (Part B of this Handbook). The clutter signal not removed, called residual clutter or clutter residue, will remain as part of many of the products. Normally, the clutter residue echoes are weak, in the range of 10 dBZ to 30 dBZ.

4.2.1.1 Recognition of Residual Ground Clutter. A low elevation Reflectivity product will show ground clutter close to the radar or distant mountainous terrain if intercepted by the beam. It will normally appear as a cluster of points (having a speckled nature) or as a large area of contiguous returns (Figure 4-1). Residual clutter is often characterized by relatively weak echoes, random velocities, and random but usually rather broad spectrum widths. A time lapse of Reflectivity products will show no movement of these returns. With small, but increasing antenna elevations, ground clutter returns will very often rapidly disappear.

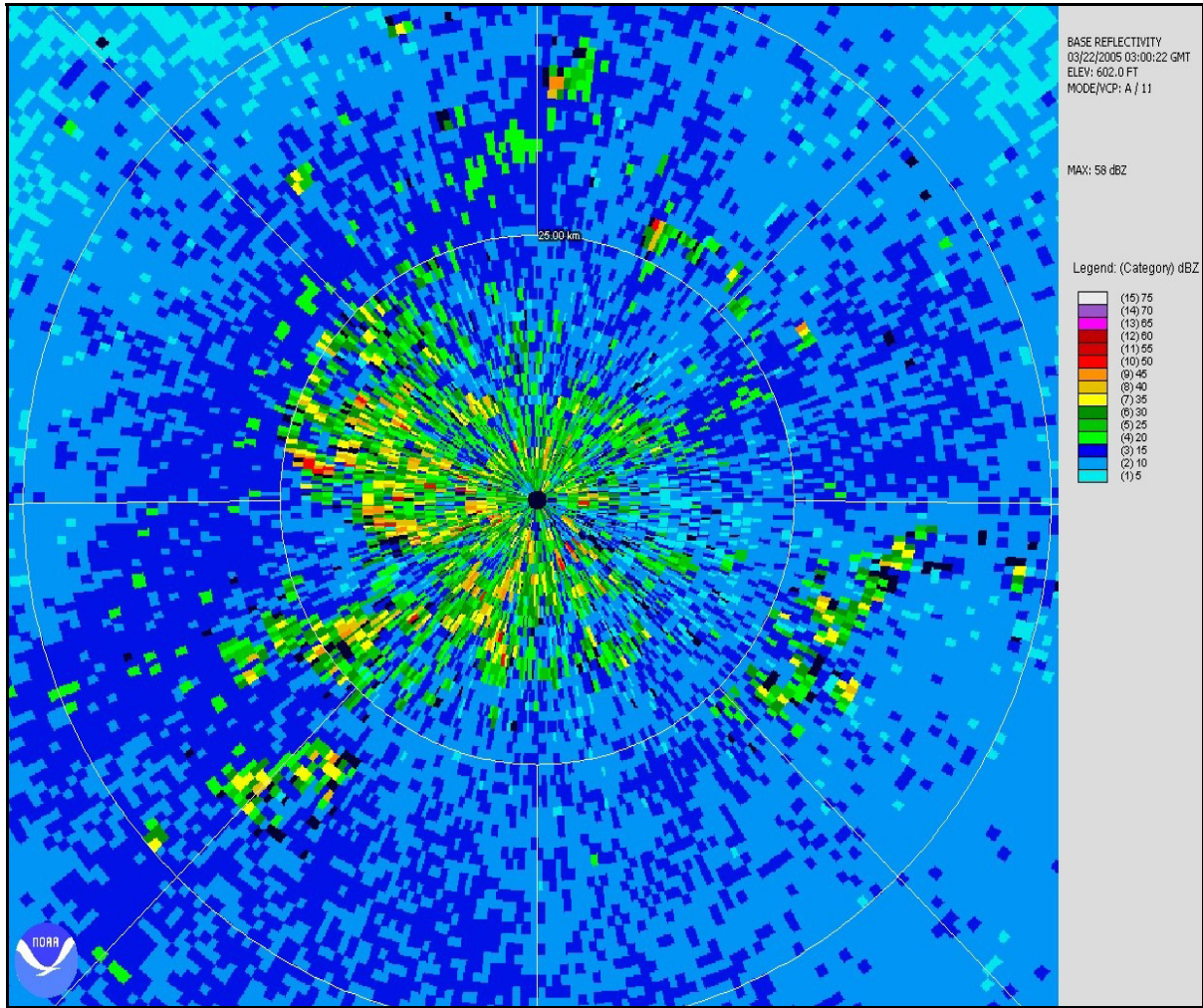


Figure 4-1
Residual Ground Clutter

This WSR-88D Reflectivity product (NCDC NEXRAD Viewer) shows "residual" ground clutter in excess of ~30 dBZ remaining, even after filtering all bins using high suppression. Range rings are at 25 and 50 km. Radials are at every 45° of azimuth.

4.2.1.2 Assessing Impacts of Residual Ground Clutter. Residual ground clutter near the radar may be recognized by its speckled appearance. When it is imbedded in a weak meteorological signal over the radar and as a result of the random velocities in the clutter residue, the Velocity Dealiasing Algorithm may introduce errors in the velocity field due to large radial and azimuthal gate-to-gate shears greater than the Nyquist velocity. This problem is most likely to occur in the Clear Air Mode using VCP 31 where the Nyquist velocity is about 10.8 m s^{-1} (21 kts) and the gate length with the long pulse is 0.75 km (0.4 nm). The net affect of long pulse is in an apparent increase in radial gate-to-gate shear amplitude and increase in dealiasing failures. Although less frequent, if this problem occurs in the Precipitation Mode, the induced shears may be picked up by the legacy Mesocyclone, Mesocyclone Detection Algorithm (MDA), or the TDA, and carried as a feature.

Clutter residue can also have deleterious affects on other products, as well. For example, in the Precipitation Mode, the Precipitation Processing algorithms will interpret these echoes as precipitation and accumulate, over time, large amounts of rainfall where none has fallen.

4.2.2 Ground Clutter Returns from Anomalous Propagation. Anomalous propagation of the radar beam is caused by non-standard atmospheric temperature or moisture gradients (Part B of this Handbook). Superrefraction, which is frequently caused by temperature inversions, bends the beam toward the earth and can cause the radar to detect ground returns from distances far exceeding the normal ground clutter area. Anomalous propagation surrounding the radars is especially common in the desert southwest and develops shortly after sunset and during the nighttime hours because of the rapid cooling of the dry boundary layer and development of a sharp radiational temperature inversion.

4.2.2.1 Recognition of Ground Clutter Returns from Anomalous Propagation. Anomalous propagation is characterized by many very small “popcorn echoes” with very high reflectivity (abnormally high for the small echo size) and extreme reflectivity gradients (Figure 4-2). Even with small changes but increasing antenna elevation, these returns will usually rapidly disappear. A time lapse of Reflectivity products may show rapidly changing patterns but without echo motion. In the absence of precipitation there can be a 20 dBZ_e, or more, difference between adjacent returns, mean velocities near zero, and narrow spectrum widths. Ground returns from anomalous propagation mixed with precipitation may result in large spectrum width values and low velocities. Erratic movement of ground returns from AP, in comparison with the motion of precipitation echoes, may also be seen.

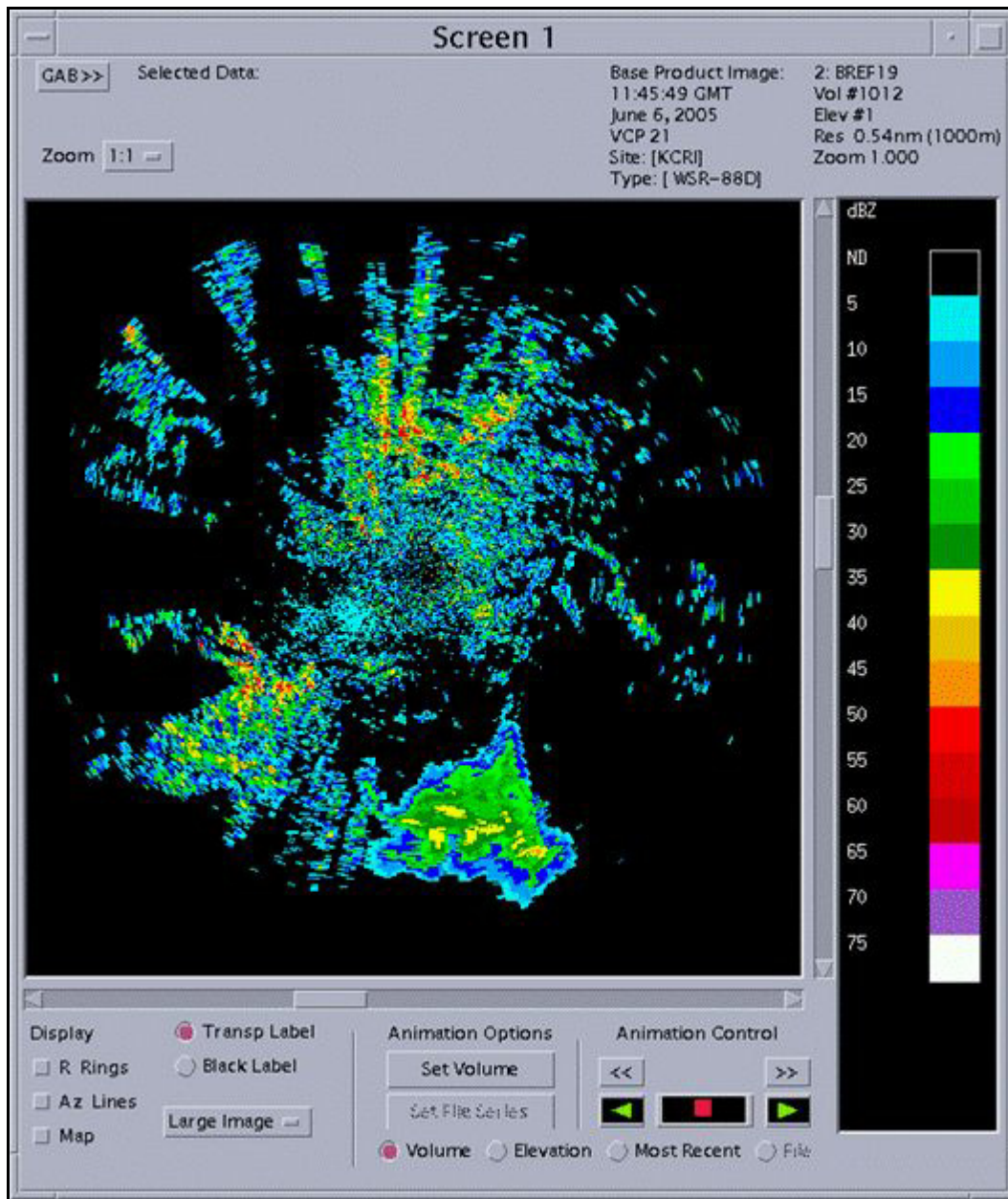


Figure 4-2
Anomalous Propagation

Norman, OK WSR-88D (KCRI, test bed radar) at 11:45 UTC on 6 June 2005 (CODEview graphics). The major areas of Anomalous Propagation (AP) are induced by a nocturnal inversion.

4.2.2.2 Assessing Impacts of Ground Clutter Returns from Anomalous Propagation. Ground returns from AP primarily impacts precipitation accumulation algorithms wherever the AP is located. But super refraction of the radar beam also frequently occurs behind the cold air outflow regions of thunderstorms. As in the case of clutter residue, in these instances, the Precipitation Processing algorithms will often erroneously interpret the ground returns as precipitation echoes and overestimate the precipitation with these storms. It may also affect other algorithmic output, e.g., if reflectivity is large, erroneous identification of a storm may occur (but is rare) and its centroid location (and therefore motion) will be altered. Additionally, it can be more difficult to interpret reflectivity echoes in the affected areas.

4.2.2.3 Removal of Ground Clutter Returns from Anomalous Propagation. The Radar Echo Classifier (REC) algorithm has been introduced to remove or flag AP (see Part C of this Handbook). While the REC assigns a likelihood estimate for echo classification, it offers a means of identifying AP in real-time. Additionally, the low-level layer of the Layer Composite Reflectivity product can be selected such that it omits the echoes from the lowest 1.52 km (5000 ft). This is also intended to remove residual ground clutter and AP. Finally, AP can be removed, to a large extent, by application of the clutter filter to the elevation angles affected. This is accomplished by overriding the clutter map resident in the RDA through editing of the Clutter Suppression Regions menu at the MSCF. Up to 15 clutter suppression regions can be edited in which three levels of suppression can be defined for the reflectivity and Doppler channels. Unit Radar Committee agreement on the use of the clutter map editor must be developed.

When weather is not a factor, i.e., operating in the Clear Air Mode or ground clutter or anomalous propagation are in a precipitation-free sector in the Precipitation Mode, it is reasonable to apply the clutter filter. It is also possible to apply the filter even in precipitation regions. In most conditions the clutter filter should be applied.

4.2.3 Sidelobes. An occasional source of data contamination is simultaneous reception of signals at comparable power levels through both the main antenna pattern and its sidelobes (Part B of this Handbook).

4.2.3.1 Recognition of Sidelobes. While obvious WSR-88D sidelobe returns are rare, they can be found to the right, left, above, and below high reflectivity areas. Potential interference from sidelobes can be diagnosed by knowing the power difference between the main beam and the sidelobe. The WSR-88D one-way sidelobe is nominally 29 dB down. The location of potential sidelobe interference will be slightly offset from the axis of the main beam (Part B of this Handbook). In most cases, the velocity field of sidelobes will display noisy or erratic values. Spectrum widths will often be extreme values and are often the best indicator of sidelobe interference. Typically, two-way reflectivity differences between the mainlobe and the sidelobe will be 50 to 54 dBZ for sidelobe detection to be a problem. Thus, owing to beamwidth considerations, strongly reflective storms with very strong reflectivity gradients must be within moderate ranges of the RDA for sidelobes to be a problem.

4.2.3.2 Assessing Impacts of Sidelobes. The presence of sidelobes may indicate erroneously high storm tops or new storm growth where there is none. Sidelobes can also impact velocities in weak echo by providing noisy or erroneous values that mask true velocity patterns. Algorithmic output, especially of the TDA and MDA, may be affected in rare cases.

4.2.4 Solar Effects. Due to the sensitivity of the WSR-88D, anomalous returns near sunrise or sunset usually appear along one to two radials as the radar scans the sun's location. These returns are generated because the sun radiates energy in the same microwave region of the electromagnetic spectrum that is used by the WSR-88D.

4.2.4.1 Recognition of Solar Effects. When the antenna scans the sun, a long radial of weak echo return is displayed. These returns are most often observed at both local sunrise and sunset. These echoes may be expected to appear as continuous returns, in a narrow "baseball bat" shape, out one or two radials, at the solar altitude. Reflectivity values generally range between 5 and 20 dBZ_e (Figure 4-3) and will typically increase with range. Solar effects will appear for one or two volume scans at a single elevation of the base products and, in very rare situations, for up to 30 minutes on a Composite Reflectivity (CR) product.

4.2.4.2 Assessing Impacts of Solar Effects. In the absence of other echoes, typical reflectivity values from solar effects are from near zero dBZ_e in close to the radar to 20 dBZ_e or higher at 460 km (248 nm). The apparent reduction in the sun's signal nearer the radar is due to the range normalization correction applied to reflectivity. The velocity and spectrum width fields indicate range-aliased data out to the maximum range of these products, i.e., 230 km (124 nm). Another reflectivity-derived product that will show this contamination is the CR and, only rarely, the Layer Composite Reflectivity or Echo Tops products. Most meteorological algorithms will not be affected, since the reflectivity values are below the significant thresholds and the occurrence is confined to one or two volume scans and one or two azimuths.

Velocity-derived products that will be contaminated are the SRR and SRM. In very rare instances and at longer ranges, the contaminated radial may disrupt pattern vectors used to identify circulations in the MDA and TDA algorithm, where the sun's signal is stronger than the corresponding storm echo. At close-in ranges, the sun's signal is too weak to impact most algorithms.

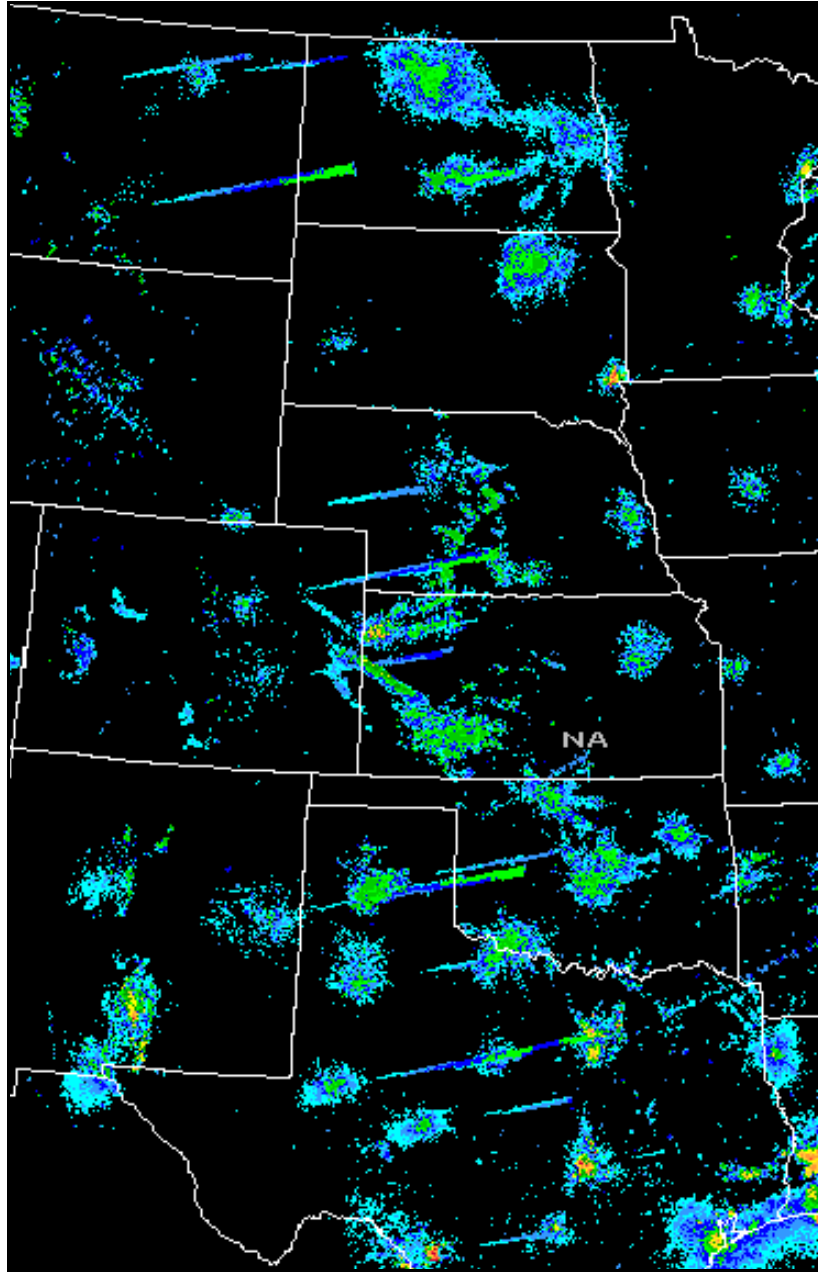


Figure 4-3
Solar Effects

Mosaic of WSR-88D Composite Reflectivity from 12:34 UTC on 21 April 2003. The streaks of low reflectivity extending outward to the east northeast from the radar locations are caused by sunrise effects. That is, the radar is detecting radiation incident from the sun in the same wavelengths as the radar backscattered power. Source: NWS Meteorological Development Laboratory.

4.2.5 Range Folded Data. Range ambiguities in the Doppler velocity and spectrum width fields caused by the WSR-88D's pulsed Doppler sampling interval (Part B of this Handbook) can be very significant. For any pulsed Doppler system, the product of the unambiguous range and the Doppler Nyquist co-interval is a constant function of the wavelength of the radar and the speed of light. By decreasing the PRF, the unambiguous range of the radar can be increased; however, the Nyquist velocity range interval will decrease. The WSR-88D's unambiguous range for Doppler velocity and spectrum width measurements varies from 120 km (65 nm) (at a Nyquist co-interval of $\pm 31 \text{ ms}^{-1}$ (60 kts)) to 174 km (94 nm) (at a Nyquist co-interval of $\pm 21 \text{ ms}^{-1}$ (41 knots)). The reasons for range folding and methods to dealias the velocities are covered in Part B of this handbook. However, it can be summarized here.

The WSR-88D scanning strategies combine Doppler waveforms having high PRF and short unambiguous ranges with a surveillance cut with low PRF and long unambiguous range in order to attempt to resolve range ambiguities of the Doppler scans. The surveillance waveform is unambiguous out to a 248 nm range. One dealiasing method uses the “split-cut,” which first scans an elevation with the surveillance waveform and then scans it a second time using the Doppler cut.

The second method, the “batch cut,” interleaves the surveillance and Doppler waveforms. In each case the dealiasing algorithm uses the surveillance waveform to do a gate by gate power comparison of the Doppler waveform multiple “trip” ambiguous ranges. This gate by gate power comparison will reveal which, if any, of the ambiguous range gates dominates. In cases where there is potential range ambiguity or overlaid echo, to summarize the algorithm processing, those gates that dominate in power returned are those range gates determined to be where the Doppler information is originating. The remaining gates with significantly weaker power returns are displayed as “overlaid data” and unusable for Doppler measurements. If returns are present, but none of the ambiguous gates dominate in power, then the data is determined to be range overlaid for all those gates.

In more detail, the dealiasing algorithm functions in the following manner. The radar interprets the locations of velocity and spectrum width returns from beyond the unambiguous range as occurring within that range, as well as beyond. The range-unfolding algorithm has been implemented in the RDA preprocessing to attempt to replace range-folded Doppler data from as many as four trips to their proper locations in range. The range-unfolding algorithm compares the return power from all possible ranges given the Doppler PRF used for that slice. This is done range gate by range gate for all possible ambiguities. If the power return from one possible range gate exceeds the power return from all other possible ambiguous or “matching” range gate locations by more than the defined threshold (TOVER, default 5dB), the Doppler data are assigned to that range and all other possible ranges are flagged as range obscured (overlaid). If the power return from one possible range does not exceed the power return from the other possible ranges by the defined threshold (TOVER), all ranges are considered range obscured (overlaid) and the Doppler data are not assigned to any of the possible ranges. Range obscured (overlaid) data are flagged as range folded, treated as missing by all downstream algorithms, and are displayed as purple (adaptable) in the display (Figure 4-4).

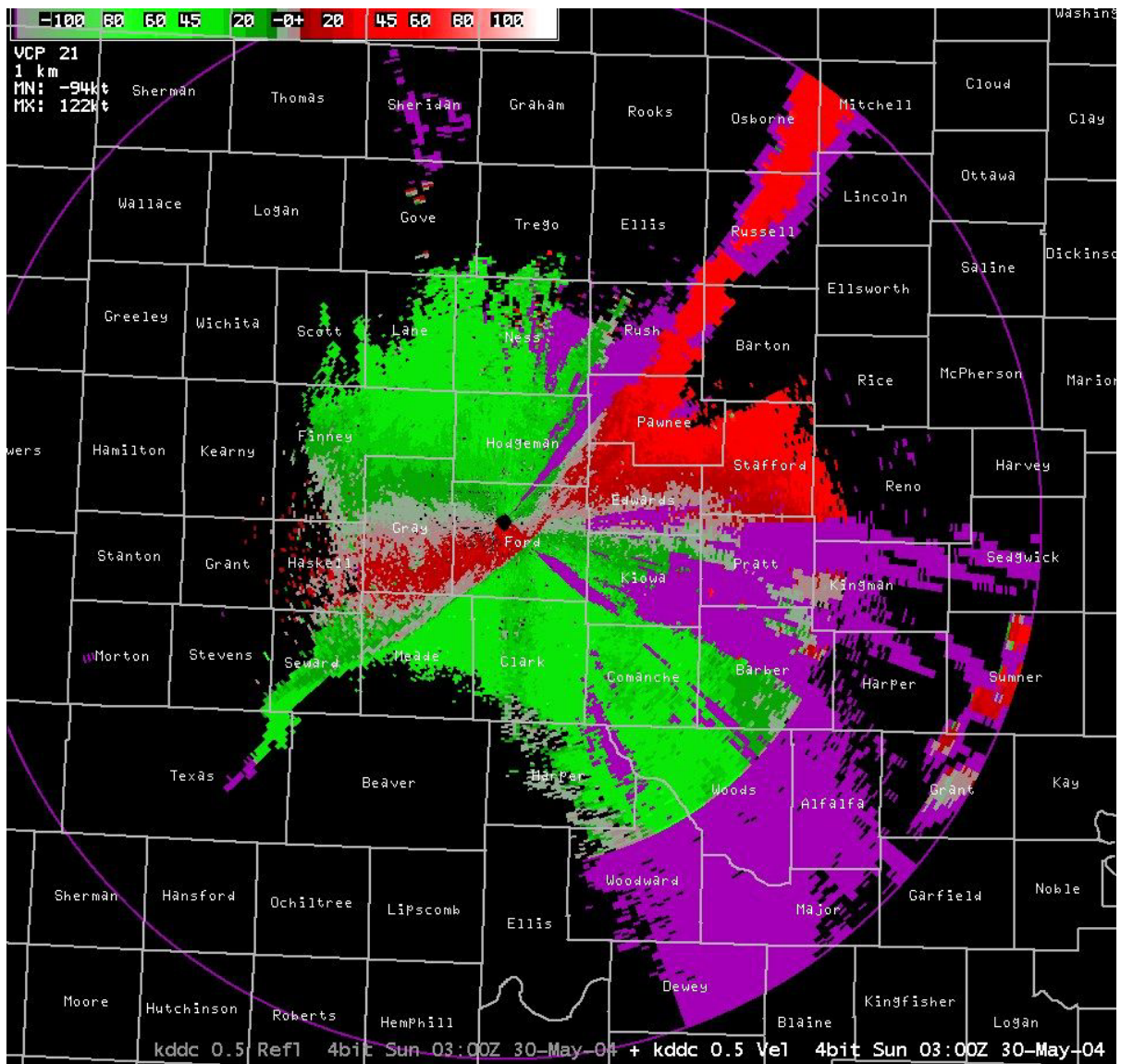


Figure 4-4
Range Overlaid Echoes

Dodge City, KS WSR-88D Base Radial Velocity Data Array product at 03:00 UTC on 30 May 2004 (AWIPS display). This product depicts significant range obscured (overlaid) or range folded echoes (color coded purple), mostly northeast through south of the radar. A strong cold front and associated wind shift is passing the radar.

4.2.5.1 Recognition of Range Folded Data. Within the WSR-88D, range folding affects only the Doppler data, that is the velocity, and velocity spectrum width data and products. However, through the use of the surveillance scan, the affected Doppler data are flagged and color-coded.

Range overlaid echo is especially a problem when the near-radar ground clutter residue or even clear air echo is repeated just beyond the edge of the 2nd and 3rd trip echoes. This can account for substantial range folding in each range interval. Range folding may also occur under conditions of anomalous propagation where the radar beam is constrained to follow a path close to the Earth's surface. Range folding is also a significant problem when strong convection occurs beyond the first trip or within widespread precipitation echo such as with tropical storms.

When possible, the range-unfolding algorithm will place the Doppler velocity and spectrum width data at the proper range. When this software cannot determine the proper range, i.e., the data is determined to be overlaid, the data will be flagged and displayed as range folded.

An alternative dealiasing method employs the MPDA (Part C, Chapter 3, of this Handbook), currently confined to VCP 121. Its primary application is velocity dealiasing, but it is also effective in range unfolding. The Doppler data for the first PRF are automatically range unfolded by the RDA. Doppler data for the 2nd and 3rd scans must be range unfolded at the RPG using the MPDA preprocessor algorithm. This algorithm reduces range folding by 50% to 70%. The algorithm implements three different PRFs and monitors the changes, if any, of Doppler data placement. In this way, the correct data placement can be determined.

4.2.5.2 Assessing Impacts of Range Folded Data. Range folded data can impact products and algorithms that use velocity data. However, there is essentially no impact on reflectivity data and products.

The impact of Doppler velocity and spectrum width range folding is significant, both in the Doppler waveform's unambiguous range limits and in 2nd or 3rd trip areas where significant velocity data loss due to range obscuration (overlaid) returns also occur. Range obscured (overlaid) data are flagged as range folded and treated as missing by the velocity-based algorithms and can, therefore, seriously impact those algorithms. But perhaps more importantly, overlaid data significantly impacts the human interpretation of the data.

4.2.5.3 Assessing Impacts of Range Folded Data on Velocity Products. The presence of range folded (overlaid) data on Mean Radial Velocity products is inevitable. The inability to determine velocity estimates for these sample volumes results from the inability of the range unfolding algorithm to distinguish between nearly equal power returns from two or more sample volumes at the same relative location within different trips. Therefore, valid velocity estimates can be derived for only one corresponding sample volume along each radial if the power returned from the sample volume dominates. If the power returned from any of the ambiguous sample volumes fails to dominate, then all will be flagged and color-coded as range overlaid echo.

The ring of range folded (overlaid) data at the beginning of the second and subsequent trips is caused by the first trip ground clutter and is a common result of this range unfolding limitation. The result, as mentioned above, is the inability of either the human or the algorithm to interpret or use this overlaid velocity or spectrum width data.

4.2.6 Velocity Aliased Data. Velocity aliasing occurs when frequencies too high to be analyzed with the given sampling interval appear as a frequency less than the Nyquist co-interval. In other words, wind speeds greater than the unambiguous velocity (Nyquist co-interval) for the current PRF are wrapped around into the incorrect Nyquist co-interval. A sophisticated velocity dealiasing technique is implemented in the WSR-88D (Part C of this Handbook). However, improperly dealiased data (Figure 4-5) occasionally occurs where the first sample volume intercepted by the radar beam already exceeds the unambiguous velocity or where gate-to-gate shears are very large. What we deal with is not aliased data, but with incorrectly dealiased data or dealiasing failures.

4.2.6.1 Recognition of Velocity Dealiasing Failure. Data that are incorrectly dealiased can often be identified by inspection. Typically aliased velocities that, for some reason, cannot be dealiased properly are actually passed through as incorrectly dealiased. Velocities may appear reasonable until the sample volume is encountered where the failure occurs. Errors are recognizable as wedges or radials having sharp radial discontinuities from adjacent regions and whose predominant colors differ markedly (Figure 4-5). Errors may also appear as radial spikes several volume samples in length, whose velocities are shifted toward high positive or negative values. When it is noted that there is no zero crossing between these high values of opposite sign along a radial or between this and the adjacent radial, then it is certain that a dealiasing failure has occurred. Moreover, if the maximum listed velocities in a velocity product are shown as $\pm 62.8 \text{ ms}^{-1}$ (122 kts) or $\pm 63.2 \text{ ms}^{-1}$ (123 kts), this often (but not always) signals that incorrectly dealiased velocities are present somewhere in the product.

Instances of incorrect dealiasing may occur when there are shifts in the inward and outward bound velocities along the radials of data that do not fit those allowed by the algorithm. In these cases, the actual values may be off by a factor of twice the unambiguous velocity of the PRF in use at that time. Typical unambiguous velocities for the WSR-88D, in the Precipitation Mode, range from 20.6 ms^{-1} (40 kts) to 30.9 ms^{-1} (60 kts). Very rarely, groupings of data appear along a small set of radials that could not be successfully dealiased. These should be obvious. However, the vast majority of time, velocity data having passed through the dealiasing algorithm is altered to the point that the non-dealiased data and its actual value are irrevocably lost.

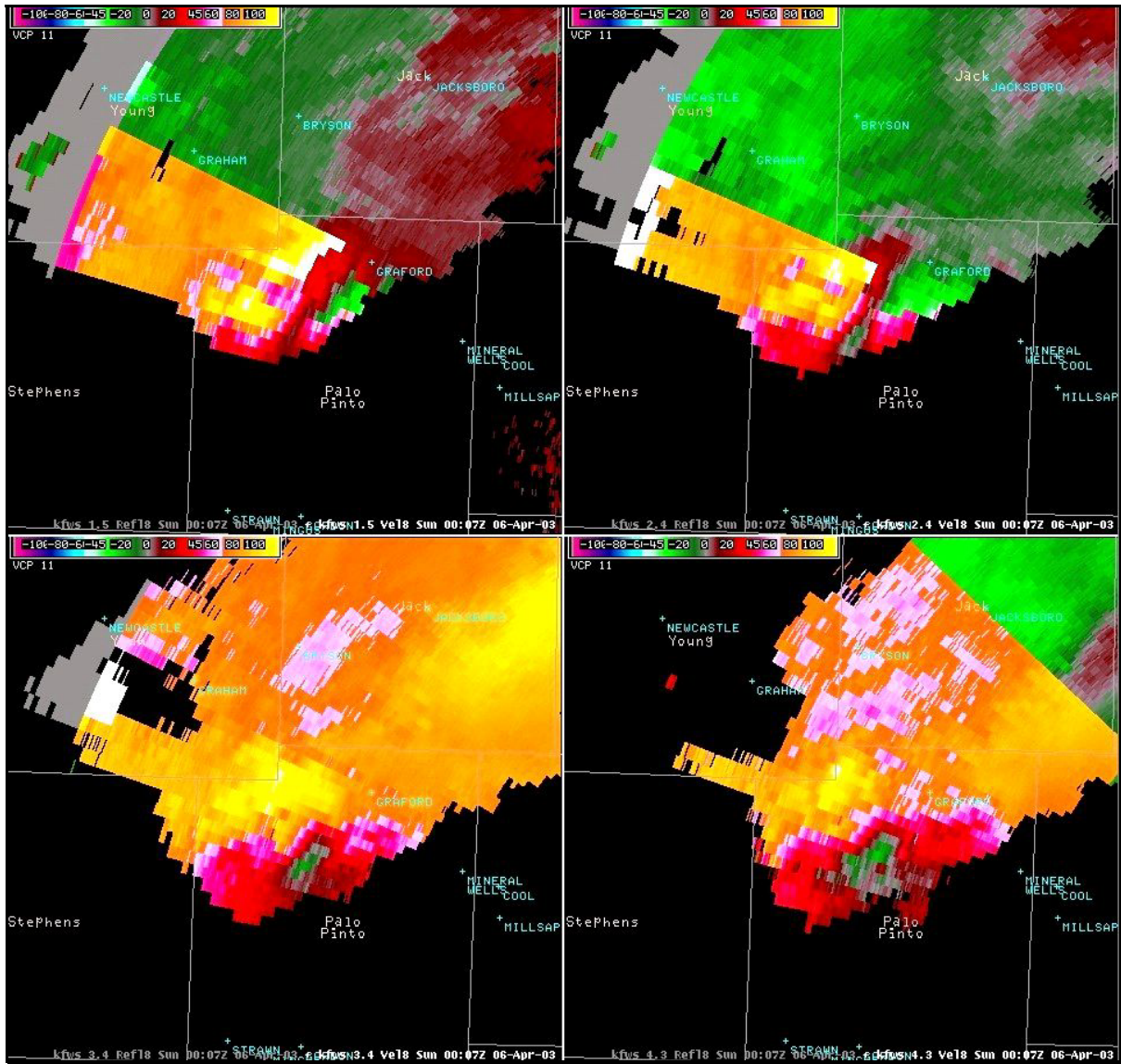


Figure 4-5
Velocity Dealiasing Errors

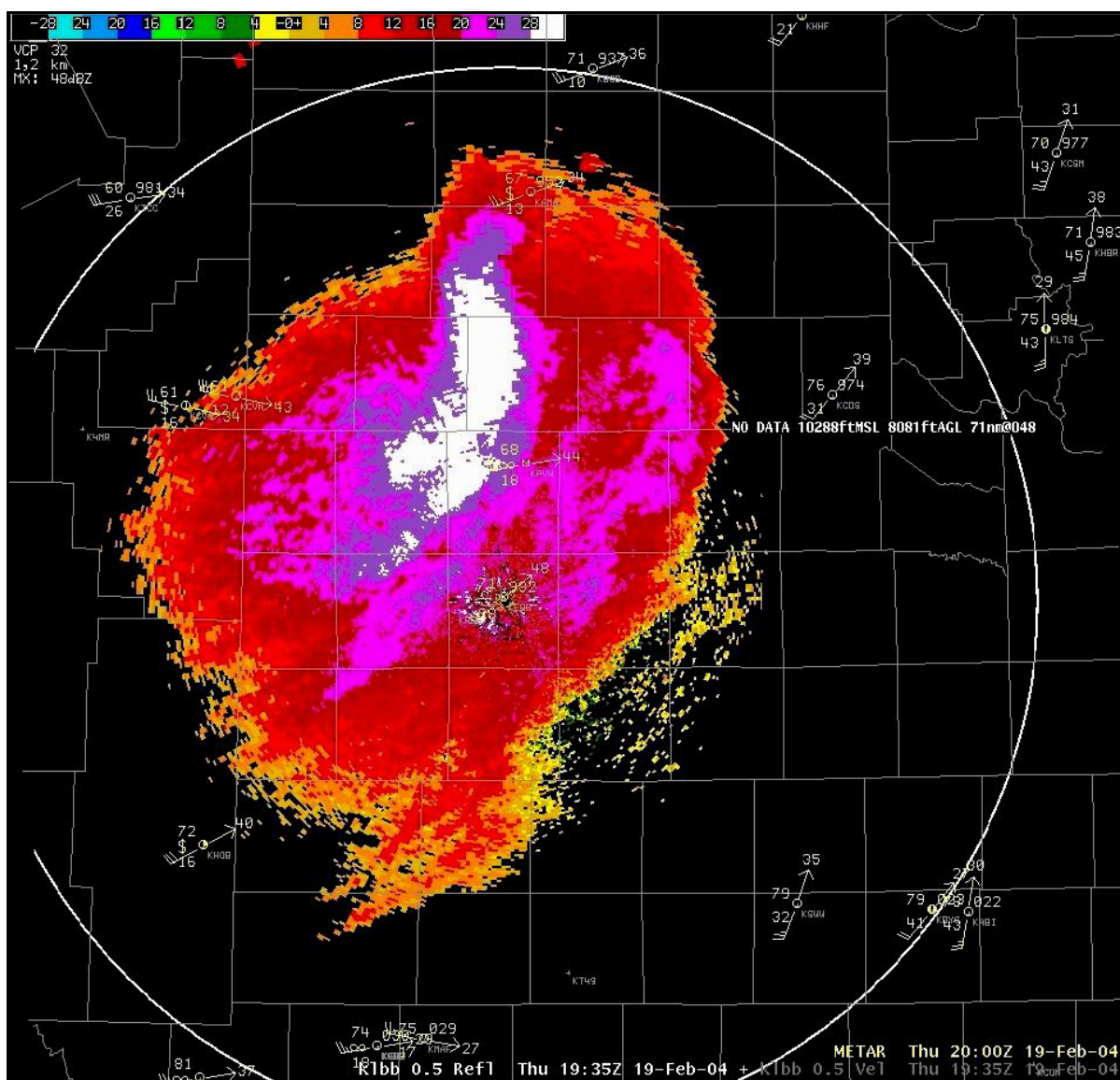
Fort Worth, TX WSR-88D 4-panel, Base Velocity Data Array product at 00:07 UTC on 6 April 2003 (AWIPS display). There are extensive areas of velocity dealiasing errors southwest of the sharp velocity discontinuities from mostly moderate radar inbound (green) velocities adjacent to the very strong (yellow and pink) outbound velocities. There is no zero crossing along these radial-aligned velocity discontinuities giving indication that there is a dealiasing error in that location.

4.2.6.2 Assessing Impacts of Velocity Dealiasing Failures. Incorrectly dealiased velocity data can seriously impact certain WSR-88D algorithms and products. Velocity products of all types (V, SRM, SRR, VCS, SWV, DV, and ITWSDBV) will be difficult or impossible to analyze when contaminated with incorrectly dealiased Doppler data. This will significantly degrade the front line of human data interpretation. In order to determine the extent of the dealiasing problem, it is recommended that earlier displays of these products be examined to determine if there is temporal or spatial continuity. In addition, other elevation angles of the velocity products may be used to determine if there is vertical continuity.

Algorithms and products that ingest mean radial velocity data can output incorrect results when such data are used. In the case of the legacy Mesocyclone, MDA, and TDA algorithms, there will likely be a lack of vertical continuity of incorrectly dealiased data. Consequently, only uncorrelated shears should result from using incorrectly dealiased velocity data. In the rare event of contaminated Mesocyclone, MDA, or TDA output, other products should help verify the existence of these circulations. However, base products should always be the primary tool for mesocyclone and Tornado Vortex Signature (TVS) detection in any case. (Algorithm output should function only as an imperfect “safety net”).

4.3 Non-Precipitation Radar Echoes. The WSR-88D provides the capability to monitor the atmosphere in the absence of precipitation-size backscattering particles in the optically clear air. Clear air return is very useful because it will often allow measurement of low-level environmental winds (i.e., those within the boundary layer) in all but the coldest months in moderate or cold climates. The capability can also prove important in recognizing early or pre-convective development, turbulence, and the onset of severe wind events.

These “clear air” returns are associated typically with two target types. The first source of clear air backscattered power is the refractive index variation or density gradients within the atmosphere. These are caused by temperature and humidity variations. Reflectivity with these variations is less than about 5 dBZ. The second source is associated with insects, birds, and sometimes bats (Doviak and Zrnic, 1984). Reflectivity often varies from 5 dBZ up to over 50 dBZ depending on the size and concentration of these biological targets. However, there is also smoke, dust (with sufficient particle size for S-band radar detection), volcanic ash, chaff, and other sources of non-meteorological echo (Figure 4-6).



Lubbock, TX WSR-88D Base Reflectivity Data Array product at 19:35 UTC on 19 February 2004 (AWIPS display). A dust storm is responsible (with significant refractivity gradients and sufficiently large particulates for S-band detection) for this large area of Clear Air Mode echo. The overlaid surface observations (20:00 UTC) indicate wind gusts ranging from ~15 to 25 ms⁻¹ (30 to 50 kts), blowing dust, and sky obscuration due to blowing dust.

4.3.1 Recognition of Non-Precipitation Radar Echoes. Non-precipitation echoes can be seen in the Precipitation Mode as well as the Clear Air Mode. In the Clear Air Mode non-precipitating returns will be seen out to about 185 km (100 nm) in extreme cases, depending on environmental conditions. In the Precipitation Mode, it may be expected that recognition of non-precipitation echoes will be confined to ranges closer to the antenna (out to ~ 46 km (25 nm) to extremes of ~ 130 km (70 nm)). In most radar locations insects and birds increase markedly at sunset and the convective boundary layer is seen to “bloom” on radar. At other times migratory birds can be detected and even tracked by radar (Kelly et al. 2000; Bruderer 1977a, 1977b, 2000).

Using the WSR-88D, it is possible to attain significant radar measurements in optically clear air. With enough atmospheric scattering, the WSR-88D can measure a return of -8 dBZ_e at a range of 50 km (27 nm) and -28 dBZ_e at a range of 5 km (2.7 nm). When operating in the Clear Air Mode, use can be made of the 16-level R and V products, as well as SW and VAD products.

4.3.2 Considerations. In the Clear Air Mode, the option exists to select either long or short pulse (VCP 31 or 32, respectively). Operation in the long pulse results in a better signal-to-noise ratio permitting lower reflectivity levels to be detected (-16 dBZ_e at 50 km (27 nm)). The long pulse, while providing better sensitivity, results in coarser resolution in velocity and spectrum width fields (~0.75 km (0.4 nm) range gate resolution) and a lower Nyquist velocity value ($\pm 10.8 \text{ ms}^{-1}$ (21 kts)). In Clear Air long pulse Mode (VCP 31), the actual pulse width is 0.75 km (0.4 nm) which restricts velocity and spectrum width product resolutions to 1 km (0.54 nm). The long pulse mode is best suited to situations where the atmospheric boundary layer is well mixed, such as during daytime heating. In the short pulse, the sensitivity is only slightly reduced and the ~250 m (0.13 nm) gate resolution is maintained in the velocity and spectrum width fields. Since the higher Nyquist velocities are available in the short pulse, this VCP may be used when strong winds characterize the environment.

4.4 Boundaries. Various airmass or airflow boundaries can readily be seen on the WSR-88D. Some of these boundaries include: synoptic fronts, gust fronts, pre-frontal trough lines, drylines, thunderstorm outflows, land and sea breezes, and other convergence zones that may be inherent to particular regions. While the mechanisms for inducing each of these boundaries may be somewhat varied, their presentation on the displays are similar enough to discuss them in a broad sense collectively. Examples can be seen in Figures 4-7 through 4-9.

4.4.1 Recognition of Boundaries. In general, boundaries are characterized by narrow zones of shifting convergent winds or density differences, or both. They will appear on Reflectivity (Figure 4-7) and Spectrum Width products (Figure 4-59) as narrow lines of enhanced values (sometimes called thin lines). The enhanced reflectivity is produced by a combination of converging particulates, e.g., insects and the birds and sometimes refractive index gradients from temperature or moisture differences or both. Enhanced spectrum widths are typically produced by wind shear, changes in wind speed and direction within individual sample volumes.

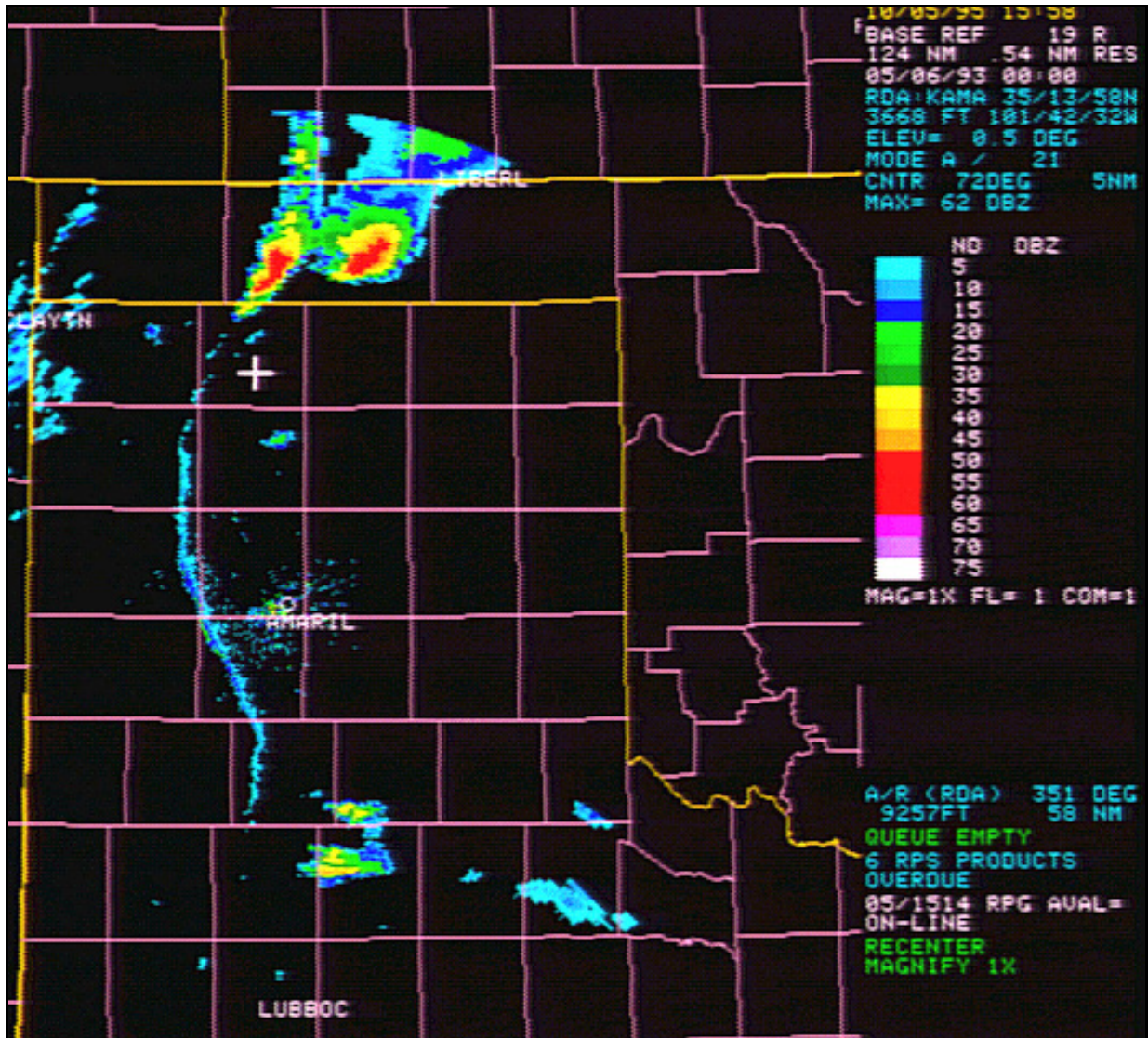


Figure 4-7
Dryline Reflectivity

Amarillo, TX WSR-88D Reflectivity product at 00:00 UTC on 6 May 1993 (legacy PUP display). This product, collected in Precipitation Mode, shows a linear thin-line echo along the "dryline" just to the west of the radar and convective storms to the north associated with the boundary. The thin-line echo is likely associated with particulates, insects and birds, and with a change in refractivity associated with the dryline.

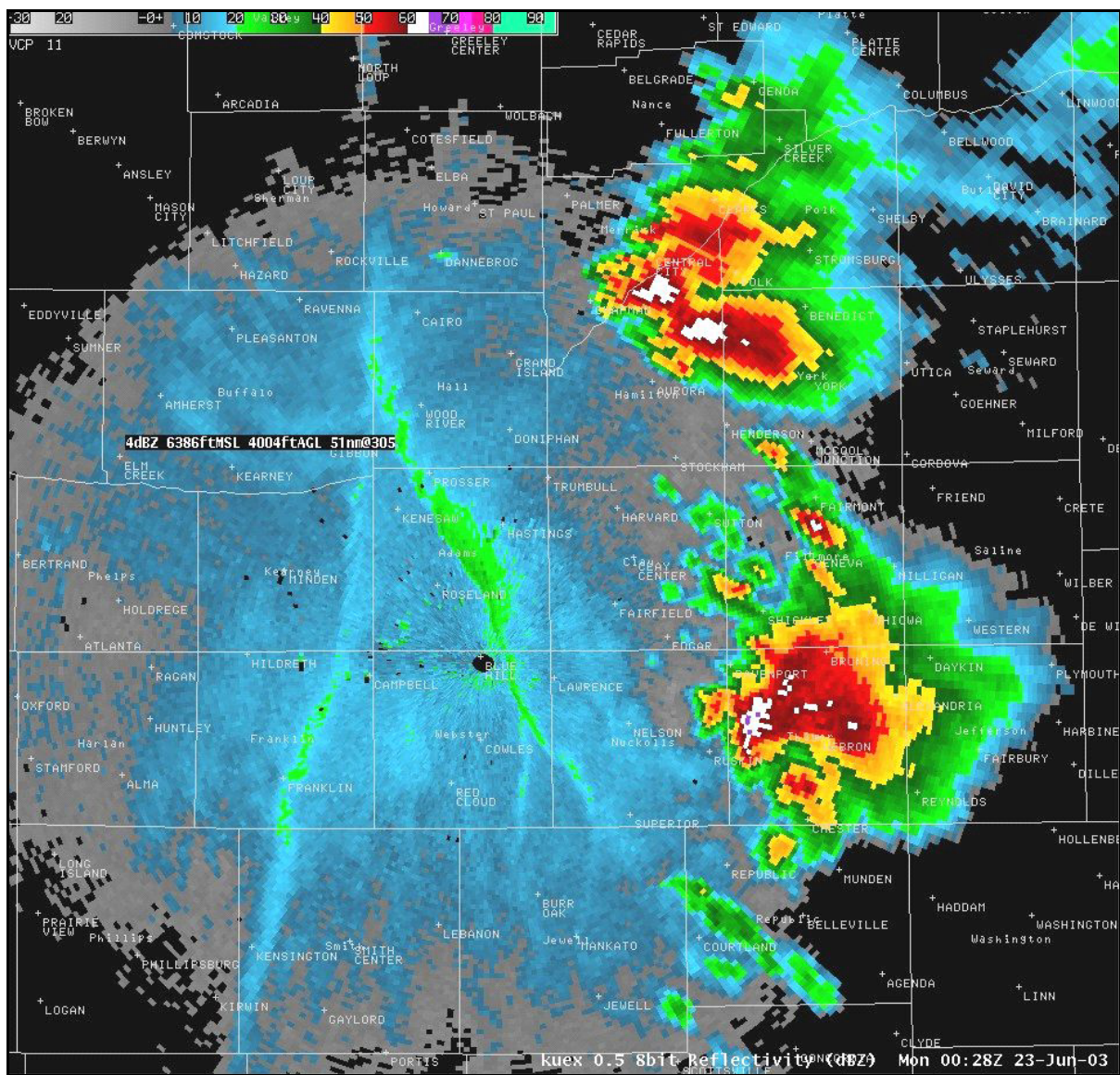


Figure 4-8
Boundaries and Severe Convection Reflectivities

Hastings, NE WSR-88D Base Reflectivity Data Array product at 00:26 UTC on 23 June 2003 (AWIPS display). This product, collected in Precipitation Mode, shows two boundaries. The thin-line to the left of the radar is along a stationary frontal boundary while that to the right is along an outflow boundary from earlier thunderstorm activity. The boundaries are delineated by echoes likely associated with insects, birds, and refractivity differences. The storm complex to the north northeast of the radar had, shortly before this image, produced the largest hail ever recorded, measuring 7.0 inches (17.78 cm) in diameter with an 18.75 inch (47.63 cm) circumference, and weighed 1.33 pounds (0.6 kg). The complex to the southeast of the radar produced the strongest mesocyclone ever recorded (Wakimoto et al. 2004).

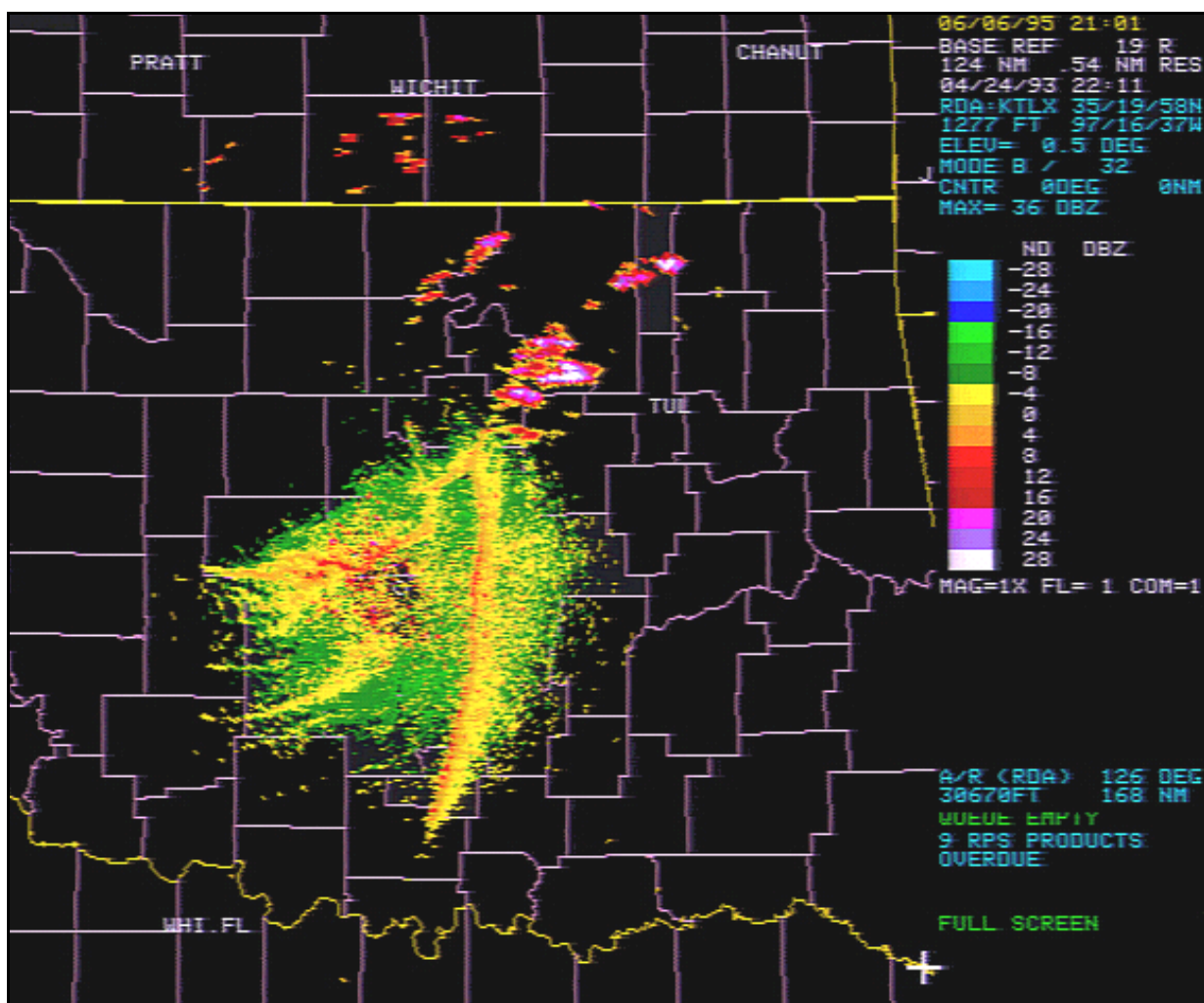


Figure 4-9
Dryline – Cold Front Intersection Reflectivity

Oklahoma City, OK WSR-88D Reflectivity product at 22:11 UTC on 24 April 1993 (legacy PUP display). This product, collected in Clear Air Mode, shows thin-lines associated with a cold front (northwest of the radar), dryline (east of the radar), and a third boundary-like feature of unknown origin between the other two. Echo intensities less than about 5 dBZ are associated with refractive index gradients. Convective echoes soon developed near the “triple point” of boundary confluence and led to a tornadic supercell storm.

The changing winds across the boundary will show up on Mean Radial Velocity products as radial convergence or azimuthal shear, depending on the orientation of the winds with respect to the radar-viewing angle. When the radar beam is perpendicular to the long axis of the boundary, radial convergence will be detected. When the beam is parallel to the boundary, the wind shift will produce a long, narrow zone of azimuthal shear and broadened velocity spectrum width. Boundaries of sufficient horizontal extent will be defined by a combination of convergence and shear on the same display.

4.4.2 Considerations. Boundaries will be better detected in the Clear Air Mode as opposed to the Precipitation Mode because of increased sensitivity with clear air sampling parameters. This is especially true with the increased sensitivity of the long pulse employed in VCP 31. At 50 km (27 nm) range, returns of -16 dBZ_e can be detected in the Clear Air Mode, but when in Precipitation Mode the lower bound reflectivity displays are typically limited to 5 dBZ_e and higher using the 16-level Reflectivity product (Figure 4-7). However, using the DR product, the lower bound reflectivity threshold, even in the Precipitation Mode is -30 dBZ_e and is clearly applicable for boundary detection (Figure 4-8). In the Clear Air Mode, boundaries are best detected by the 16-level Reflectivity product which, in this mode, as indicated above, has a much lower threshold than the same product in the Precipitation Mode (Figure 4-9). In the Precipitation Mode, boundaries can often be detected, but not as well as in the Clear Air Mode; boundaries away from precipitation areas will most frequently be seen closer to the radar (often within ~ 55 km (30 nm) or less) unless using the DR product. Gust fronts in association with squall lines and fronts that are attended by mesoscale precipitation bands most often have reflectivity factors of +5 to +25 dBZ_e and their boundaries will sometimes be detectable at longer range increments.

Display system software that implement “feature tracking” can be used to calculate boundary motion. Time lapse loops can be used for this purpose, as well. In addition, the intersection or collision of boundaries, which may lead to further convective development, can often be easily anticipated or observed by viewing time lapse sequences.

When a boundary passes the radar and a frontal “airmass” covers the radar for some distance, then the VWP product may be used to detect the cold air depth (typically 1 to 3 km (3,000 to 10,000 feet deep)), its changes, and vertical frontal structure. The vertical extent of land or sea breezes can also sometimes be determined using the VWP as an indicator.

4.5 Cloud Layers. Strictly speaking the WSR-88D, because it is an S-Band weather radar, cannot detect cloud droplets owing their very small size. This is the case with warm clouds that is clouds above freezing that do not contain precipitation. However, often and under certain circumstances the sensitivity of the WSR-88D provides the user with the capability of detecting cloud layers due to precipitation size particulates (~0.1 to 1 mm) or refractive index gradients. The WSR-88D has revealed that many clouds, even some which are translucent, contain S-band radar detectable precipitation-size particles. Moreover, refractive index gradients sufficient to create radar returns

can reveal a variety of other clouds. Smoke plumes and smoke layers (with sufficiently large particulates) are often revealed in the same way as are volcanic ash plumes. The Reflectivity products in both Clear Air and Precipitation Modes are commonly used to determine the existence and extent of the cloud layers. Thus, in this Handbook when referring to WSR-88D “cloud” detection, we are considering detection of either precipitation-size particles within cloud or cloud-associated refractive index gradients. This capability is important because it has application to aviation forecasting, and forecasting or observing the early evolution of precipitation.

The WSR-88D can detect large ice crystals and precipitation size particles that are present in middle and high-level clouds. Of course, virga descending from these same clouds is also detectable. Reflectivity may range up to and in excess of +30 dBZ_e within these precipitation bearing clouds. Thunderstorm anvil “blow-off” and middle- and upper-level precipitating cloud layers associated with stratiform precipitation and warm fronts are prominent examples. Because these clouds can be easily detected, other aspects of the middle troposphere can be observed. The VAD algorithm, for example, will use Doppler velocity measurements from middle and high-level clouds to generate profiles into the middle troposphere. These wind profiles allow the operator / meteorologist to observe the movement of synoptic and smaller scale waves and troughs and can be used to monitor numerical model performance.

4.5.1 Recognition of Cloud Layers. With the high sensitivity of the WSR-88D, it is possible to obtain reflectivity estimates within clouds at all heights which generally reflect at levels between -12 and +5 dBZ_e (Figure 4-10). Moreover, it has been observed that refractive index gradients within atmospheric layers that are undergoing cooling and lifting prior to actual cloud formation are also sometimes detectable.

The depth of cold cloud layers may often be inferred from particulate detection and warm cloud layers from detecting refractive index gradients. Cloud layers very often appear as concentric rings about the radar location. The inner edge of the ring marks the cloud base while the outer edge marks the cloud-layer top. Using the Reflectivity product for the elevation that intersects the cloud layer, place the cursor at the point where the base appears to be and note the azimuth, range, and height. Then, place the cursor at the apparent top of the cloud layer noting the same information. This reveals the cloud depth at those points. These layers are, however, often not of uniform depth and may slope with height (Lemon and Quetone 1994).

4.5.2 Considerations. In the Clear Air Mode, cloud detection may be best achieved using VCP 31 due to a better signal-to-noise ratio. As explained above, cloud droplets characterizing warm clouds (stratus and fog absent of precipitation) are too small to be detected by S-band radars. Horizontal cloud rolls or cumulus cloud streets can also occasionally be detected with reflectivity often ranging from -10 dBZ_e to +10 dBZ_e. This is again because of refractive index gradients or convergence of particulates such as insects, birds, etc. Gravity waves and undular bores atop an inversion can also be detected at times in the velocity and reflectivity fields. Gravity waves should coincide with parallel bands of alternating increases and decreases in reflectivity.

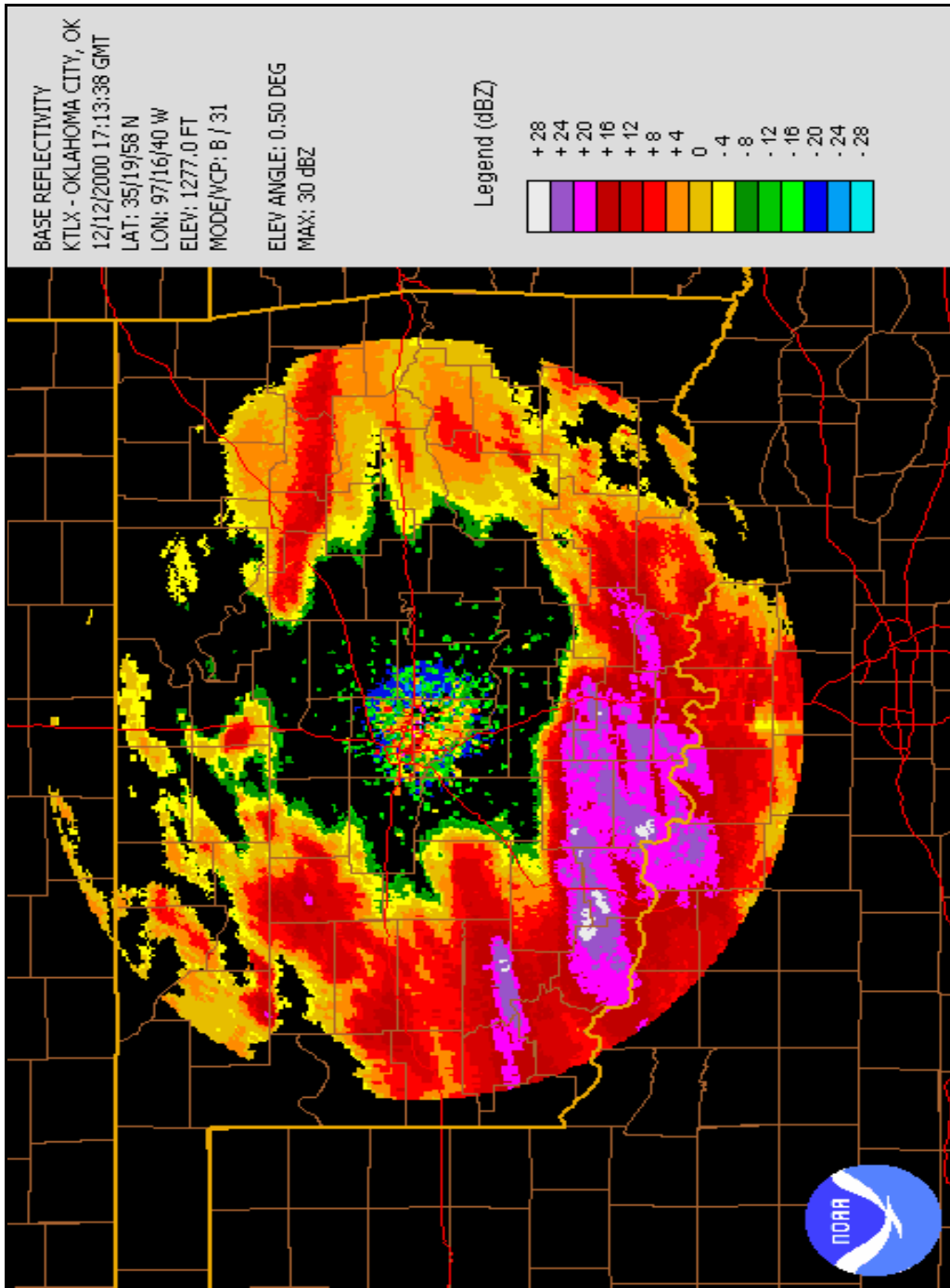


Figure 4-10
Clear Air Reflectivity Product

Oklahoma City, OK WSR-88D Reflectivity product at 17:13 UTC on 12 December 2000 (NCDC NEXRAD viewer). In this product, collected in Clear Air mode, the radar-centered "donut" echo is an ice crystal cloud and a virga layer aloft surrounds the radar.

4.6 Pre-Convective Development. Of importance to all forecast programs is the ability to observe and forecast development of clouds and convection.

4.6.1 Recognition of Pre-Convective Development. In areas of warm advection, small, weak, echoes may begin to appear in bands or clusters. These echoes will then increase in numbers and intensity at various rates. In other cases lines of broken convection become apparent when these small, weakly reflective echoes rapidly increase and become strong within a few volume scans. Observations of this can be accomplished in the Clear Air Mode using all three base moments. At other times in an otherwise noisy field, the user can begin to detect velocity coherency and low values of spectrum width. Reflectivity returns may appear to be small and essentially circular in nature.

4.6.2 Considerations. Evidence of convective development will sometimes appear in the spectrum width and velocity before any significant return is detected in the reflectivity field. Selection of the long pulse in the Clear Air Mode may produce better results because of increased sensitivity. For the earliest evidence of convective development, observations at or near the altitudes of the 0° C to -15° C isotherms are often used.

4.7 Convective Storms. Deep moist convection develops in a conditionally unstable environment with sufficient moisture and lift. Lift and updraft may be produced in a variety of ways including by warm advection, low-level convergence, cold advection aloft, jet streaks aloft, orography, etc. Once precipitation particles form and precipitation drag and evaporation begin, corresponding downdrafts will soon develop. It is important to realize that convection and convective storms are compact regions of airflow and heat exchange. These storms and their corresponding radar echoes are not “things” or objects, but rather four-dimensional airflow processes.

Many of the radar products in the WSR-88D are designed to examine convective storms and the features that mark them as severe. The WSR-88D is a diagnostic tool in the hands of the meteorological researcher and practitioner. Through the use of WSR-88D products, characteristics of single cell, multicell, and supercell storms are investigated with the intent to determine storm existence, motion, strength, and severity. In this section we discuss WSR-88D detectable storm features and the analysis methods and products used to discriminate between severe and non-severe storms. (The user is urged to use not only radar data, but all observations).

4.7.1 Single Cell Storms. Modern concepts of convective storms owe their origin to the Thunderstorm Project of the 1940's (Byers and Braham 1949). Of fundamental importance identified in this project was the basic organizational structure of deep, moist convection that is the “cell” (Figure 4-11). The meteorological scientific community recognizes the buoyant bubble or plume of updraft and cumulus cloud as a thunderstorm “cell.” This rising bubble or plume gives rise to a precipitation ensemble detectable on the radar as an echo center or echo reflectivity core. As precipitation begins to form and descend a downdraft will quickly result through entrainment of dry potentially cold air aloft and precipitation drag. In time, this downdraft will spread and in non-

severe convection will not coexist with the updraft for long periods but will overtake and dominate the “cell” leading to updraft demise and demise of the cell, leaving only an “orphan anvil.” Commonly, the life cycle of a single cell ranges from perhaps 20 to 40 minutes.

In meteorological operations, the cell concept has been somewhat modified and based on the primary observing system, that of the radar. The thunderstorm “cell” has come to mean a discrete, typically low-level, individual convective radar echo (see Part B, Chapter 8, of this Handbook). Over the years, taxonomy of convective storm types has developed around this concept. Most recently, convective storms have been seen as “ordinary” and “supercell” convection. However, here we persist with the former system emphasizing both cell and storm organization. The first, or fundamental, storm type in this system is the “single cell storm” (Figure 4-12). Arguably, single cell storms do not, in reality, exist; however, for our operational purposes we will begin with what is called the single cell storm. (We neglect for now the “new cell” development shown in Figure 4-12.)

4.7.1.1 Recognition of a Single Cell Storm. The environment for the single cell storm is normally one of relatively deep moisture, weak wind shear of the horizontal winds with height, and modest instability. An ordinary, non-severe, single cell storm typically has a radar pattern in which the reflectivity distribution is vertically aligned; no weak echo region or echo overhang is present. Displays of successively higher elevation angles of the Reflectivity product in a 4-panel display should confirm the vertical alignment and a narrowing of the echo (Figure 4-13). A Reflectivity Cross Section product, generated for an appropriate axis through the storm, may also confirm this alignment (as in Figure 4-12). Storms having this structure are not normally severe. They may produce lightning and thunder, brief heavy rain and infrequently small, non-severe, hail and gusty surface winds. Other products normally used are Mean Radial Velocity; VIL; STI; HI; and CR with the Combined Attributes Table; and the OHP, THP, and the STP/Digital Storm Total Precipitation (DSP) accumulation products.

Single cell storms generally move in the direction and with about 70% of the wind speed of the mean wind through the cloud-bearing layer. With reflectivity values typically above 40 dBZ_e, and easily identified storm reflectivity centroids or centroid, the Storm Cell Identification and Tracking (SCIT) algorithm should adequately track movement of these storm cells. However, with the storm’s typically abbreviated life cycle, these single-cell storms may be tracked for only 3 to 6 volume scans while the total lifetime of the overall echo will be longer.

4.7.1.2 Considerations. As single cell storms intensify, they invariably become multicell cluster storms. Moreover, and especially when in a sheared environment, these storms will often begin to propagate, and occasionally deviate, to the right or left of the mean flow. In this event, the STI product will be unable to accurately project the change in its movement since a linear track is assumed.

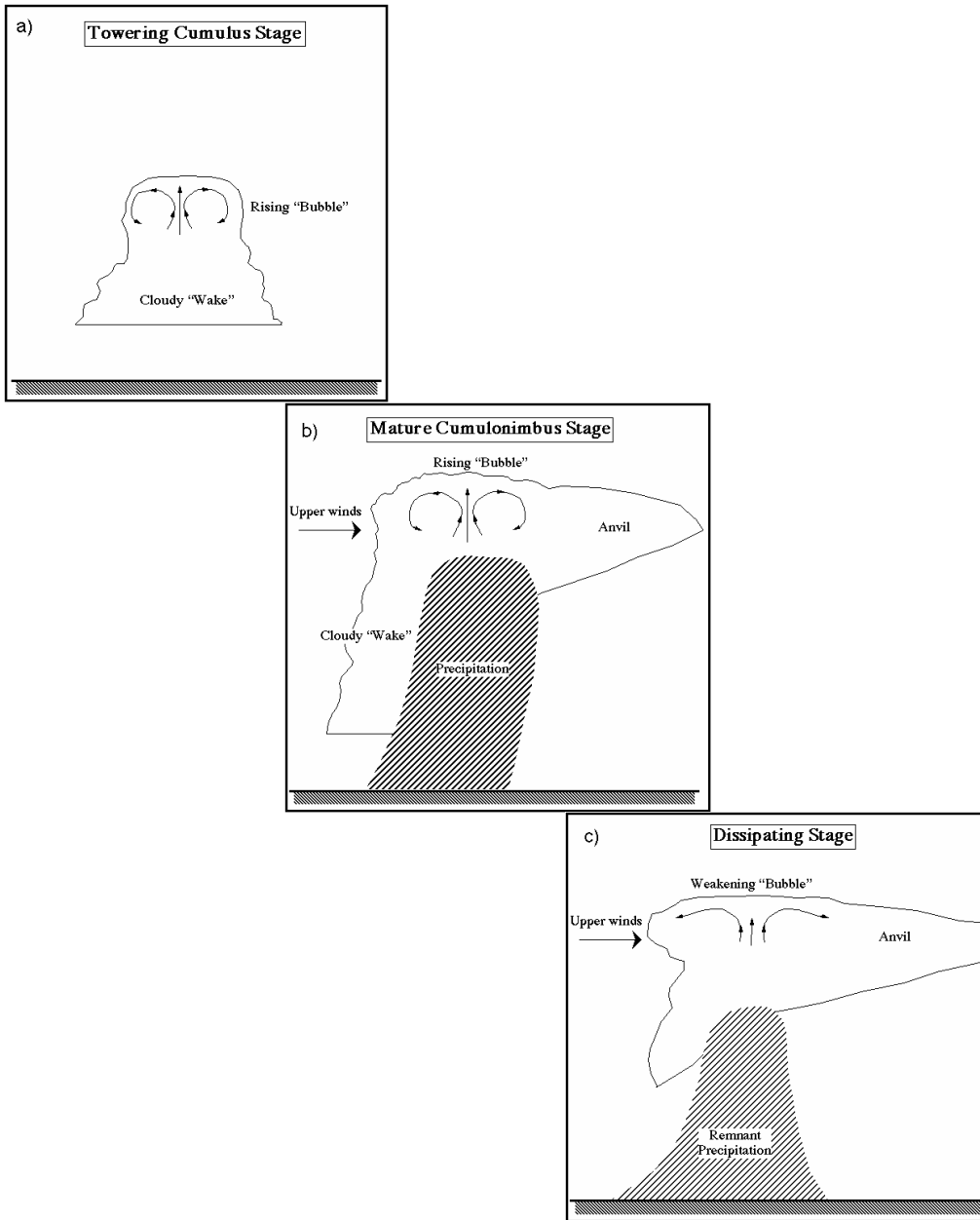


Figure 4-11
Ordinary Cell

The three stages of an ordinary cell life cycle, a) towering cumulus, b) mature, c) dissipating are depicted. Features of the figure are labeled showing distributions of cloud (outlined) encompassing updraft and precipitation encompassing downdraft. (From Doswell 2001 after Byers and Braham 1949).

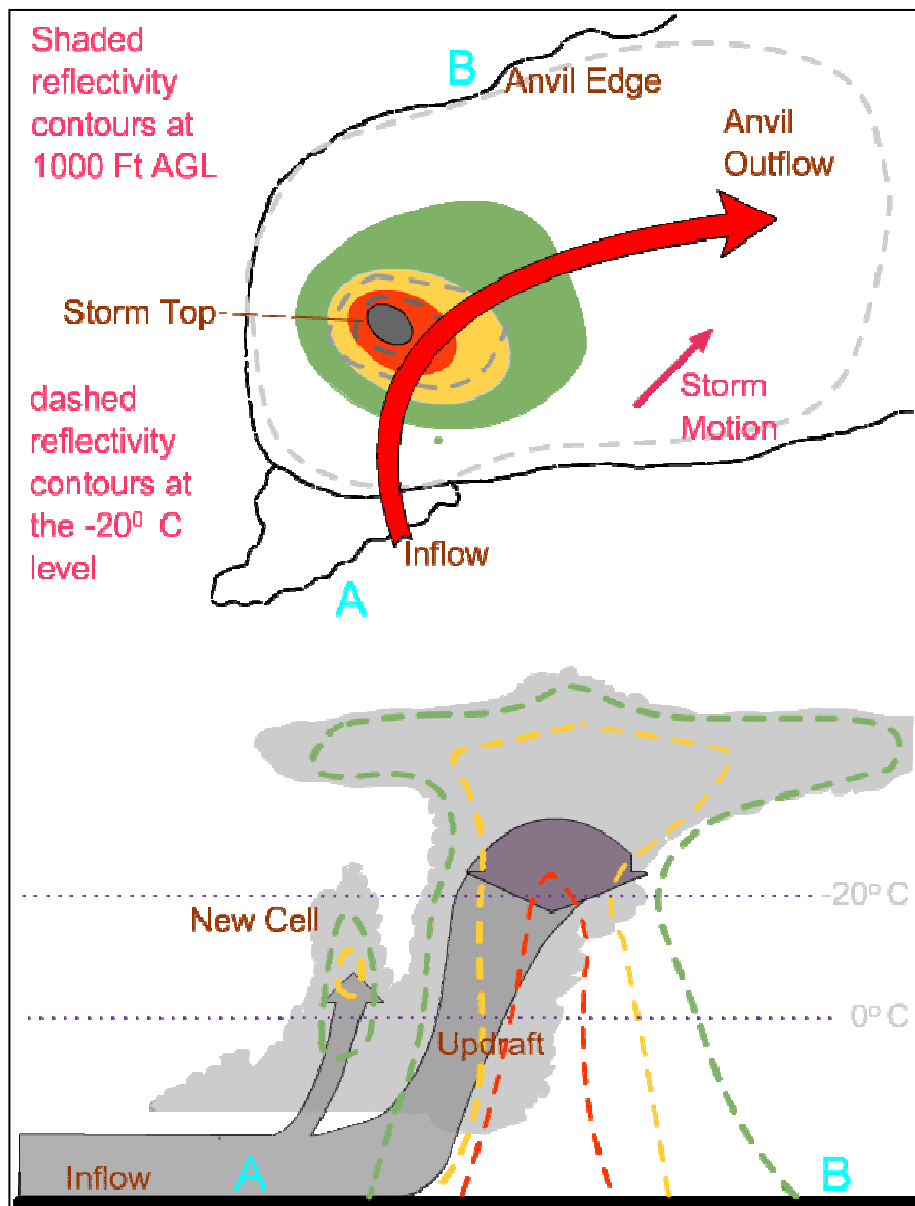


Figure 4-12
Non-Severe Thunderstorm Schematic

Schematic diagram of a non-severe thunderstorm in a sheared environment. In the upper panel is seen the cloud outline and the radar echo and features as labeled. Placement of the vertical cross section (A – B) in the lower panel is shown in the upper panel. Vertical cross section includes dashed echo contours, cloud outline, and low-level inflow and high-level outflow is indicated by the shaded arrow. After Lemon (1980).

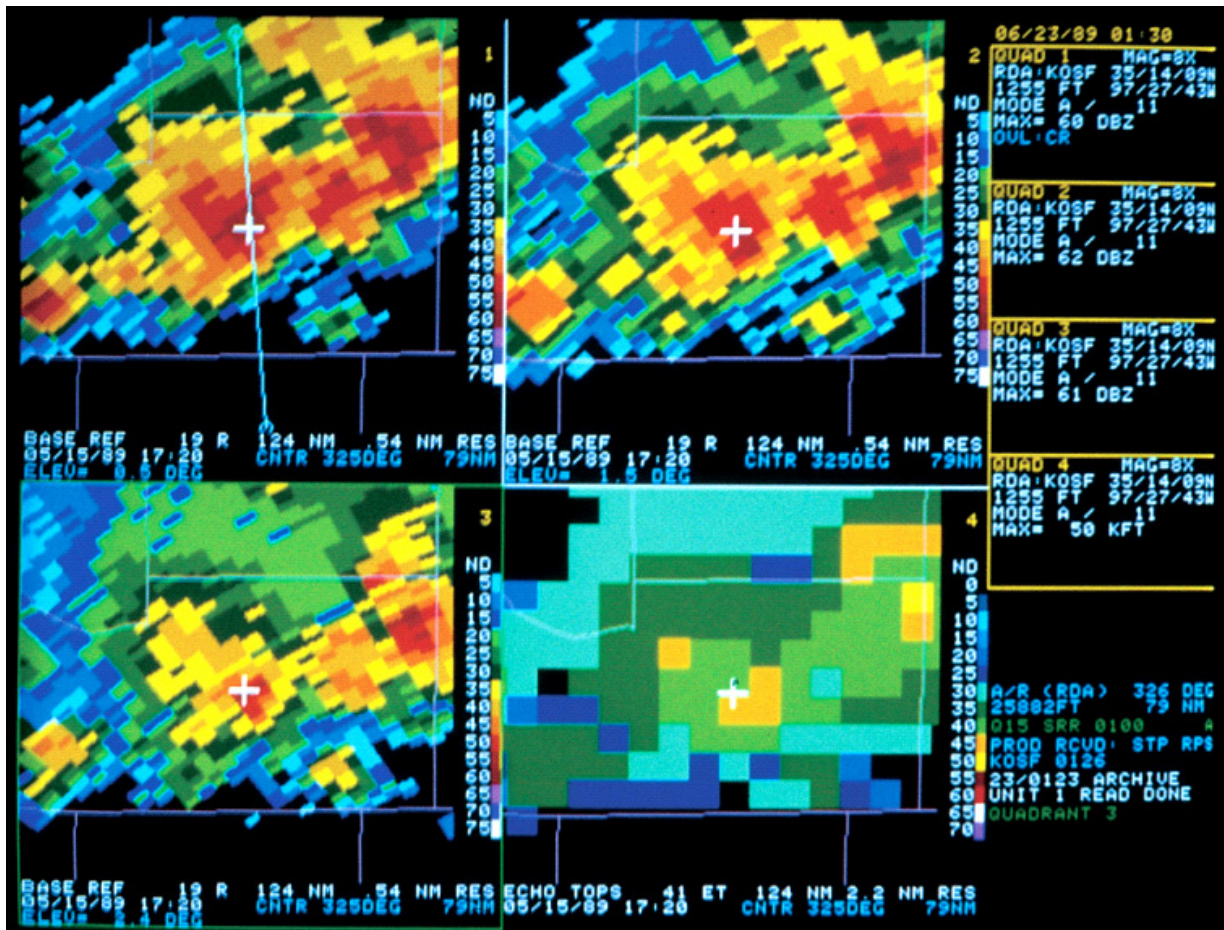


Figure 4-13
Ordinary Non-Severe Thunderstorm

Norman, OK WSR-88D (test bed radar) 4-panel display of Reflectivity products at 01:30 UTC on 23 June 1989 (legacy PUP display). The white cross at the 0.5° elevation upper left, 1.5° in upper right, 2.4° in lower left, and Echo Tops product in the lower right is at the same geographical location. The white cross is at the location of the echo summit and the high reflectivity echo core aloft of this nearly vertical thunderstorm.

4.7.2 Multicell Storms. A multicell storm consists of a cluster of single, short-lived cells in different stages of their life cycle (Figure 4-14). Often, each multicell cluster storm is one contiguous echo in low-levels on the display but the multicell nature of the echo can be seen in mid- and upper-levels of the echo. The outflows from each cell frequently combine to produce a low-level gust front, and the convergence along the boundary triggers new cell development on a preferred storm flank. This is especially true when the storm is embedded in an environment of deep layer shear.

4.7.2.1 Recognition of a Multicell Storm. A multicell cluster storm is evident when two or more (often mid-level) echo cores and/or echo tops become apparent within the echo mass (Figure 4-12). These cells will usually be in various stages of development, as indicated by increasing and decreasing values of reflectivity and fluctuating echo tops, over time. A time lapse of a Reflectivity product should help identify development of new cells on a preferred flank (“updraft” flank) of the storm. As each new cell develops and matures it becomes the dominant updraft and cell within the complex only to be replaced by successive new cells and associated updrafts. As each cell is replaced it moves downstream as it weakens and dissipates.

In a multicell storm, an indication that there is a transition to severe activity is the appearance of a cell with its first significant echo at higher levels than the earlier cells. However, this is often difficult to recognize in real time.

In a sheared environment, several changes in the echo may indicate a transition to a severe thunderstorm. Most of the echo features indicating severity will be discussed in Section 4.7.4., but a few will be mentioned here. If the multicell storm in a sheared environment becomes severe, a mid-level echo overhang on the updraft storm flank will develop with a weak echo region beneath. In low-levels, a strong reflectivity gradient develops on the updraft storm flank. This overhang and strengthened reflectivity gradient reflects invigoration of the updrafts and the subsequent enhancement of upper level divergence. This can be recognized by displaying successively higher elevations of the Reflectivity product in a 4-panel/multi-panel or “all tilts” display, with each panel centered and magnified identically. This can be done in an automated fashion using Reflectivity products on the current RPS list. Moreover, in this same fashion V, SRM, or SW can be displayed revealing the matching kinematic storm structure. The overhang and Weak Echo Region (WER) features can also be identified using Reflectivity Cross Section (RCS) products, but the axis and endpoints must be very carefully chosen. In order to be certain that the three-dimensional reflectivity storm structure has been best delineated, several RCS’s will probably be required and even then, it cannot be certain that the proper axis was selected. This process and the serious limitation in placement are not present with a 4-panel, multi-panel, or all tilts Reflectivity product display. Rather, much of the structural ambiguity is removed through quasi-horizontal display of Reflectivity multi-panel displays. Therefore, the multi-panel method of product display is recommended over the vertical cross section method.

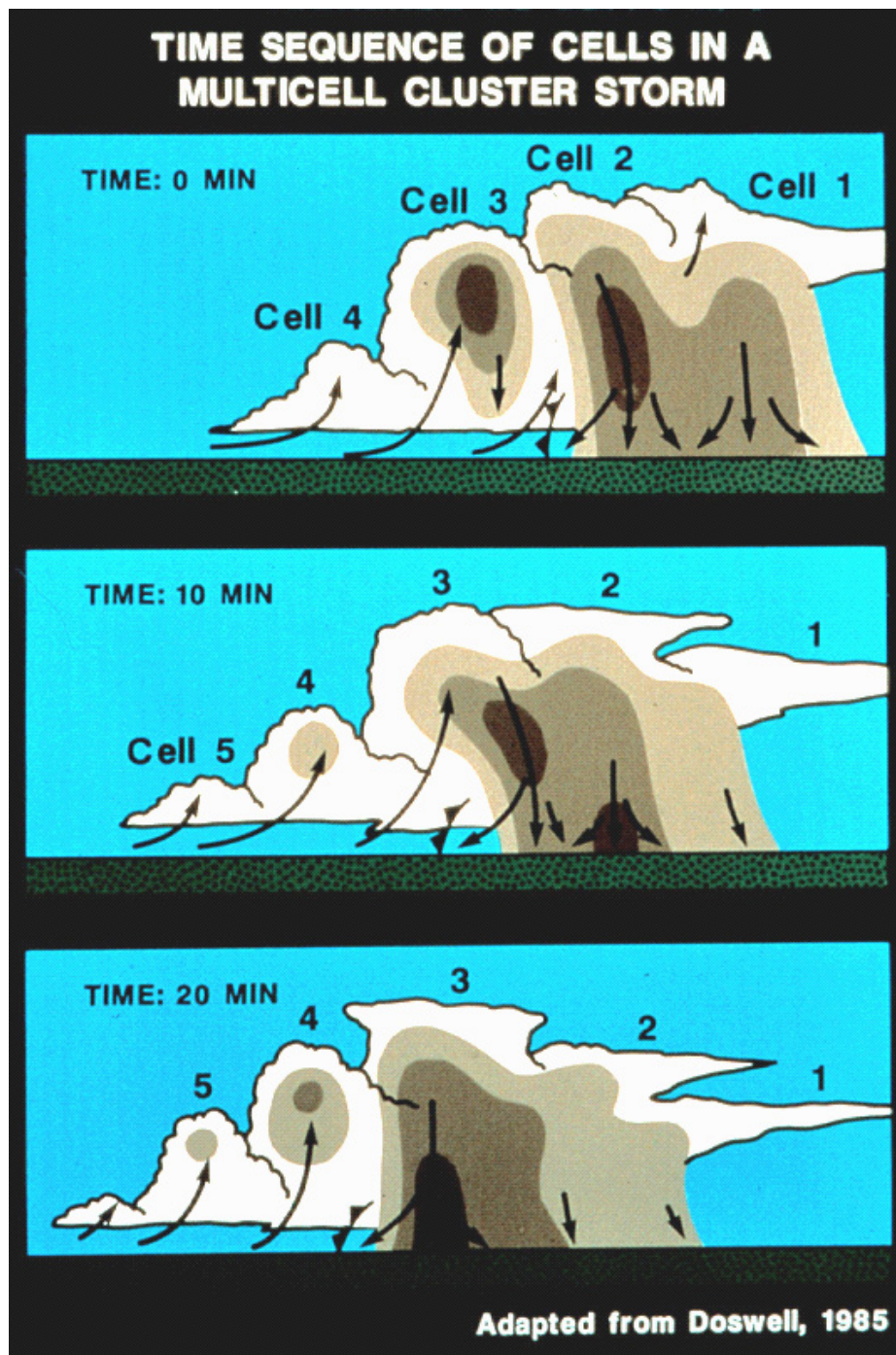


Figure 4-14
Multicell Storm Sequence Schematic

Schematic illustrating the evolution of convective cells moving through a multicell storm over a 20-minute period.

As each new cell of the multicell cluster storm tends to develop in the up-shear direction, often to the right of its predecessor, the storm as a whole will usually deviate in the direction of updraft propagation and move more slowly than the individual cells and the mean wind. At other times new cell development on the storm front flank may accelerate storm motion. Then again, with downstream cell motion but upstream cell propagation offsetting each other, the result can be a stationary storm. There are many and varied combinations of propagation and cell translation. A time lapse of low-level Reflectivity products will help in showing deviant motion and new cell development, often in the direction of the updraft storm flank.

When, with a multicell radar echo, the low-level echo core is displaced toward a developing updraft-flank along with enhanced reflectivity gradients, an echo overhang, and WER aloft, with the storm top directly above, then that storm is a developing severe storm. The dominant severe weather phenomena are typically large hail (> 1.9 cm ($\frac{3}{4}$ inch) hail) and occasionally severe or damaging surface winds (> 25.7 ms⁻¹ (50 kts)). Most often the severe weather occurs in an episodic manner as each new cell developing on the updraft storm flank matures and begins to decline.

In a squall line, a linear multicell system, the portion of the line with the most intense updrafts can be located by using the multi-panel method to identify the area of strongest low-level reflectivity gradient, displaced low-level echo core, the mid-level echo overhang and WER beneath, and the displaced echo top. These features, when associated with the squall line, are normally along the advancing edge and again indicate a severe storm. In fact, as a segment of the line begins to intensify, the use of the multi-panel or quarter-panel display with appropriate reflectivity slices may signal this with a shift of echo top from over a storm core to along the leading edge of the line as the WER develops. As with other storms in a sheared environment, these same structural features are consistent with a storm producing large hail and sometimes damaging winds (Figure 4-15). With squall lines, however, damaging winds are a substantially greater threat than are the very large hailstones.

Further, when squall lines or Bow Echo events are located near the radar (within about 40 miles), damaging winds may be detectable if the viewing angle is largely parallel to these winds. At longer ranges the “Deep Convergence Zone” (DCZ) (Lemon and Parker 1996) or the Mid Altitude Radial Convergence (MARC) (Schmocker et al. 1996) signatures can be used to infer the presence of damaging surface winds.

4.7.2.2 Considerations. While the SCIT algorithm should readily identify the individual storm cells, incorrect forecast movement by the STI product will occur if a storm begins to change direction in a nonlinear fashion or, occasionally, when reflectivity components are incorrectly assigned by the SCIT algorithm. Thus, with several cells in close proximity to each other in a multicell storm complex, the product may not adequately track storms. When storm cell tracking may not forecast storm movement as a whole; a time lapse of Reflectivity products will often provide a better estimation. Correcting these limitations of the SCIT algorithm is the subject of ongoing research.

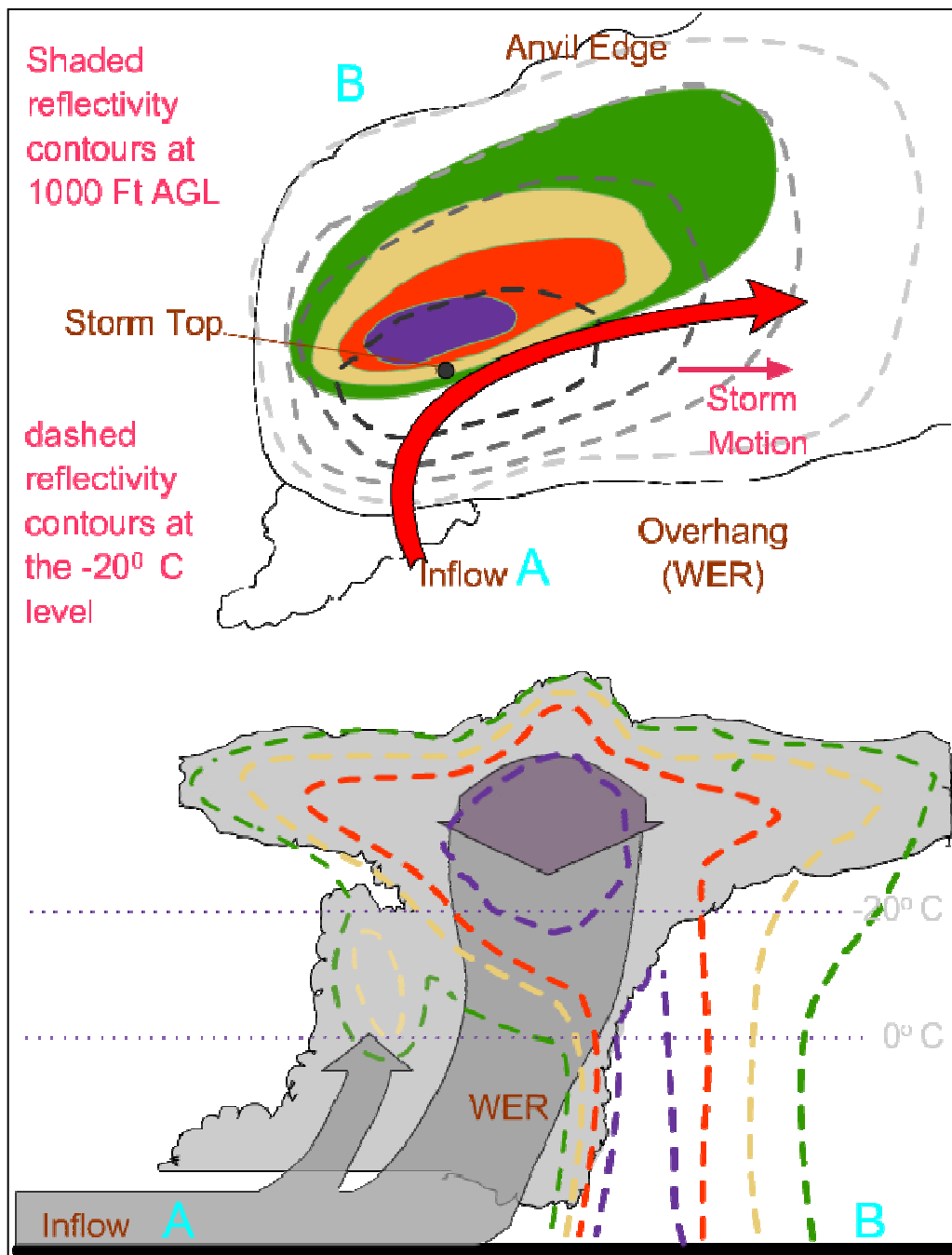


Figure 4-15
Severe Thunderstorm Schematic

As in Figure 4-12 except schematic diagram of a severe thunderstorm in a sheared environment. After Lemon (1980).

“Deviant” storm movement as compared to the mean wind or motion of most other echoes may indicate that the storm has become or is becoming severe. This deviant movement will best be identified using the time lapse capability and specifying a continuous update.

As before, one method of identifying the overall echo structure is to generate a multi-panel display of different elevation angles of Base Reflectivity centered and magnified on the storm (Figure 4-13) or via an “all tilts” product. Reflectivity Cross Sections may also be useful, but as emphasized earlier, placement is critical and several cross sections may need to be generated. This is both time consuming and of questionable value owing to placement uncertainties. Another method to determine storm structure is to build a quarter-screen display with four different elevations of reflectivity, all centered, and magnified at the storm location. Linked cursor readout will then enable the user to visualize the relationship of weak echo regions, overhang, and other structural features of interest. Use of typical RPS Reflectivity products in the multi-panel display is superior to this. In any case, use of the background maps (maps in foreground) with quarter-panel displays and magnification will aid in WER extent recognition.

Vertically Integrated Liquid can be used for convective storm diagnostics. Rapid changes in VIL values may signify the onset of severe activity, but gaps in the VCP elevation angles can induce these changes strictly as an artifact of sampling. For this and other reasons, caution is recommended in its use.

4.7.3 Supercell Storms. Supercell storms occur in unstable, highly sheared environments, very often producing large hail, heavy rainfall, high winds, and sometimes strong or violent tornadoes. Supercell convective storms are defined by the presence and persistence of a distinguishing characteristic, that of the deep mesocyclone (vorticity of $1 \times 10^{-2} \text{ s}^{-1}$ or greater) (Browning 1977). These storms are of great importance due to their disproportional production of damage and nearly all strong or violent tornadoes. There are arguably three types of supercells (Doswell and Burgess 1993): Classic, High Precipitation (HP), and Low Precipitation (LP) Supercell storms. While considerable subjectivity is involved in discrimination of these types and sampling parameters have a strong influence on radar typing, these supercell types will be discussed here. Much of the discrimination as to supercell type deals with the location of the updraft and downdraft, as well as the distribution, intensity, and type of precipitation near and around the primary updraft. This, in turn, is often a function of storm relative winds over the storm depth. For example, the so-called “Classic” supercell typically maintains updraft to the right and rear of the precipitation cascade and downdraft which are positioned on the left storm flank. The so-called HP Supercell typically maintains a larger and more intense precipitation cascade to the rear of the front-flank updraft. In both cases there is the very important “Rear Flank Downdraft” (RFD) across the storm’s rear flank and into the hook echo area. Much of the RFD in the HP case is within the precipitation cascade region, whereas in the Classic case some of the RFD is within the hook echo and behind; more is outside the storm echo as a whole. However, these storms, like the LP supercell, all contain a mesocyclone. It should be noted that there are often attempts to type supercell storms via visual appearance. However, because distributions of large raindrops and hail are easily detected by radar, while visually these same hydrometeors often are not, these attempts

are very often in error and should not be completely relied upon. These three types of supercells are depicted more clearly by radar.

Again, it is stressed that regardless of which supercell type is being discussed, the fact that a storm is a supercell (i.e., it possesses a deep, persistent mesocyclone) is very important and fundamental. As we shall see, this fact has enormous implications concerning the severe weather expected, the typical lifecycle, and magnitude of storm severity.

4.7.3.1 Classic Supercell Storm. The supercell model was first conceived as a persistent, quasi-steady state storm consisting of a single cell that may have a lifetime of several hours while typically propagating continuously to the right of, and more slowly than, the mean winds. Common characteristics of a mature supercell storm are echo ellipticity, an echo diameter of 15 nm or more, a hook echo at times, and the presence of a mesocyclone. With much better observations we now recognize that while these storms are persistent, they often are not quasi-steady and they commonly have some multicellular characteristics.

4.7.3.1.1 Recognition of a Classic Supercell Storm. Development of a supercell storm can be monitored through the use of the 4-panel/multi-panel or all tilts (used in AWIPS) reflectivity display and velocity displays. Supercell development typically begins as a non-severe cell in a multicell cluster storm with the reflectivities initially aligned vertically or even with a down-wind slope. As the updraft strengthens the reflectivity echo core is displaced toward the updraft flank and the adjacent reflectivity gradient strengthens. Sometimes, the reflectivity pattern will begin to elongate, with the strongest gradient on the right and rear storm flank. The development and/or existence of a weak echo region or a bounded weak echo region can be determined from the multi-panel display of different elevation angles of Reflectivity products (Figures 4-17 and 4-18). With sufficient radar resolution and with a storm sufficiently close to the radar, a supercell storm will typically exhibit a bounded weak echo region that will last for an extended period of time, normally until the collapse phase.

The storm top will shift from over the reflectivity echo core region to a position either above the strong low-level reflectivity gradient or the WER/Bounded Weak Echo Region (BWER) as the storm develops those structural features during transition from non-severe to severe (Figures 4-15, 4-16, and 4-17). These characteristics can be seen when comparing the lower elevation slices with the higher elevations on the 4-panel reflectivity display. A four panel/multi-panel display of different elevation angles of Storm Relative Mean Radial Velocity products (SRM or SRR) can provide information on the existence of a mesocyclone. It will also allow the detection and monitoring of the height of the strongest mesocyclonic shear and rotational velocities. Often, that strong shear will first appear aloft and, with time, lower toward the surface. When, and if, that most intense shear is seen to lower near the earth's surface, tornadogenesis may be imminent. Moreover, if the storm is within about 102 km (55 nm), the development of possible TVSs can be monitored by the same multi-panel SRM or SWA velocity products. At other times high shears within the mesocyclone will develop initially in low-levels or within the boundary layer, Trapp et al. (1999).

When the environment is characterized by a linear or unidirectional hodograph with sufficient shear, as the storm evolves further, splitting may occur with intense “mirror image” supercells on the left and right flank. The low-level echo may begin to lengthen in a direction normal to the storm movement as the splitting process begins. In addition, the echo aloft may split into separate convective cores earlier than at the lower levels. Along with the 4-panel/multi-panel product, continuous updates of Reflectivity products in a time lapse will aid in recognizing these trends. The left flank storm typically has the WER/BWER on the forward left storm flank. Note the left-moving supercell in Figure 4-16. This storm was the left-moving portion of a splitting storm and the front flank WER and echo overhang are obvious in the 4-panel product. Left-moving supercells typically move appreciably to the left of the winds in the cloud bearing layer and move more rapidly than those winds. A deep, persistent anticyclonic circulation (“mesoanticyclone”) signature is common with the “left-mover.”

Severe weather with the left-mover is typically large hail (sometimes > 5 cm (2 inches) diameter) and damaging surface winds. Tornadoes are uncommon.

The right-moving counterpart that results from this splitting storm is typically a Classic supercell that moves to the right of the environmental winds and often produces large hail, damaging winds, and sometimes tornadoes. When the environmental hodograph is less unidirectional and veers increasingly with height, the left-splitting storm is suppressed and the right moving storm is favored.

Large values of VIL may be present with a supercell storm. Rapid increases in VIL values may signify the initial stages of severe weather activity; rapid decreases in VIL values may indicate the collapse phase of the storm. However, caution is recommended because gaps in the VCP may artificially create abrupt and large decreases in VIL simply as an artifact of sampling. In addition to the use of VIL, the M and TVS products can also be used along with vertical cross sections (again, when properly placed). Mean Radial Velocity products may be used to determine the flow patterns in and around severe convective storms. However, the SRR, SRM, and SWV may all be used more effectively to monitor the kinematic storm structure and the existence of mesoscale/storm-scale circulations. Storm Relative Motion products, with storm motion removed, make mesocyclone signature identification easier and should be used to ascertain a mesocyclone’s presence and rotational velocity.

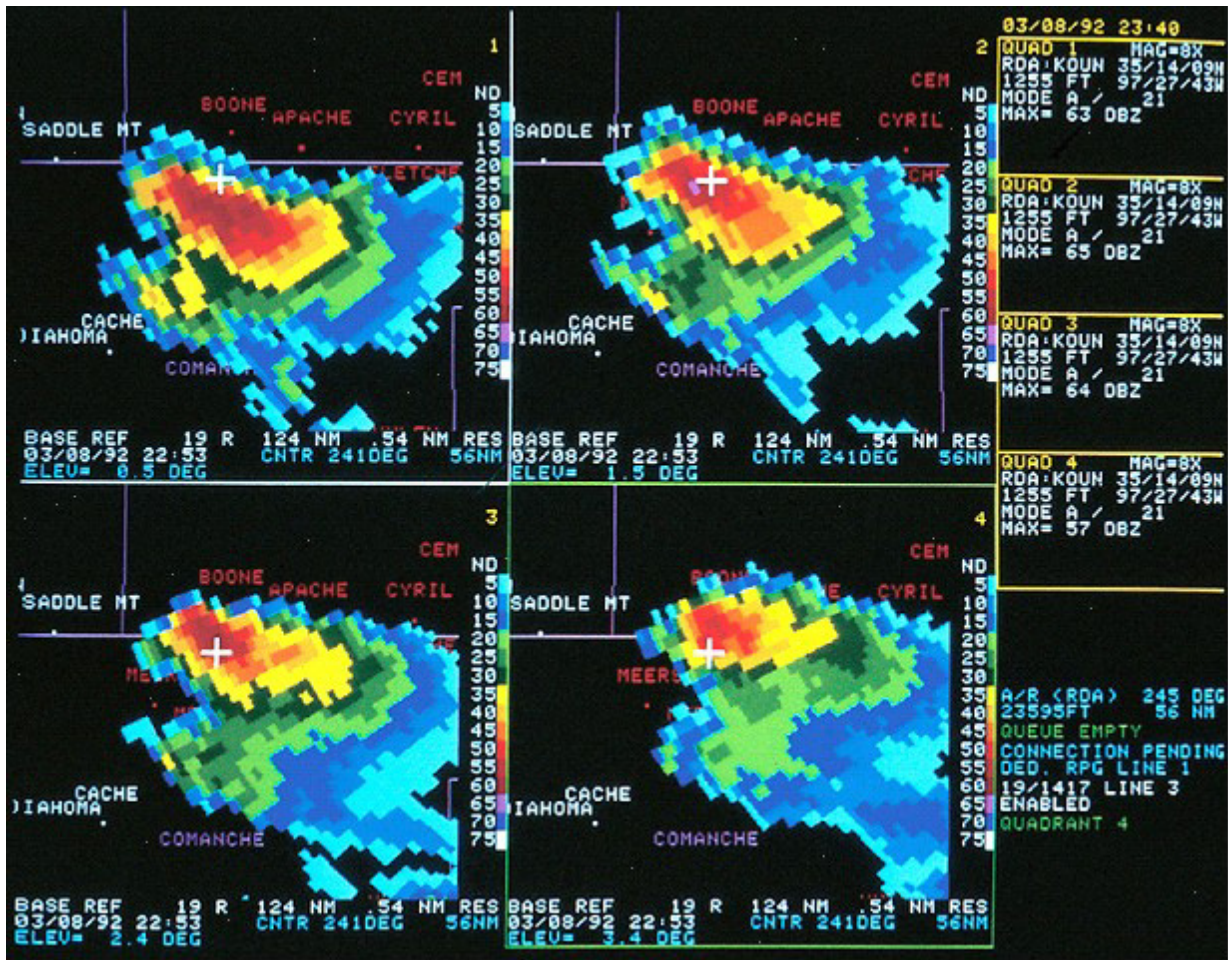


Figure 4-16
Left-Moving Severe Thunderstorm Reflectivity

Norman, OK WSR-88D (test bed radar) 4-panel display of Reflectivity products at 22:53 UTC on 8 March 1992 (PUP display). This display shows a left-moving supercell thunderstorm that developed from a storm split. The front flank Weak Echo Region and echo overhang is revealed by noting the position of the geographically fixed cursor location and the storm core as seen in this four elevation angle sampling of the storm. Storm motion was 200° at 24.7 ms^{-1} (48 kts), which is over 10° to the left and over 9.3 ms^{-1} (18 kts) faster than the mean environmental wind.

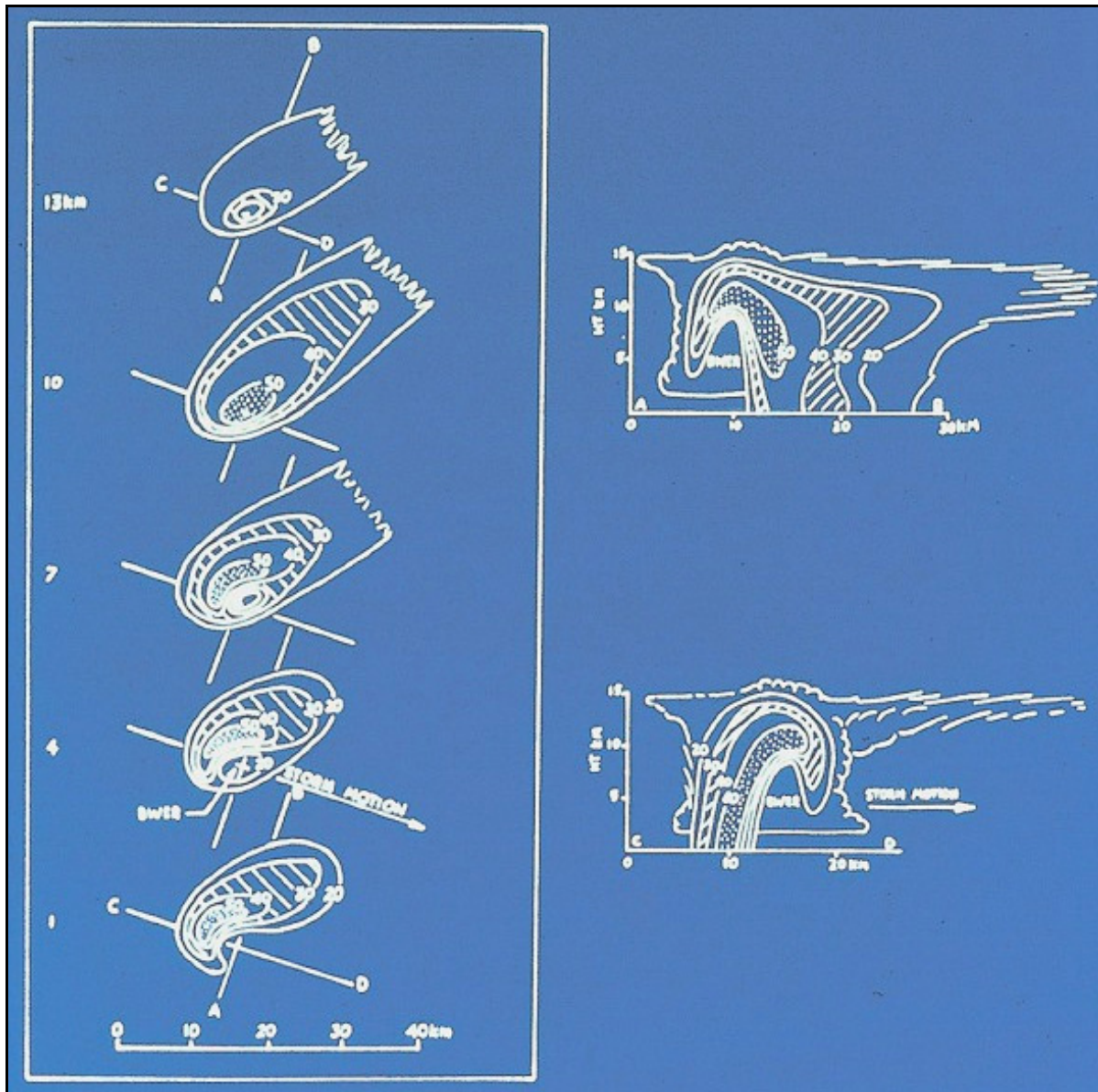


Figure 4-17
Classic Supercell Thunderstorm Schematic

Schematic of a classic supercell storm with vertical cross sections along and at right angles to storm motion. This cross section schematic shows a BWER as well as the WER, echo overhang, and low-level hook echo. Note that while there is essentially no tilt in this schematic, not uncommonly there is some storm tilt. From Chisholm and Rinick (1972).

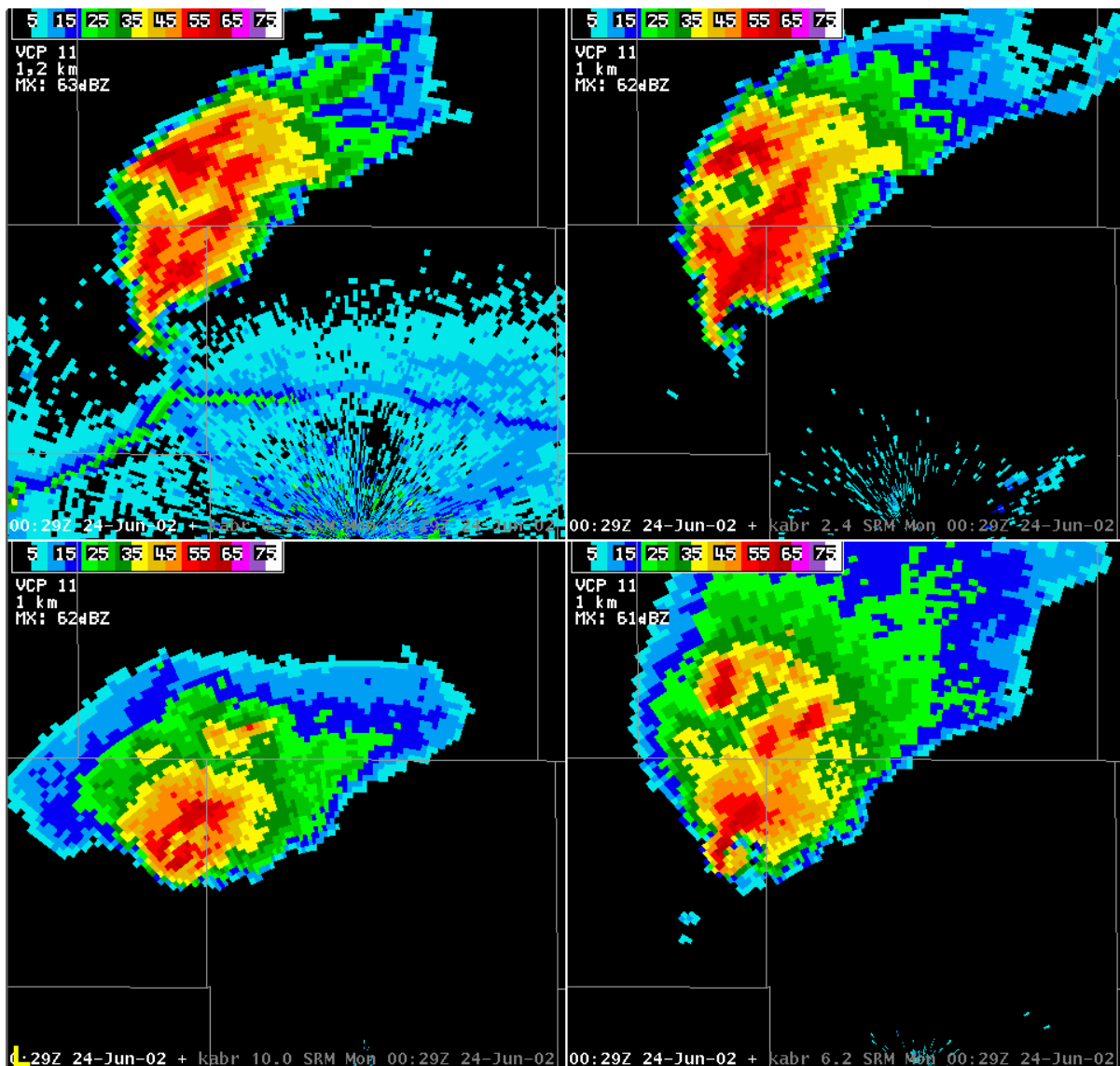


Figure 4-18
Supercell Thunderstorm Reflectivity

Aberdeen, SD WSR-88D 4-panel display of Reflectivity products at 00:29 UTC on 24 June 2004 (AWIPS display). This display of a supercell storm has reflectivity slices at 0.5° in the upper left, 2.4° in the upper right, 6.2° in the lower right, and 10° in the lower left. Note the boundary across the lower portion of the upper left panel and the storm gust front trailing from the storm hook echo intersecting. The low-level hook echo partially surrounds, with height, a BWER.

4.7.3.1.2 Considerations. With a single Doppler radar providing velocity data, only a portion of the flow in and around the storm will be seen. Moreover, velocity data can be sampled only where and when sufficient tracers are available. Note, as well, that while the M and MDA algorithms and associated products can be used with some success for mesocyclone and supercell identification, these algorithms will not identify the mesoanticyclones of left-moving supercells.

The storm reflectivity and velocity structure must be monitored continuously. This is done most effectively through the use of the multi-panel reflectivity and velocity products during all successive volume scans (Figures 4-16 and 4-19). Typically, supercells will have one major storm top (often among other lesser tops) which will persist for a long period of time. Normally, the SCIT algorithm will adequately identify and track the storm and provide storm structure information. However, the forecast movement by the Storm Tracking algorithm will lag motion changes. Very pronounced veering to the right will sometimes occur during supercell development. Sometimes pronounced left deviation will occur during weakening.

4.7.3.2 High Precipitation Supercell. High Precipitation (HP) supercells produce a variety of severe weather, including very large hail and occasional tornadoes, but they also sometimes produce flash flooding (Moller et al. 1990). An HP supercell, like many Classics, may exhibit some characteristics of both a multicell cluster and a supercell storm. As mentioned earlier, the HP supercell typically is characterized by a front-flank updraft and mesocyclone, as well as heavy precipitation to the rear and partially surrounding the storm's primary updraft (Figures 4-19 and 4-20). However, at times a Classic supercell can transition into an HP as the mesocyclone (and a tornado, if present) becomes embedded in heavy rain. Thus, for a short period, HP structure may result when a Classic supercell undergoes the collapse phase. In addition, HPs are often characterized by a highly reflective and broad hook echo when the hook is present. Visual observations indicate that heavy precipitation exists in areas where the classic supercell is typically rain-free or includes only limited precipitation. These characteristics sometimes make HP supercells more difficult to recognize.

4.7.3.2.1 Recognition of a High Precipitation Supercell Storm. The radar reflectivity pattern of an HP supercell will often indicate a broad, highly reflective (over 50 dBZe) pendant or hook echo. Because HP supercells often have a front flank updraft, the WER and BWER are generally located on the front flank. In these cases, the high precipitation supercell has a front flank mesocyclone, in contrast to the right rear flank mesocyclone typically observed with classic supercells. Occasionally, there may also be a central heavy precipitation region with very strong or damaging outflow behind a bowing gust front. This region often has sharp lateral edges to the damaging outflow and is typically to the right of the mesocyclone center. It is not uncommon for these storms to produce very large hail and very damaging surface winds. Occasionally, these storms are extremely severe or "high-end" events (Miller and Johns 2000; Miller et al. 2002).

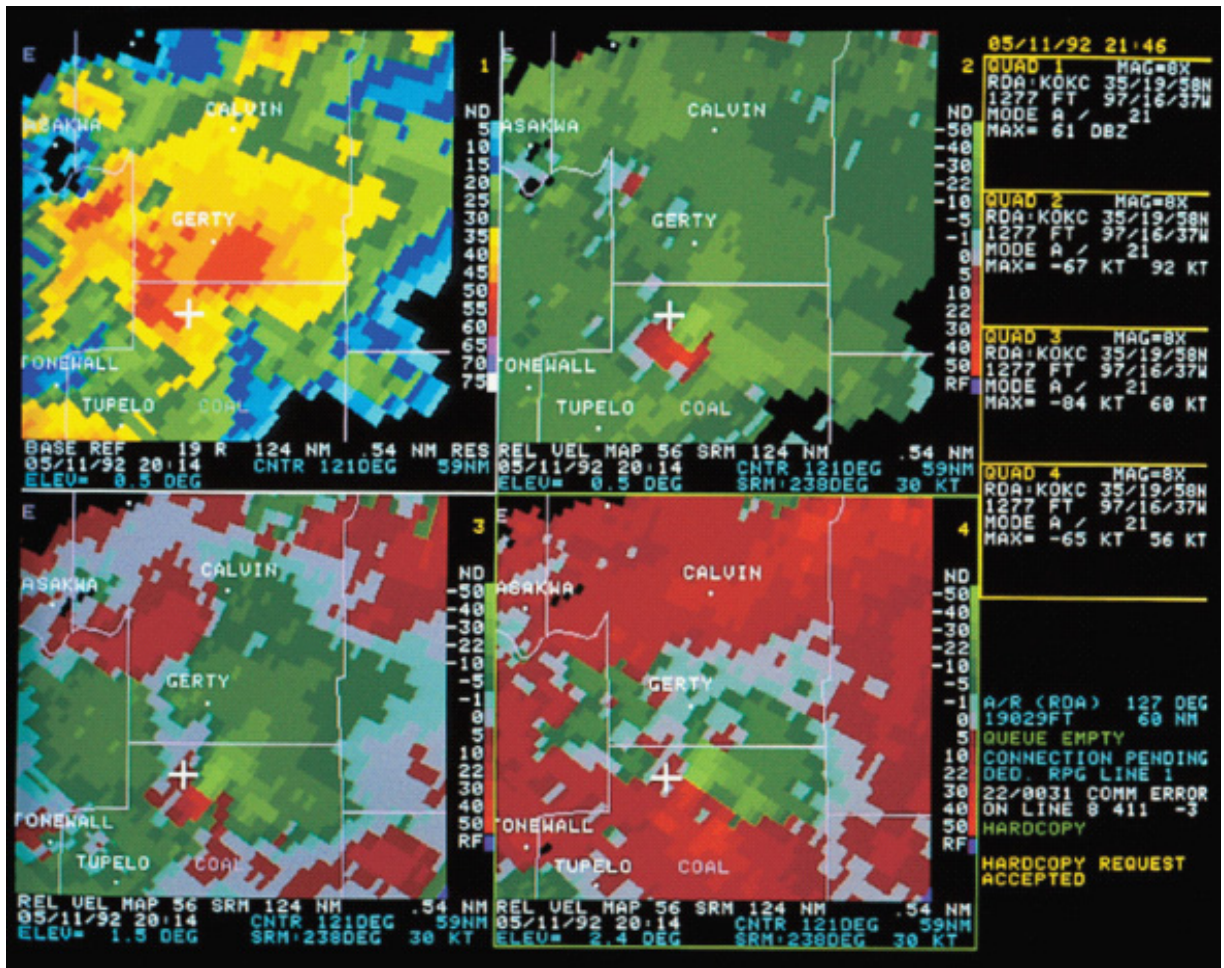


Figure 4-19
High Precipitation Supercell Thunderstorm

Oklahoma City, OK WSR-88D 4-panel display of products of a HP Supercell storm at 20:14 UTC on 11 May 1992 (legacy PUP display). The upper left display is 0.5° Base Reflectivity, the upper right is a 0.5° SRM, the lower left is a 1.5° SRM, and the lower right is a 2.4° SRM. The mesocyclone velocity couplet is near the white cross (109 km (59 nm) from the radar) with inbound velocities being green and outbound velocities being red.

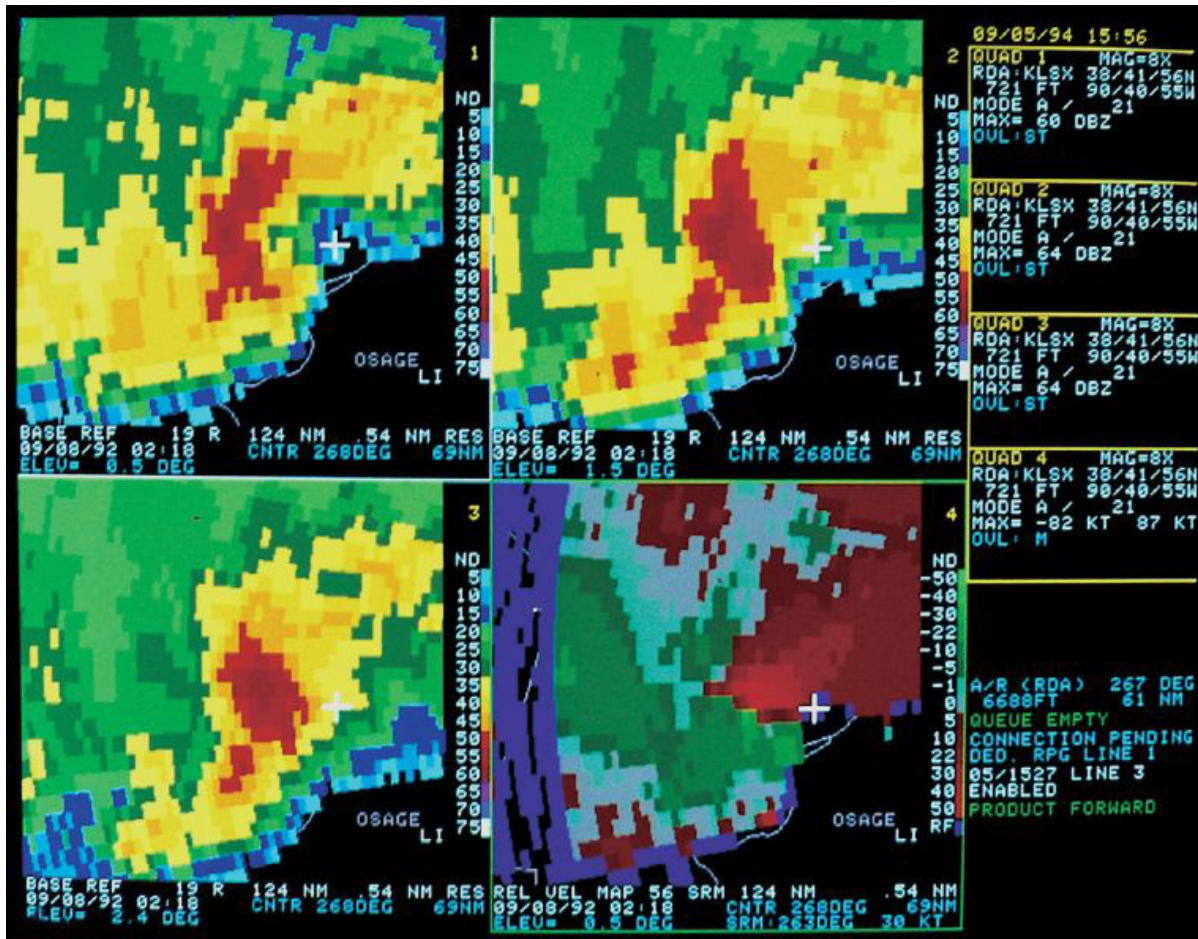


Figure 4-20
Reflectivity and Mean Radial Velocity Display of a High Precipitation Supercell

St Louis, MO WSR-88D 3-panel Reflectivity products and a single quarter-screen SRM product of a HP Supercell storm (legacy PUP display) at 02:18 UTC on 8 September 1992. Note the front flank notch (upper left) and the mesocyclone in the lower right SRM product. The mesocyclone and TVS velocity signatures (right panel) are embedded within moderate to heavy rain as indicated by the surrounding (red) reflectivity echo.

A low-level Reflectivity product will reveal the inflow notch on the side of the mesocyclone characterized by inflow and updraft. Again, with the HP, this is typically on the storm's front flank. The weak echo region, storm overhang, and highest storm top are typically on the leading edge of the storm. This is best monitored via the multi-panel Reflectivity and Velocity (V, SRR, SRM, and SWV) displays.

The existence of a mesocyclone may be apparent in an SRM or SRR product, a Mean Radial Velocity product, or, to a limited extent, the VCS product oriented perpendicular to a radial through the storm. As always, placement of the vertical cross section is critical and the meanings of the velocities are much more difficult to determine when not radially aligned. Heavy rainfall is easily identified with the OHP product. In fact, especially with HP supercells, the precipitation accumulation products OHP, THP, STP/DSP, and the User-Selectable Rainfall Accumulation Precipitation (USP) are of critical importance. When applying the WSR-88D, the user must be careful not to neglect certain potential threats (e.g., flooding) when dealing with others (e.g., tornadoes, wind, and hail). If an event is not anticipated, when it occurs it is often not recognized in a timely manner (Quoetone and Huckabee, 1995).

Significant changes in a high precipitation supercell, such as rapid transition to a bow echo with a rotating comma head, or movement of a mesocyclone to the northeast within the echo mass, can be monitored through the use of Reflectivity, and Velocity product time lapses. Climatologically high VIL values, large accumulations of rainfall, and high values of reflectivity are likely with High Precipitation supercells. Time lapse sequences of VIL, precipitation accumulation, and Reflectivity products should be extremely useful in monitoring storm evolution and in anticipating a transition from an HP into a Bow Echo.

4.7.3.2.2 Considerations. Due to the amount of precipitation, front flank mesocyclones, and broad embedded hook echo structures of high precipitation supercells, they are sometimes difficult to identify on radar. At other times, these structures are prominent making the HP more easily identified. Moreover, the SCIT algorithm may be unable to adequately track an HP supercell when the storm is embedded within considerable surrounding strong convection such as within a Mesoscale Convective System (MCS). At times, storm components may be interchanged between adjacent echoes. This can create abrupt changes in tracking forecasts and can impact the output of other algorithms such as the hail algorithms. This underscores the importance of doing base data analysis with decreased reliance on algorithm output. The time lapse capability of base data can be useful in monitoring a storm's evolution and changes in motion. But the multi-panel displays of base data are critical in monitoring storm structural changes and storm intensity/severity changes via the three-dimensional echo structure.

Microbursts are common with Classic and HP supercell storms, especially in the vicinity of the hook echo, mesocyclone, RFD, and front flank notch. In fact, the RFD actually promotes them. However, because the most intense and damaging outflow from microbursts commonly occur within about 300 meters of the ground, they are very difficult to detect via radar. Moreover, they are usually not axis-symmetric, thus they may be even more difficult to detect depending on the

viewing angle. Base velocity data with high resolutions are preferred, as is use of VCP 12, which includes increased and overlapping low-level sampling over previous VCPs.

4.7.3.3 Low Precipitation Supercell Storm. Low precipitation supercell storms are rather rare, and to the limits of our knowledge, virtually unique to dryline environments within the Great Plains and High Plains east of the Rocky Mountains. While appearing benign in reflectivity fields and even in velocity fields at times, low precipitation supercells frequently produce large hail, but rarely wind damage, because of the lack of a significant downdraft. While damaging tornadoes can be produced, they are rare with the LP supercell (Doswell and Burgess 1993) (Figure 4-22).

4.7.3.3.1 Recognition of Low Precipitation Supercell Storms. Radar reflectivity of 50 dBZ_e or less is common with low precipitation supercells. Occasional higher reflectivity caused by hail at mid-levels of the storm may be detected at higher elevation angles of Reflectivity products. Storm Tracking Information products typically function well with LP storms because they tend to be more isolated than HPs, for example. In addition, the Hail Detection Algorithm (HDA) may provide data that will allow some assessment of the hail potential.

Due to the sparsity of rainfall, low precipitation supercells rarely contain a pendant or hook echo, especially when the storm is beyond close radar ranges (Figure 4-22). The mid-level mesocyclone can often be identified as with other supercell storms through use of multi-panel displays of V or SRM, SRR, or a series of 4-panel Severe Weather Analysis (SWA) products. With these products the user can inspect the displays for symmetry, depth, and rotational velocities as a function of range from the radar. But with less precipitation sometimes detection of the mesocyclone and other structural details are more difficult. Further, mesocyclone detection may be confined to storm mid-levels. Moreover, since LP storms typically exhibit few, if any, distinctive reflectivity features and, since detection of the classic echo features is so range- and resolution-dependent, these storms are often difficult to identify, especially without adequate velocity field examination.

As always, Velocity products may be used to determine the flow patterns in and around LP supercell storms. However, SRM products, with the correct storm motion removed, make mesocyclone signature identification easier for the user and should be used to determine mesocyclone shear and rotational velocity. But, because shear is invariant to storm motion, algorithm detection does not depend on storm motion removal.

4.7.3.3.2 Considerations. Reflectivity structures of low precipitation supercells may be much more difficult to resolve because of the scarcity of precipitation and their typically small storm size. In addition, the lack of significant reflectivity may cause a low precipitation supercell to be overlooked, or its strength underestimated for most radar distances.

Significant hail formation within a low precipitation supercell can adversely affect the Precipitation Processing algorithms. These storms will frequently produce 0.2 inches or less of rain at locations along their paths. But with hail, radar estimates of precipitation will often be somewhat greater.

4.7.3.3.3 Mini-Supercells. During the past decade, supercellular convection has been observed to take place on much smaller scales than the larger counterparts just discussed (Figure 4-21). So called “mini-supercell” storms are typically much smaller in all dimensions. These miniature supercells have been discussed by McCaul (1987); Burgess et al. (1995); Grant and Prentice (1996); and others. While these storms appear to be small, they still can, and do, produce significant and sometimes substantial severe weather, including tornadoes. Indications are that in mid-latitudes, the environment for at least some of these storms appears to be marginal Conditional Available Potential Energy (CAPE) but strong shear. In other cases, the CAPE and steep lapse rates are confined to a limited, but lower-level depth, of the atmosphere. (This is also the case with “low-topped” supercells which are very similar to the mini-supercell, except that other dimensions are somewhat larger.) Moreover, it appears that most of the storms producing tornadoes associated with land-falling tropical storms are of the mini-supercell variety (Figure 4-47). In these cases much of the environmental shear is confined to the lowest few thousand feet above ground.

However, because of the small dimensions, low-tops, and small mesocyclones, these storms can only be resolved when relatively near the radar. The 4-panel Reflectivity and Velocity products are still appropriate, but high resolution products are advised. It will also be appropriate to use VCP 12, with its concentration of sampling via overlapping beams in lower levels.

4.7.4 Severe Thunderstorm Identification. Of great importance are the characteristics of a thunderstorm radar echo that indicate the storm is severe. Of equal importance are those characteristics that indicate a transition from a non-severe to a severe thunderstorm. Analysis of the three-dimensional structure of a thunderstorm cell provides fundamental insight into the severity of a storm. For example, the presence of a WER or BWER and strong storm top divergence are important indicators of an intense updraft and storm severity. When mid-level reflectivity is strong, the storm WER is large, and the storm echo top is over the WER, the likelihood of at least a severe hailstorm is virtually certain (Lemon 1980; Lemon and Doswell 1979; Burgess and Lemon 1990; Moller 2001). The presence of a BWER enhances the probability of a thunderstorm producing a tornado. It is these and other features we will address here.

4.7.4.1 Storm Structure. We have been, and will be, speaking of the “updraft flank” or “storm inflow flank.” The updraft storm flank in the northern hemisphere is often to the right or right rear relative to storm motion. However, relative to squall lines, the updraft storm flank is normally along the advancing or leading edge (forward flank) of the line. In reality, the flank of the storm where the updraft is located is unimportant; it can be any flank. But the echo characteristics we address below are independent of storm flank and, to a great extent, storm type, as well. It is not the storm flank that is important, rather the characteristics of the updraft positioned there.

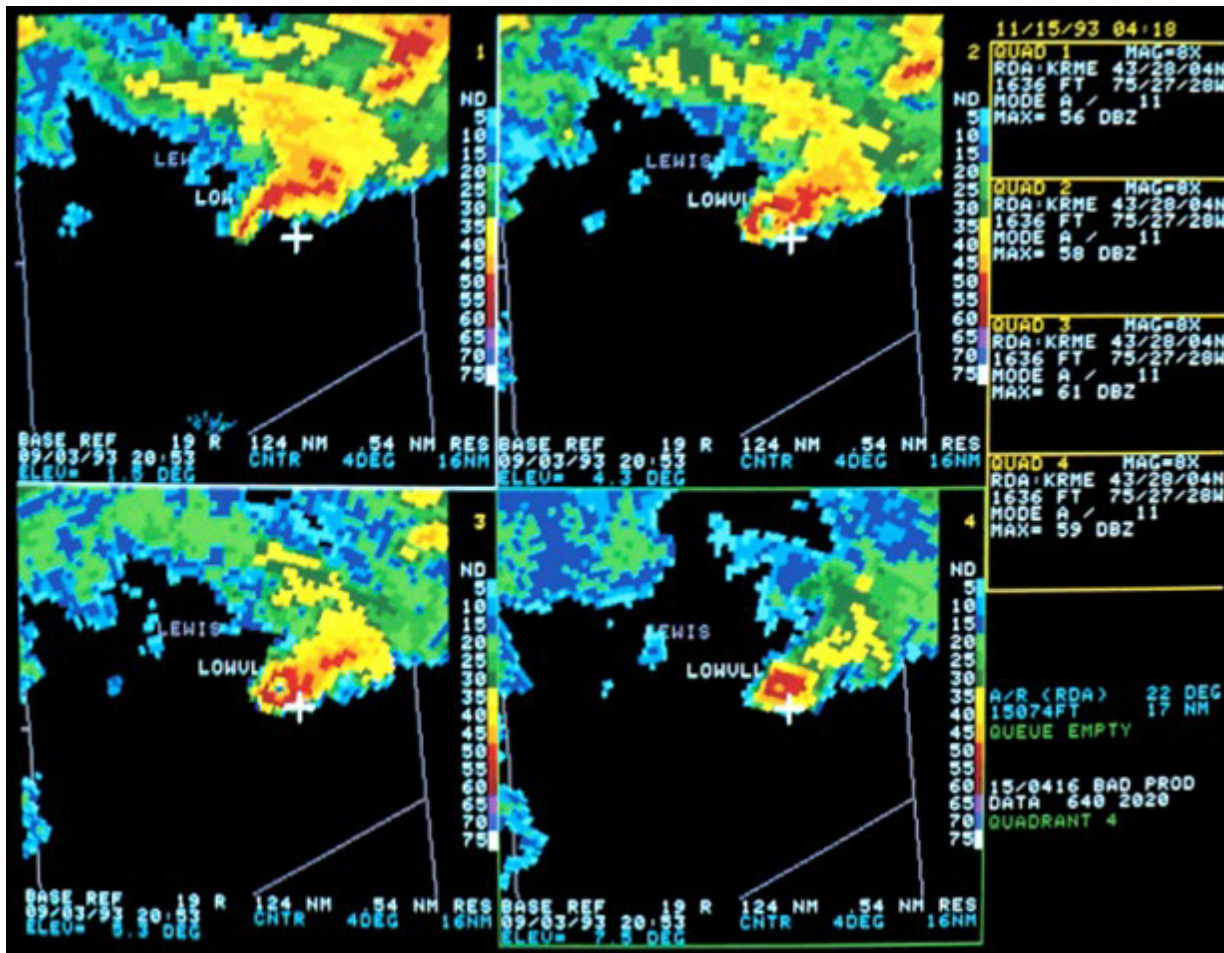


Figure 4-21
Mini-Supercell Thunderstorm Reflectivity

Fort Drum, NY WSR-88D 4-panel Reflectivity product display at 20:53 UTC on 3 September 1993 (PUP display). A mini-supercell storm (near the white cross) is 16 nm from the radar. These Reflectivity products are slices with the following elevation angles: 1.5° upper left, 4.3° upper right, 5.3° lower left, and 7.5° lower right. The low-level pendent echo partially surrounds a BWER with increasing height in this very small and shallow storm.

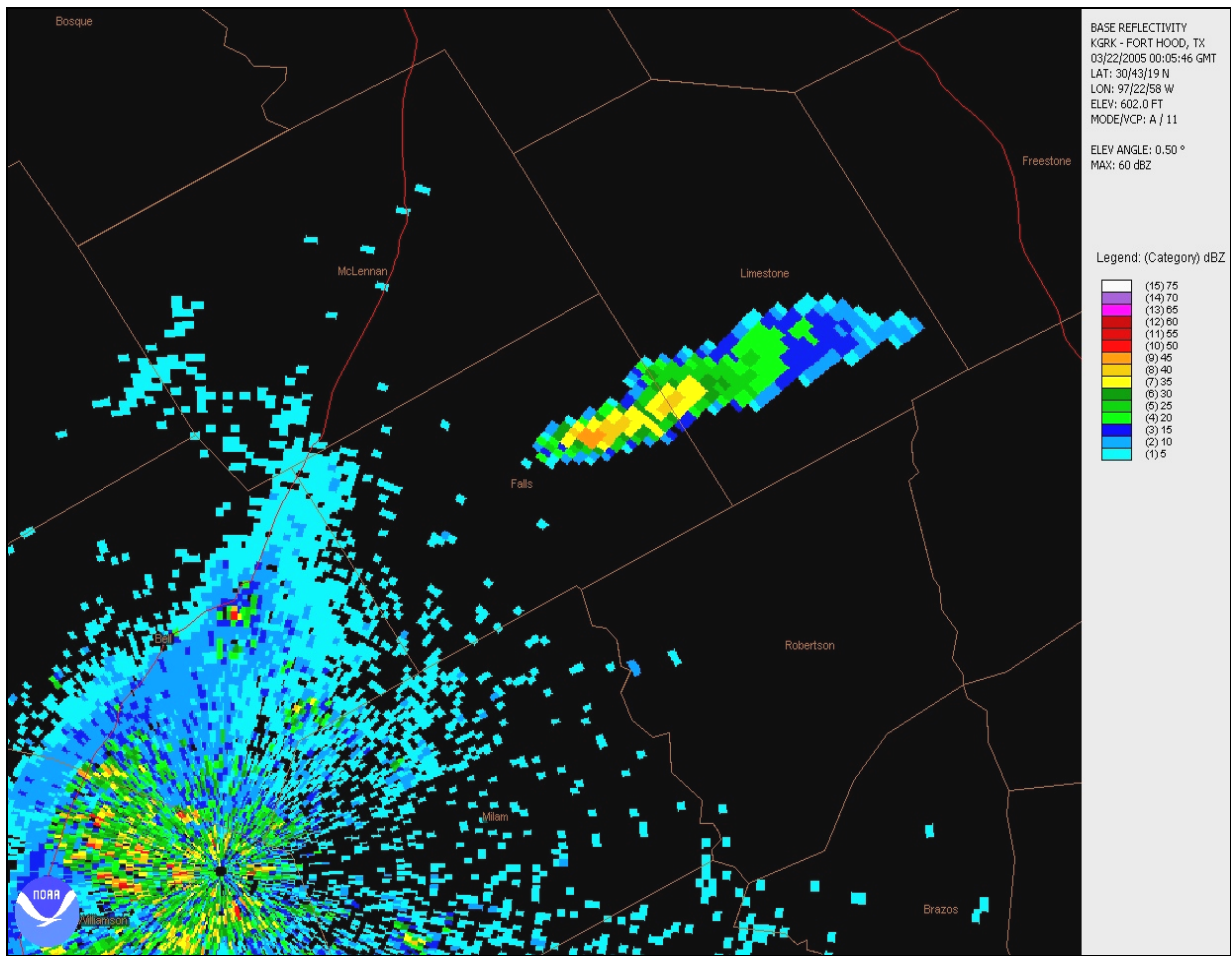


Figure 4-22
Low Precipitation Supercell Thunderstorm Reflectivity

Fort Hood, TX WSR-88D Reflectivity product at 00:05 UTC on 22 March 2005 (NCDC graphics). This LP Supercell storm located in Falls and Limestone counties of central Texas produced a weak tornado and hail.

Storm severity is most often a function of updraft strength. The stronger and more intense the updraft, the more severe the storm is (Burgess and Lemon 1990). Thus, radar is used to diagnose updraft trends or strength. In a “pulse” severe storm or multicell storm environment, an indication that there is a transition to severe activity is the appearance of a cell with its first echo at a higher level than the earlier cells owing to an invigorated updraft. Viewing higher elevation angles of a Reflectivity product, especially by using the multi-panel display, can aid in determining this. However, this is often very difficult to recognize in real-time.

There are other more obvious and more significant changes that take place in a radar echo within an environment of deep layer shear and moderate to strong instability that signal the onset of a strengthening updraft and a severe storm (Lemon and Doswell 1979; Lemon 1980; Browning 1977; Burgess and Lemon 1990). We have previously covered a portion of this material in Section 4.7.3 but it is reviewed and summarized here because of its importance.

What are these changes or echo characteristics of a strengthening updraft in a sheared environment? First, as illustrated in Figures 4-15 and 4-18, in the low-level echo, a tightening reflectivity gradient will occur on the storm inflow and updraft flank. At times, this storm flank will also develop a concavity open to low-level inflow in association with the strong reflectivity gradient. A second related change is that the dominant low-level reflectivity echo core is typically displaced toward this storm flank.

With increasing storm summit divergence and rapid expansion of echo aloft, a mid-level echo overhang develops and extends over and beyond the strong low-level reflectivity gradient, producing a WER. The overhang and WER can be identified by comparing several elevation angles of Reflectivity in the multi-panel display, or with an RCS that is well-placed. However, the first choice is the 4-panel or multi-panel display as explained previously. At the same time the storm VIL will be increasing, reflectivity at all levels will be strengthening, and hail algorithm probabilities (Probability of Hail (POH), Probability of Severe Hail (POSH), and Maximum Expected Hail Size (MEHS)) will be increasing. Depending on the VCP and other scanning characteristics, the storm echo top may be characterized as increasing.

Within the developing echo overhang associated with the WER is development of a strong mid- and upper-level reflectivity echo core, again located above the tight low-level reflectivity gradient. As updrafts have become stronger, the echo top shifts over the tight low-level reflectivity gradient or above the WER on the updraft storm flank. Note that it is not the height of the echo top that is important, it is the location of the top relative to the low-level echo. A multi-panel velocity product during this early phase of supercell development may begin to show a mid-level (often cyclonic) shear signature, but it is not of sufficient strength as of yet to indicate a mesocyclone.

Storms growing within an environment of deep layer shear and moderate to strong instability that develop this structure are severe storms. The dominant severe weather phenomena these storms produce are large hail (> 1.9 cm ($\frac{3}{4}$ inch hail)) and significantly less often damaging surface winds (> 25.7 ms⁻¹ (50 kts)).

4.7.4.1.2 Recognition of Severe Storm Structural Features. As emphasized within this document the most useful technique in analyzing the structure of a storm is the generation of multi-panel Reflectivity and Velocity products (V, SRR, and SRM) with progressively higher elevation angles and magnification on the storm in question (e.g., Figures 4-18, 4-19, 4-29). This can often reveal the WER and echo overhang resulting from intense storm summit divergence. At times, if generated correctly, an RCS product will also show a strong midlevel reflectivity field and its overhang position creating the WER below, again indicating the presence of intense divergence from a strong updraft. Evidence of intense upper level storm summit divergence (an indication of updraft strength) can often be found through the use of a higher elevation scan of the SRR, SRM, or V products and, occasionally, through careful placement of a VCS product. (The overhang must extend horizontally for few miles to be significant.) This region beneath the overhang, the WER, should be easily identified.

The development of a conically shaped BWER extending vertically upward into the echo overhang base typically indicates an intense updraft (Figures 4-18, 4-21, and 4-23). This feature may develop in response to intensifying updraft or due to improved radar resolution, or both, because of decreasing range to the storm. In a mid-level Reflectivity product, a BWER will appear as a hole, a circular or elliptical region of low reflectivity values enclosed by higher values. At times, the BWER will be elongated and curved with the long axis parallel to the low-level gust front where the intense lifting may originate. While the BWER should be evident in an RCS product if properly placed, its presence and development is again best detected in a multi-panel Reflectivity product with magnification (Figure 4-18). Evidence of associated mesocyclone development may be found in a companion multi-panel velocity (V, SRR, and SRM) product, again with magnification (Figure 4-19). Most often, the mesocyclone makes its initial appearance in mid-levels near or within the area of the BWER.

In addition, use of the multi-panel displays can also be used effectively to determine if the storm top location is very near or over the WER, BWER, or the strong low-level reflectivity gradient.

Within the supercell life cycle, the collapse phase is critical. It often is most easily recognized in reflectivity structural features and is critical for severe weather occurrence at the ground, (Brown et al. 1973; Lemon and Doswell 1979; Burgess et al. 1982; Burgess and Lemon 1990). The wrap-up and disappearance of the hook echo, collapse or diminishment of the classical reflectivity features of BWER, WER, storm top descent, and a rapid decrease in the VIL values will often signify the decrease in surface hail size, but will also signal the onset of surface wind damage (and microbursts) and tornadoes. It is during this same time period that tornadogenesis is often typified in the velocity data by the descent and surface arrival or low-level intensification of the mesocyclone shear, rotational velocity, along with circulation diameter decrease. The development of the low-level TVS (Figure 4-29, Figure 4-31, and Section 4.7.4.4), when within radar range (< 102 km (55 nm)), is often detected at this time. Because of the importance of this storm phase the user must carefully monitor reflectivity and velocity displays. However, detection of these features near the earth's surface is heavily dependent on the radar range to the storm and related radar horizon.

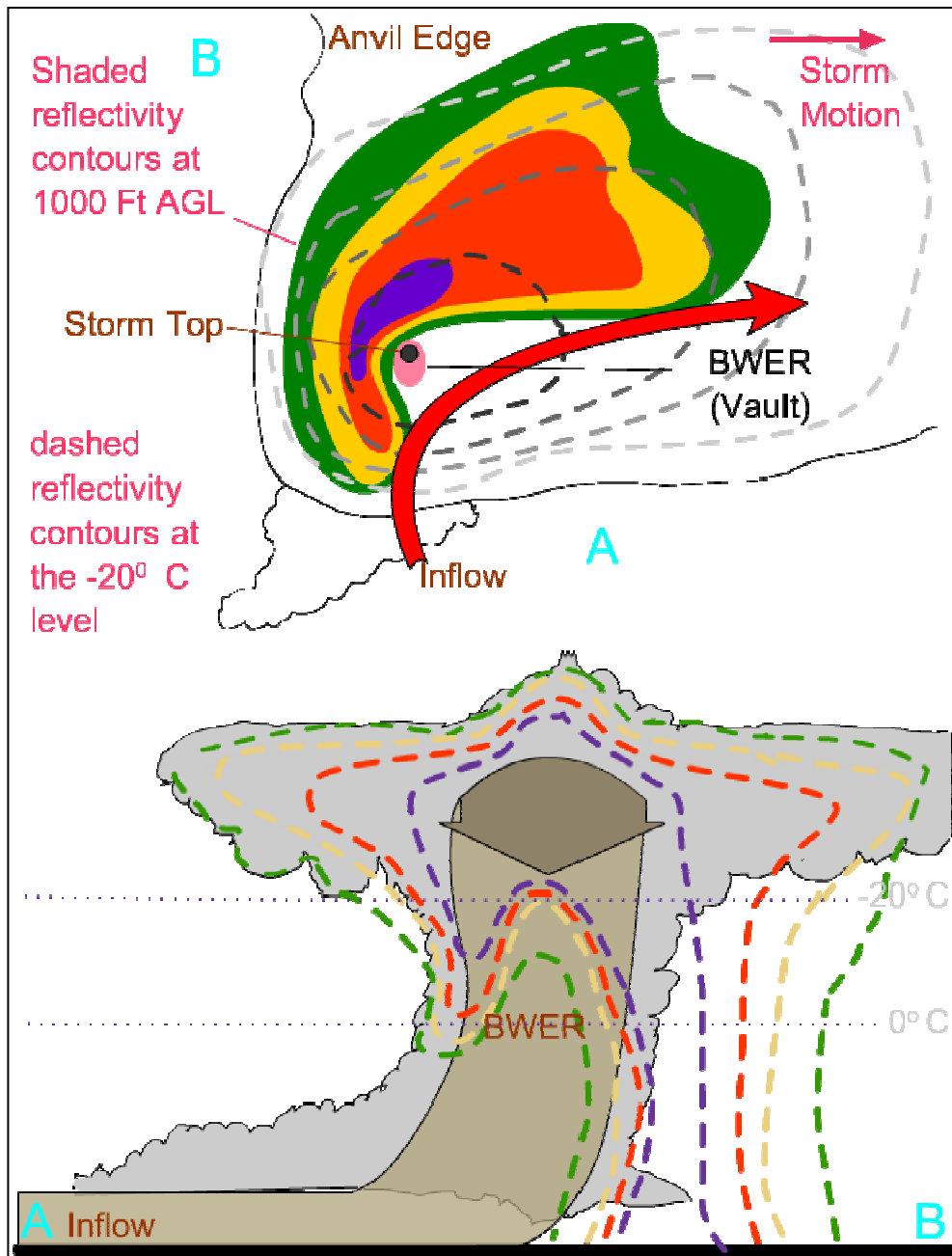


Figure 4-23
Mature Severe Thunderstorm Schematic

Same as Figures 4-12 and 4-15 except for a mature Classic supercell storm. Note the position of the BWER and storm top as is typical of these storms in the mature development phase. After Lemon (1980).

For a more detailed look at severe storm and supercell morphology and structure the reader is directed to Lemon and Doswell (1979); Lemon (1980); Burgess and Lemon (1990); Doswell and Burgess (1993); and several chapters within Doswell (2001).

4.7.4.1.3 Considerations. Alphanumeric data from the Storm Structure algorithm and the associated “trends” displays of some WSR-88D display systems can provide information on the structure and evolution of a storm. However, reflectivity and velocity product 4-panel displays may be more useful in determining the three-dimensional structure of a severe storm.

Understanding the characteristics and model of a storm class is invaluable in determining its potential surface severity and lifecycle stage. Monitoring the history of storm tops (development, location, and collapse), the intensity, and altitude of the maximum reflectivity, and other such parameters, can provide insight into where a thunderstorm is in its life cycle and the surface severe weather production. These insights may be gained through monitoring of the storm velocity and reflectivity structure. As before, multi-panel base product display is preferred for mid- and upper-levels, as well as the lowest elevation angles in order to monitor storm structure and mesocyclone development and strength. Vertically Integrated Liquid, ET, and high-level LRM may also be used to monitor storm significance. Time-lapse loops of 6 to 10 frames are often most useful.

Additionally, the user must be careful to discern a real weakening and diminishment of the supercell storm from the collapse phase. This can be done by coupling the velocity information with the reflectivity field information. Unless the WSR-88D user is careful, noting the diminishing reflectivity structure can lead the warning meteorologist to conclude that the storm is no longer dangerous when, in fact, the storm is entering its most dangerous and deadly phase.

4.7.4.2 Echo Shape, Severe Weather, and Damaging Winds. During the early years of radar development and its application to severe weather detection, echo shape was the radar practitioner’s “first line of defense.” The shape of a radar echo was viewed as an indicator to thunderstorm severity. We have since recognized that many of these shapes were highly subjective, did not rely on our physical understanding of storms, and often had a rather high false alarm rate. However, to some extent, we still do rely on echo shape as a clue to severe weather potential.

For example, hook echoes have long been associated with tornadoes and are often indicative of supercell storms, although tornadoes do not always accompany them (Figures 4-18 and 4-24). Also, a tornado may be well developed without a radar hook being present. Hook echo detection and recognition is also a function of radar range and resolution. Beyond about 60 km (100 miles) true hook echo detection is rare. Moreover, during tornadogenesis and during an increase in tornado strength the hook echo will often disappear as the other echo structural features weaken and vanish as the collapse phase of the storm proceeds. Thus, a hook echo alone has been found to be of questionable value. However, actual supercell hook (or pendant) echoes must be, or have been associated with, a WER or BWER. Thus, the overall storm structure is important in verifying such reflectivity features. Moreover, the detection of an associated mesocyclone is even better confirmation.

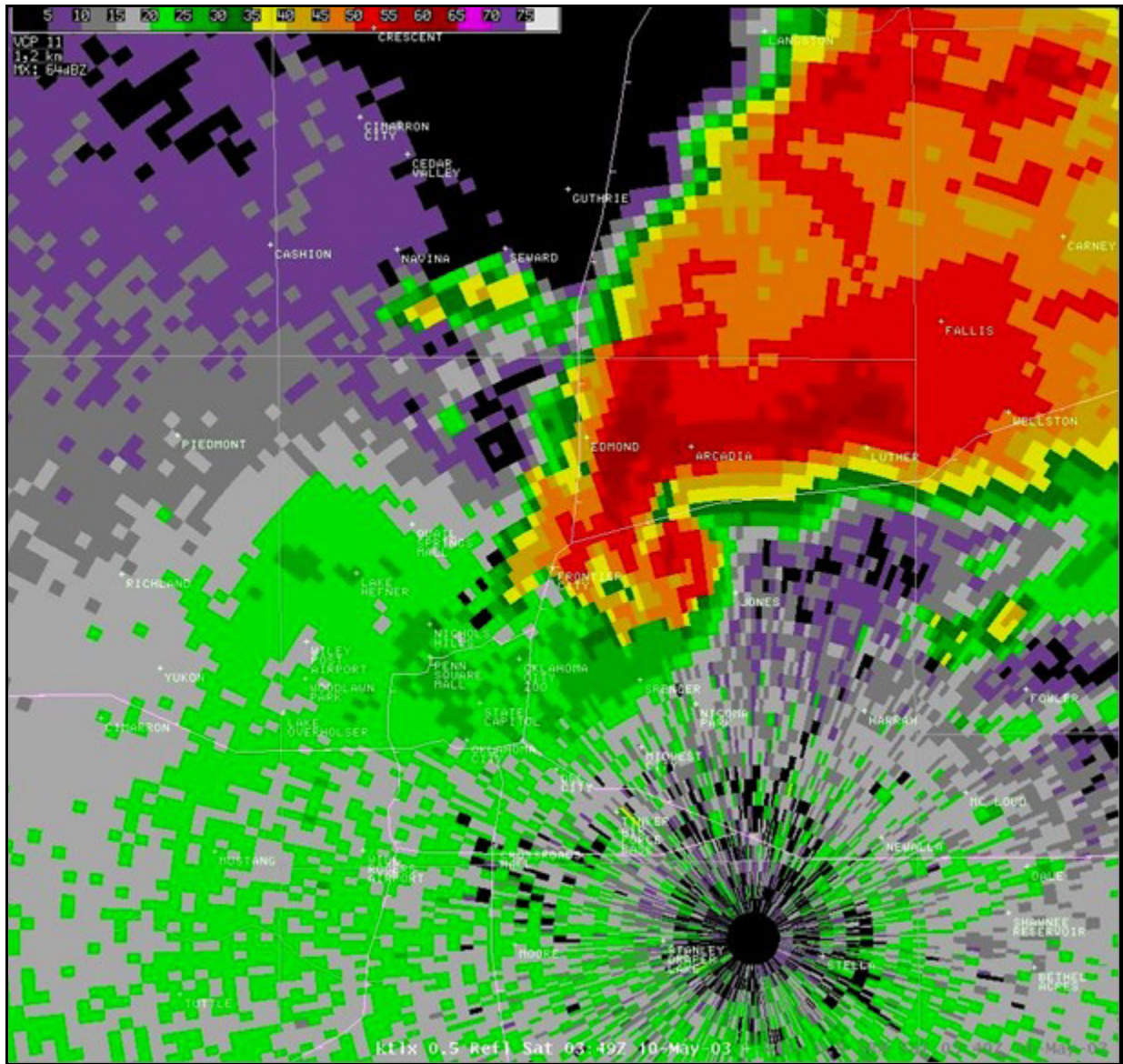


Figure 4-24
Tornadic Supercell Thunderstorm Reflectivity

Oklahoma City, OK WSR-88D Reflectivity product at 03:49 UTC on 10 May 2003 (AWIPS display). A supercell with a hook echo is north of the radar. A strong tornado was occurring within the hooked or curl-shaped echo appendage on the southwest portion of the storm located north-northwest of the radar.

Echo shape has especially been useful as severity indicators of thunderstorm lines. For example, a thunderstorm Line Echo Wave Pattern (LEWP) may develop, then a portion will take on a bow echo shape. These bow echoes will occasionally develop a “rotating comma head.” Like the LEWP, the bow echo is often accompanied by severe weather at the surface such as damaging, low-level diverging winds with macrobursts or microbursts. The rotating comma head is often indicative of a mesocyclone and, at times, may be accompanied by tornado development. Przybylinski and Gery (1983) reported that “distinctive” bow echoes are convex in shape, with a strong, low-level reflectivity gradient along the leading edge, the maximum echo top displaced over or ahead of the gradient, and an evident weak echo channel. Note that most of these echo features are the same radar echo features emphasized previously that mark an intense updraft and severe weather-producing storm. Thus, Przybylinski and Gery (1983) offered further confirmation of the importance of these echo features and shapes.

4.7.4.2.1 Recognition of Echo Shape and Attendant Features. A low-level Reflectivity product will show the presence of bow- and comma-shaped echoes (Figures 4-25 and 4-26) and attendant features, but the three-dimensional storm structure should also be viewed along with the low-level echo. The 4-panel/multi-panel reflectivity and velocity displays can be used to verify the impression of low-level echo shape. Moreover, the output of the MDA via the Mesocyclone product or overlay, and the TDA via the output of the TVS or overlay, can also be used for further verification. However, the output (positive or negative) of these and other system meteorological algorithms must always be verified by examination of the velocity products. The maximum echo top location can be identified from the ET and EET products. However, high-levels will provide better resolution of where the echo top is located and its height. A comparison can be made as to top location in relation to the low-level reflectivity gradient by displaying the products on a multi-panel display and linking the cursors to permit visual comparison of low-level, mid-level, and high-level echo features. Reflectivity Cross Section products can also help in identifying the low-level gradient and the maximum storm top position, as well as the general storm structure, but must be positioned properly.

With squall lines and bow echoes, the “Rear Inflow Jet” (RIJ) and low-level weak echo channel shapes (Rear Inflow Channel, RIN) to the rear of the echo line have been emphasized as being associated with damaging winds (Przybylinski 1995). Within the limits of the viewing angle, strong velocity maxima near these RINs should be identifiable and used with low-level Velocity products for verification. The weak echo channel is often located near the center of the bow and associated with the RIJ and strongest surface downburst winds (Figures 4-25 and 4-26). (See Part B, Chapter 7, of this Handbook for discussion of squall lines, MCSs, and bow echoes.)

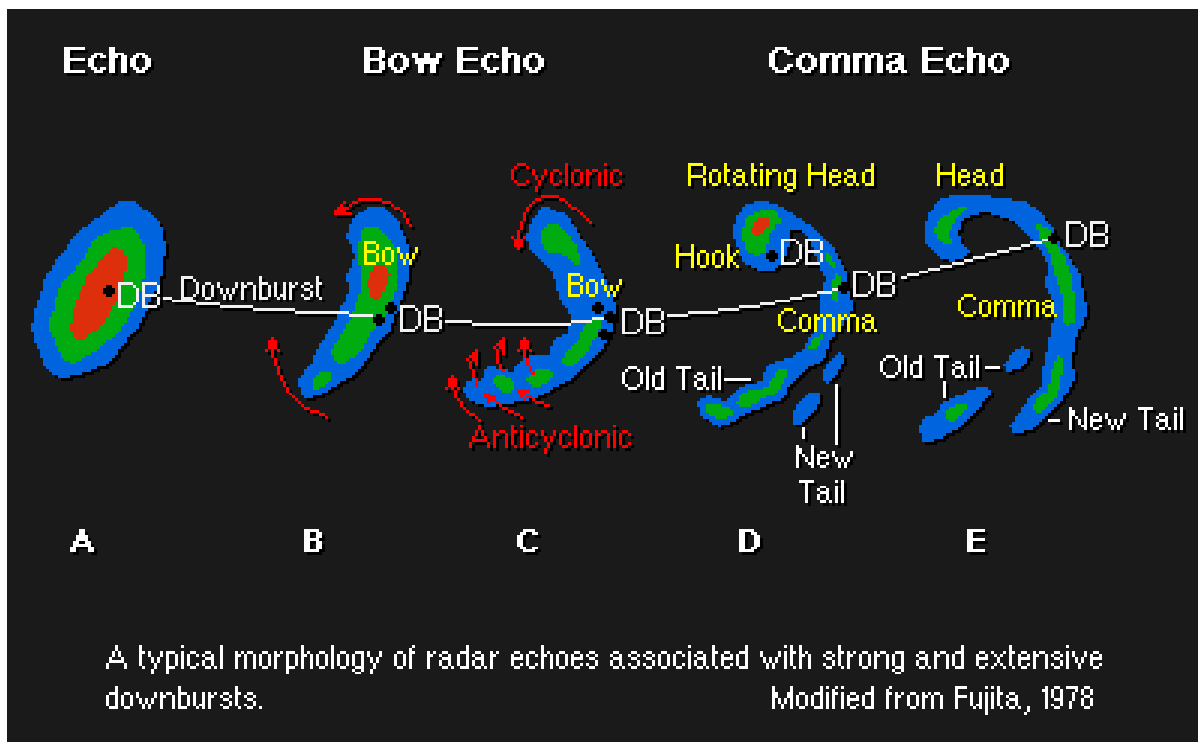


Figure 4-25
Bow Echo Schematic

Conceptual model of bow echo characteristics and typical evolution. Adapted from COMET (1999).

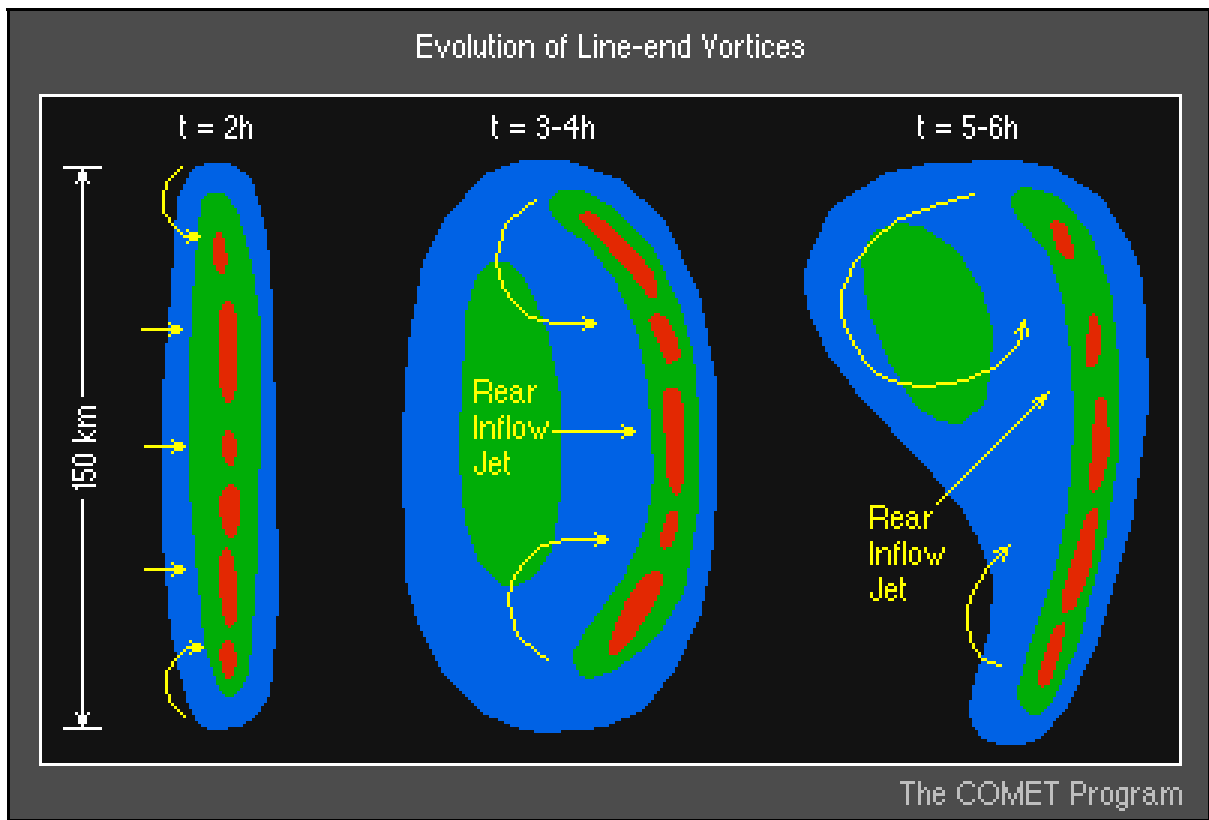


Figure 4-26
Squall Line Schematic

Development of cyclonic (north) and anticyclonic (south) "bookend" vortices in a squall line simulation. Note the Rear Inflow Jet. From the COMET *MCS module* (COMET, 1999).

A time lapse of a, specifying a continuous update, will aid in monitoring squall line feature evolution such as bow- and comma-shaped echoes. Sometimes bow echo development may be noticed first with the appearance and acceleration of a forward bulge in the echo or the line and sometimes with the development of a LEWP, a portion of which can later assume a bow shape. The bow echo may further evolve into a comma-shaped echo with a rotating head. Note that sometimes the most damaging winds associated with a Bow Echo or LEWP occur during development of these features. Once the bow shape is well developed the strongest wind damage may be past. The comma head is a mesocyclonic storm, i.e., a supercell, even though rotation may be confined to mid-levels. Rotation at the head of the comma echo may be identified in the SRM or SRR products, the Mesocyclone product, and perhaps in a time lapse of Reflectivity products.

Important three-dimensional features of damaging Bow Echoes are: elevated RIJs, line-end vortices, rear inflow notches, and the indicators of an intense updraft as given earlier: strong reflectivity gradient, WERs, displaced echo top, and supercells. The line end vortices can be very important because they can amplify the RIJ and can be associated with tornadoes at their leading edge.

Increasing velocities behind a line echo (or large echo) may signal acceleration of a portion of the line and transition into a bow shape. Very damaging winds and some large hail may occur during this phase. Bow-shaped echoes, such as within a LEWP, may move at a faster speed than the line itself owing to the rear inflow jet. If other storms do not intersect its path, or are not in close proximity, the bow echo's movement should be effectively tracked by the STI product.

The appearance of a low-level hook echo and/or the “inflow notch” along the leading edge of a squall line, comma head, or bow echo can best be identified via the three-dimensional echo structure detected in reflectivity and velocity products through the multi-panel base product display. Again, a time lapse may aid in monitoring the evolution of this feature. However, rapid changes in mesocyclone and storm strength are not uncommon and the user must be knowledgeable of the near storm environment in order to evaluate the need for short fuse tornado or damaging wind warning. The rotation of the “bookend vortices” should be noticeable in velocity products (V, SRR, SRM) in mid- and/or low-levels. One of the indications of enhanced tornado threat with linear echoes is the intersection of the line with a surface-based boundary, often located at right angles to line orientation (Przybylinski et al. 2000). This threat is further enhanced with associated hook echo development. Another sign of enhanced tornado threat is the development of strong echoes just ahead of the line and the subsequent intersection of that echo and the line itself.

4.7.4.2.2 Considerations. Windstorm identification relies heavily on echo shape, but other factors need to also be considered. For example recognition of storm-damaging wind potential relies on the LEWP, on bowing line segments, the surging supercell RFD, detection of the DCZ or the MARC, mesocyclones, WER, BWER, low-level tight reflectivity gradient along the leading edge of a squall line, and the rear inflow notch.

Severe weather can be produced during bow echo or comma echo development. Since it is often hard to identify individual echoes assuming a bow shape in real-time, the use of time lapse with continuous update of a Reflectivity product can be extremely useful in increasing warning lead-time. Storm structural features such as the WER, BWER, hook echoes, inflow notches, and echo shapes, such as the Bow Echo, often cannot be distinguished in a CR product since their shapes are low- and mid-level features and are obscured in CR products by reflectivity echo canopies (overhangs) and cores above. However, the CR Combined Attribute Table provides an excellent summary of algorithm output.

Range-overlaid echo may obscure velocity data needed to confirm a mesocyclone or TVS, should they exist, but not the reflectivity hook echo itself if it exists. Sometimes, however, the higher elevation velocity data may be free of overlaid echo. Moreover, velocity signatures should be interpreted in the context of the storm reflectivity structure.

As a review, damaging wind radar patterns/trends include LEWPs, bowing segments, surging RFDs, deep convergence on backside of mesocyclones, the DCZ and the MARC, mesocyclones (non-descending, descending, developing, strengthening), WER, BWER, tight reflectivity gradients along the leading edge, the RIN, and gust front speeds well matched to squall line speed. Descent of high reflectivity cores and associated mid-level convergence are also indications of downbursts and/or microbursts.

Types of radar products used for analyzing potential damaging wind storms include high resolution R/V, R/SRM multi- or 4-panels, all tilts, cross sections, SW, and time-lapse animations. However, keep in mind that the SRM does not display ground-relative velocities and should not be used for surface wind warnings.

4.7.4.3 Mesocyclone Signature Detection. A mesocyclone is a small scale rotation closely associated with a major convective storm updraft (in which vertical velocity and vertical vorticity are correlated) and often involves the RFD, as well. True mesocyclones meet or exceed established thresholds for: persistence, (minimum of two volume scans), vertical extent (shear extends at least 3 km (10,000 ft) in the vertical, but dependent of storm depth), and shear. The distance between maximum inbound and maximum outbound velocity peaks of the circulations are normally ≤ 9.3 km (5 nm). The rotational velocity is equal to the absolute values of the maximum inbound velocity plus the maximum outbound velocity divided by 2 (using mid-range velocity product values). While the radar system is equipped with algorithms (the legacy Mesocyclone algorithm and the recently developed MDA) for the automated identification of these features, here we confine our discussion, for the most part, to manual identification and meteorological meaning of these features. The algorithm designs are discussed in Part C, Chapter 3, of this Handbook.

An overwhelming majority (probably more than 95%) of mesocyclones (Figures 4-27 and 4-29) have been found through long-term Doppler observations to be associated with some form of severe weather (hail > 1.9 cm ($\frac{3}{4}$ inch), winds > 25.7 ms⁻¹ (50 kts), and/or tornadoes). Perhaps

26% are precursors to, or associated with tornadoes (Trapp et al 2005). They generally have the size, depth, and persistence characteristics just mentioned. Mesocyclones have been found to be associated with virtually all strong and violent tornadoes. Supercells (storms containing deep persistent mesocyclones) are responsible for a disproportionate amount of damage. Stronger mesocyclone signatures more often produce tornadoes than do weaker signatures, especially if a TVS and BWER are also present. However, as of this writing, we have yet to be able to effectively identify or discriminate via radar between mesocyclones that will produce tornadoes from those that will not.

4.7.4.3.1 Recognition of a Mesocyclone Signature. A mesocyclone typically will develop within mid-levels of a supercell storm and build upward and downward as the storm matures. Mesocyclone rotational velocity, shear heights, and shear strengths can be monitored via the velocity field revealed in multi-panel V, SWV, SRM, and SRR products. The M, MDA, and TDA algorithm products, though they have relatively high false alarm rates at times, can also act as a “safety net.” But the output of these algorithmic products must always be verified with velocity products. Time lapse capability with continuous update may also be useful, at times, in monitoring mesocyclone development. As a first approximation the velocity field of a mesocyclone will appear as a solidly rotating core (Lemon et al. 1977) (Figure 4-28). That is, the mesocyclone appears as two velocity peaks of opposite signs, separated azimuthally (Figures 4-27, 4-28, and 4-29). The surrounding potential vortex (outside of the core circulation) is more difficult to discern with radar.

Interrogation of different elevation scans of SRM or SRR products (e.g., Figure 4-19, at 0.5°, 1.5 km (5,000 ft); 1.5°, 3.6 km (12,000ft); and 2.4°, 5.5 km (18,000 feet)) can aid in determining the height continuity of a mesocyclone. As seen in Figure 4-29, the multi-panel mode can be very useful for this purpose.

If correctly oriented through the storm, storm rotation (cyclonic or anticyclonic) of a well-developed mesocyclone may be evident in the RCS product. Remember, however, that correct placement is critical. When the velocity cross sections are not oriented along a radar radial, then interpretation of these velocities displayed in the product become problematic. Therefore, for operational purposes, the multiple panel R, V, SRM, SRR, and SWA products become far more useful to the user during storm interrogation.

Removing the storm motion via SRR or SRM products may aid in the human recognition of a mesocyclone when shifted velocities caused by this storm motion make recognition difficult. Algorithm detection is, however, unaffected by this storm motion.

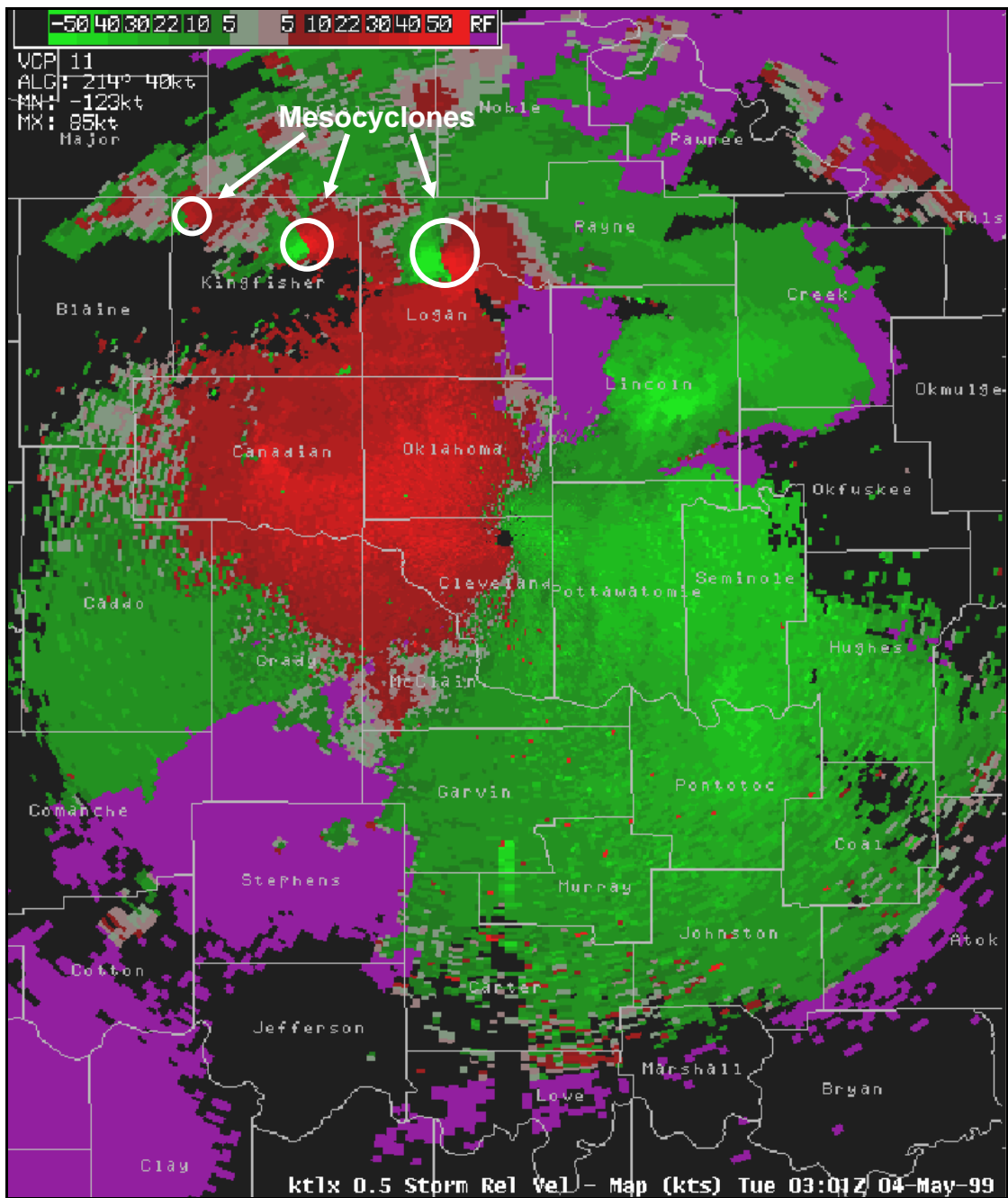


Figure 4-27
Mesocyclones

Oklahoma City, OK WSR-88D SRM product at 03:01 UTC on 4 May 1999 (AWIPS display). Three mesocyclone velocity couplets (encircled) are north-northwest of the radar and are identified by the bright green adjacent to the bright red color-coded velocities.

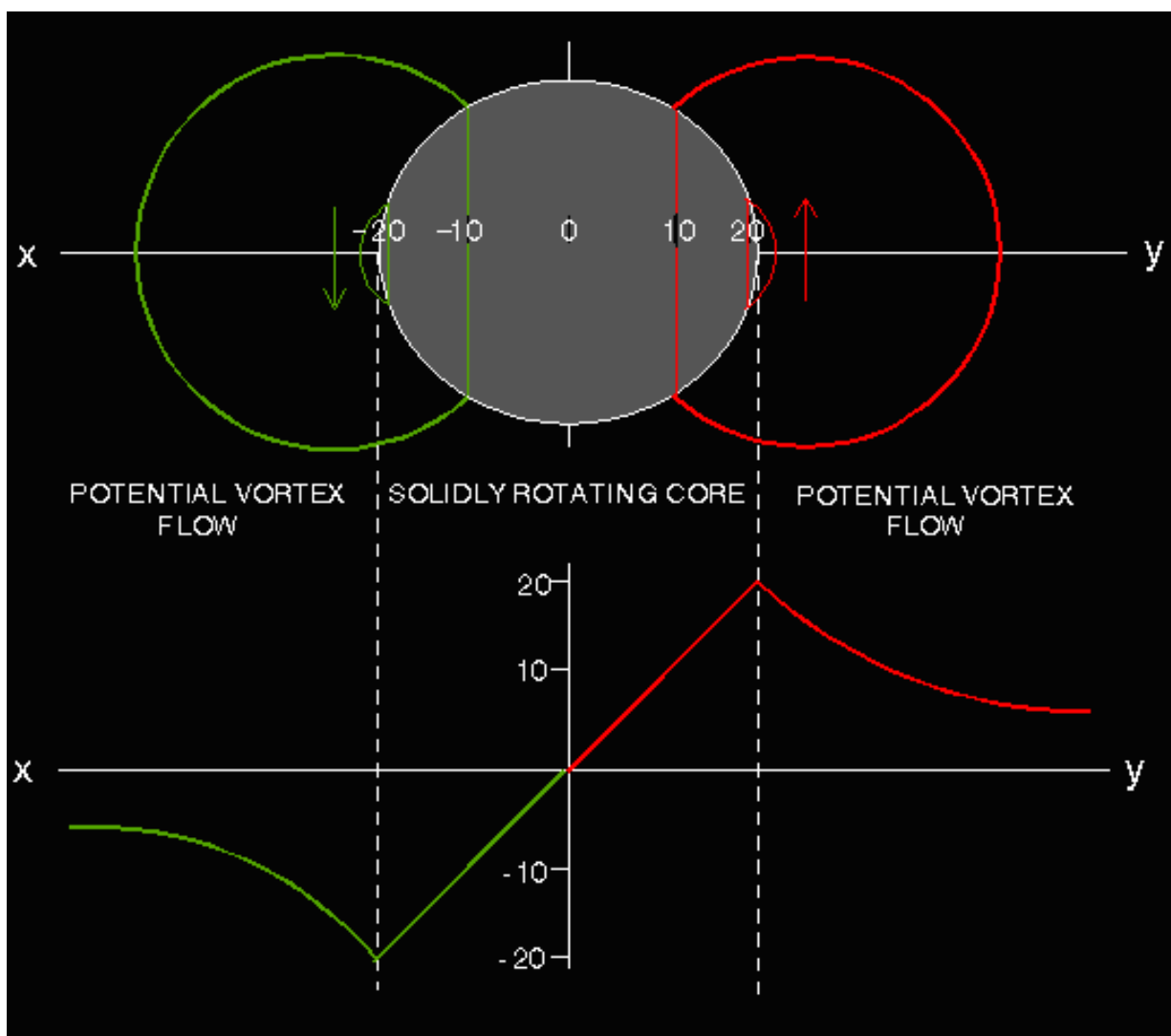


Figure 4-28
Combined Rankine Vortex Schematic

A schematic of the first approximation of a mesocyclone showing the velocity profile as a Combined Rankine Vortex. From Lemon et al. (1977).

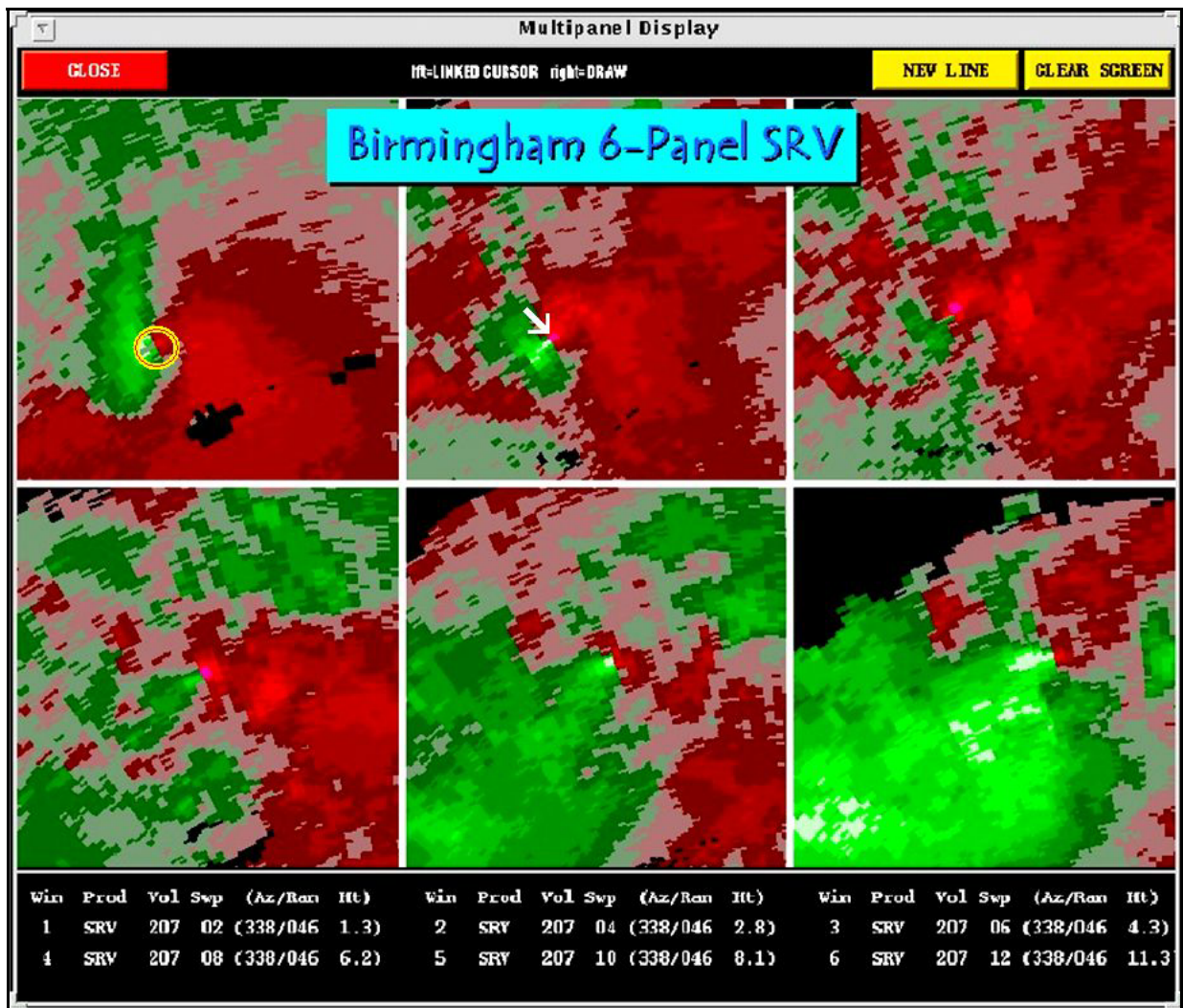


Figure 4-29
Mesocyclone and TVS Vertical Extent

Birmingham, AL, 6-panel WDSS Storm-Relative Mean Radial Velocity (SRV on WDSS display) depicting WSR-88D SRR product for 6 progressively higher elevation slices. A mesocyclone and TVS associated with the supercell and tornado that struck Birmingham, AL on 8 April 1998 are depicted. The radar is in the lower right. Outbound velocities are in red and inbound in green. The increase in color brightness indicates progressively higher velocities. In the upper left the height is 1.3 km (4,264 ft) above radar level (ARL), upper center, 2.8 km (9,184 ft), upper right, 4.3 km (14,104 ft), lower left, 6.2 km (20,336 ft), lower center, 8.1 km (26,568 ft), lower right, 11.3 km (37,064 ft) ARL. A tornado was in progress as these data were collected.

In a tornadic supercell, Doppler data have indicated many times that a separation of the mesocyclone core from the BWER occurs prior to or during the collapse of the BWER and often just prior to tornadogenesis (Lemon and Doswell 1979). With the somewhat increased likelihood of tornado development at this stage, the separation of the mesocyclone core from the BWER may be monitored via the multiple panel displays.

However, mesocyclone presence alone will not give adequate information to anticipate tornadogenesis. Nor can we sample the buoyancy of the RFD (a positively buoyant RFD is favorable to tornadogenesis). When the Lifting Condensation Level (LCL) is low (less than ~ 1000 m) and the 0 to 1 km shear is high (greater than $\sim 25.7 \text{ ms}^{-1}$ (50 kts)) these conditions then aid the storm in tornado development and suggest a buoyant RFD may be present (Carven et al. 2002; and Brooks and Craven 2002). When evidence is present indicating a source of low-level vertical vorticity and a coexistence of strong low-level updraft, beneath or with this mesocyclone, then tornadogenesis becomes even more likely (for more detail and discussion see <http://www.wdtd.noaa.gov/courses/dloc/ic57/ic57.pdf>). As before, the use of high resolution multiple panel base products provide the tools to monitor indications of tornadogenesis. While not mentioned, magnification of these base product images is essential.

4.7.4.3.2 Considerations. The legacy Mesocyclone algorithm and the new MDA provide the position of the feature on the lowest elevation angle in which the feature was detected. In this way the meteorologist/user can better warn those beneath or within the mesocyclone circulation. However, mesocyclones (and other storm features with a vertical extent) are often tilted and are, therefore, displaced at higher elevations from where they are located in lower levels and at the surface. Thus, both radar horizon and vertical slope must be considered before concluding where a mesocyclone or a TVS may actually be located at the earth's surface.

Mesocyclones are present with supercell storms and often produce severe weather and tornadoes, but severe weather and tornadoes can also be associated with non-mesocyclonic storms. For example, ordinary multicell cluster storms can also produce large hail, downbursts, or weak tornadoes produced as a result of pre-existing vertical vorticity along convergent boundaries. When present, and through the use of the MDA, mesocyclone tracking information is now supplied to the user.

However, mesocyclones can, and often do, propagate discreetly with one mesocyclone core dissipating while a second develops in a new but nearby location. In fact, about 40% of supercell storms produce multiple mesocyclone cores during their extended lifetimes and can be "tornado family producers" (Figure 4-30). Because of this fact, and because supercells often produce tornadoes during the storm's collapse phase, warnings for these storms should persist for a significant period of time, even when they appear to have lost their supercell organization and storm severity (Burgess and Lemon 1990).

In order to best resolve and characterize velocity-related storm features such as the mesocyclones and TVSSs, use of the Digital Velocity Array (DV) with 0.25 km (0.13 nm) range bins and 256 data levels should be used during severe convective storm interrogation.

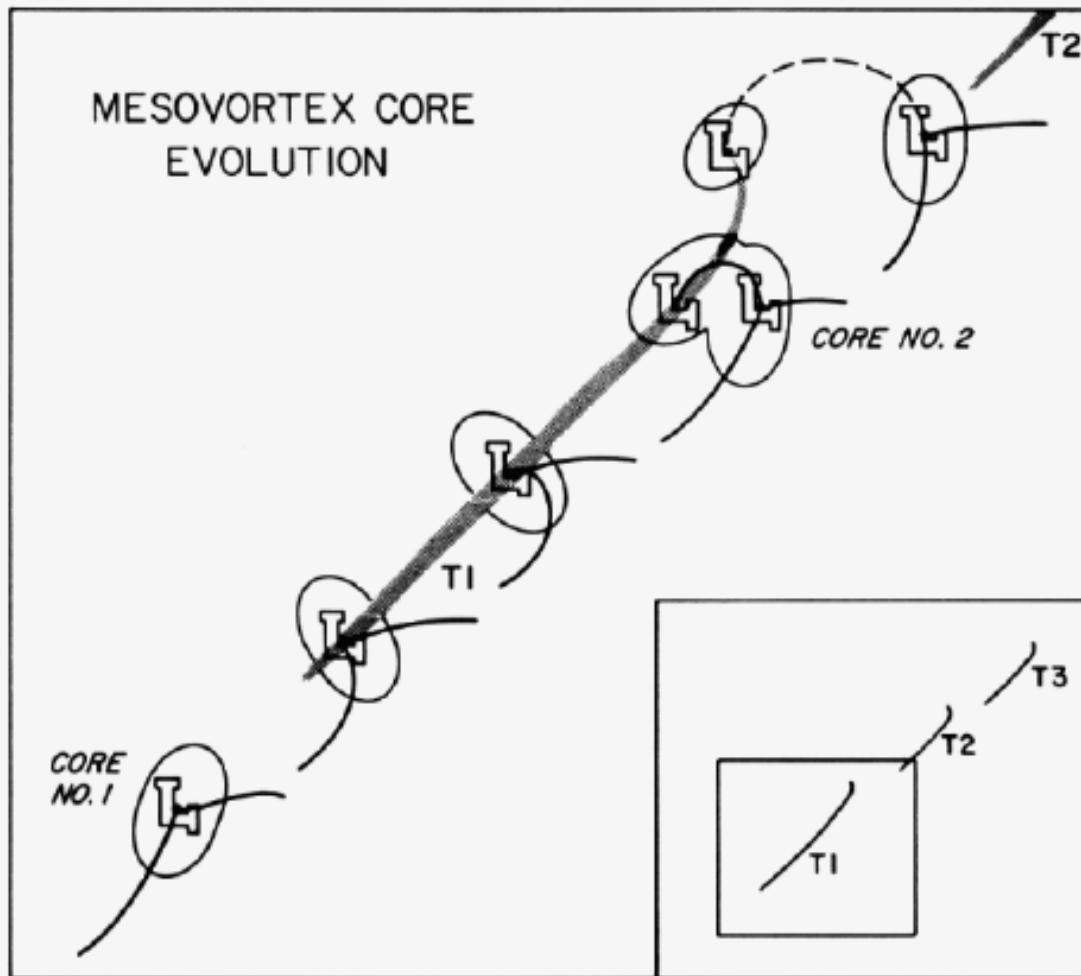


Figure 4-30
Multiple-Core Mesocyclonic Storm Schematic

Conceptual model of mesocyclone core evolution. Thick lines are low-level wind discontinuities, and tornado tracks (exaggerated for size indication) are shaded. Insert shows tornado family tracks and the small square is the region expanded in the figure. From Burgess et al. (1982).

Due to beam broadening and radar horizon, Doppler radar detection of mesocyclones is generally limited to about 230 km (124 nm). Mesocyclones range in size from 1.8 to 9 km (1 to 5 nm) in diameter. “Misocyclones” formed in weak vertical wind shear may not be detected much beyond ~ 46 km (25 nm) due to their small size ~ 500 m (1600 ft) to ~ 1500 m (4900 ft), (Lee and Wilhelmson 1997).

Mesocyclones most often imply generation of RFDs (the LP storm may be an exception) and strong updrafts. In order to increase confidence in their existence, they must have time and height continuity within the data. Mesocyclone diameter is not related to severity of the thunderstorm but, a shrinking mesocyclone diameter or increasing rotational velocity in low levels should be interpreted as signs for significantly increased tornado likelihood. The user must also monitor the data for low-level convergence with a mesocyclone above (or nearby) implying vertical stretching of vorticity and tornadogenesis. In these very dangerous situations the mesocyclone need not lower to the surface prior to tornado occurrence. In fact, when an elevated mesocyclone is situated over strong low-level convergence the user should anticipate that tornadogenesis is imminent (Burgess and Magsig 1998).

4.7.4.4 Tornado Vortex Signature Detection. The TVS is defined as a locally intense circulation indicated by strong shear on the order of 0.01 s^{-1} between two velocity gates which are azimuthally adjacent and constant in range (gate-to-gate) (Brown et al. 1978). It is an intense gate-to-gate azimuthal shear associated with tornadic-scale rotation (Figures 4-29 and 4-31). A TVS is identified manually if the gate-to-gate velocity difference is: $> 46 \text{ ms}^{-1}$ (90 kts) and the range to the feature is $< 55.5 \text{ km}$ (30 nm). But when its range is between 55.5 km and 102 km (30 nm and 55 nm) the gate-to-gate velocity difference must be $> 36 \text{ ms}^{-1}$ (70 kts) to qualify as a TVS. The gate-to gate shear is equal to the velocity difference between the maximum inbound velocity value and that of the maximum outbound velocity (absolute values), normally in adjacent azimuths and at the same range. These values are only guidelines; the user will have to adjust according to the situation, storm size, near-storm environment, and geographic or topographical location. While the system uses an algorithm for the automatic detection of the TVS, we confine our discussion for the most part to the feature and its meteorological meaning.

Precisely what causes the TVS signature within Doppler radar data is unknown. We do know that the radar beam is normally substantially larger than even the largest tornadoes even at close ranges. What is also known is that the signature is highly correlated to vortex existence of tornadic intensity, either incipient or actual tornadoes (Brown et al. 1978). Speculation concerning the signature cause has included an “intermediate” circulation immediately surrounding the tornado called the “tornado cyclone” (Burgess et al. 2002).

The hook echo, which has, in the past, been considered indicative of tornadic circulations, is, in fact, more indicative of a mesocyclone. While tornadoes are not directly observed with even Doppler weather radar, a TVS within velocity products is often a strong indication of presence of a tornado. This is especially true if located in the hook echo and mesocyclone.

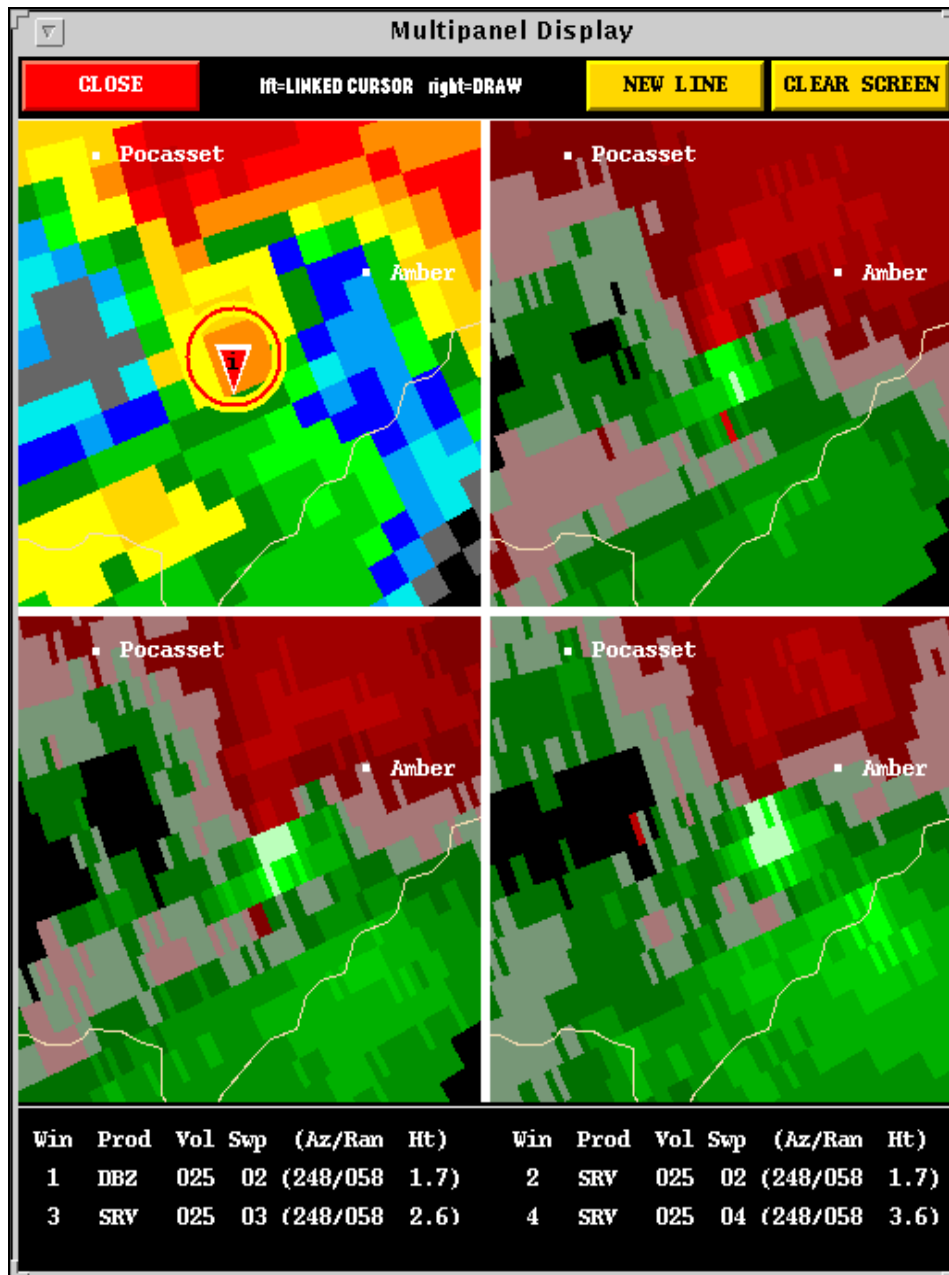


Figure 4-31
Tornado Vortex Signature Vertical Extent

Oklahoma City, OK WSR-88D 4-panel display with products from 3 May 1999 (WDSS display). The upper left display includes a Tornado Vortex Signature Product (TVS) overlaid on the reflectivity display. The remaining 3 panels contain SRR products. The TVS signature extends from 1.67 km (5500 ft) above ground level (AGL) to ~ 3.7 km (12,000 ft) AGL in these images and is associated with a tornado near Oklahoma City.

4.7.4.4.1 Recognition of a Tornado Vortex Signature. In addition to the appearance of a hook-shaped echo in a low level Reflectivity product, the mesocyclone detection capability of the WSR-88D offers clues to the existence of tornadic circulations and possible tornadoes.

Unlike the initial version of the TVS algorithm which would confine searches to only the mesocyclone vicinity, the TDA (Part C, Chapter 3, of this Handbook) will search the velocity data for a TVS signature. If identified, the TVS product provides information on potential tornadic circulations and the location of the signatures. The graphic overlay product can be used on a low-level V or R product, or the SRR, SRM, or SWA products in order to help identify the rotational phenomenon associated with the detection of the signature and to verify its existence and location. Again, base products must always be used to verify algorithm output, whether negative or positive.

Monitoring V, DV, and SRR, SRM, and SWA products can be useful in identifying mesocyclone and TVS existence and development. TVS rotation in a storm may begin in mid-levels aloft, co-located with updraft and often centered within or near the BWER, then extend downward as well as upward with time. However, these signatures are often the “non-descending” variety and develop near the surface within a strongly convergent flow and/or within or beneath a mesocyclone.

Trapp et al. (1999) examined a diverse data set, comprised of 52 events varying from southern Great Plains supercell tornadoes to tropical cyclone-spawned tornadoes. They stated that when classifying each by an objective means, they found (with a standard error of 7%) that 52% of the sampled tornadoes had descending TVSs, and 48% had non-descending TVSs. The results were stratified according to attributes of the tornado and TVS. For example, the descending TVSs were associated with greater differential velocity and greater tornado lead time. Tornadoes within squall lines and bow echoes tended to be associated with non-descending TVSs, an identification which provided a mean tornado lead time of 5 min. Based on these results, they concluded that radar operators should recognize, while interpreting Doppler radar signatures for tornado warning decisions, that a large percentage of tornadoes form in a manner different than Brown et al. (1978) who found that TVSs consistently descended. But then Brown et al. (1978) had a far smaller data set.

Tornado Vortex Signature characteristics, including the descent or non-descent, can be monitored via displays of different elevation angle velocity products in multi-panel displays. Inadequate removal of storm motion may somewhat obscure these phenomena, but this is usually minor since only a constant is added to the velocity field.

4.7.4.4.2 Considerations. The TDA is actually a misnomer. Rather than identifying only tornadoes, the algorithm detects a variety of vortices, including tornadic vortices. Thus, it must be used with caution for tornado detection.

The TDA in its current form uses a variety of adaptable parameter data sets to tune the algorithm to various conditions such as tropical cyclones, squall lines, or large Great Plains thunderstorms. These data sets better adapt the algorithm functionality to changeable conditions and improve its performance. However, even with these improvements, the TDA still has a rather high false alarm rate. Additionally the algorithm detects both surface-based (lowest radar sampling level) TVSs and Elevated TVSs (ETVSs). In most cases, the ETVS portion of the algorithm is disabled because those TVSs are not often correlated with tornadoes and may be confusing to the user. F0 and F1 tornadoes (i.e., gust front tornadoes, those developing from a bow echo, non-supercell tornadoes, and along convergence boundaries) may not have a parent mesocyclone. Tornadoes at higher altitudes (in mountainous areas) are often small and may lack well-defined signatures making recognition difficult.

Due to beam broadening, detection of a TVS is limited to a range of about 55 nm. Because of beam broadening, beyond that range, strong gate-to-gate shears are typically strong mesocyclones instead of actual TVSs. Thus, additional information regarding the increased likelihood of tornadoes gained through the TVS recognition is absent at longer ranges. However, the relative strength of the mesocyclone may provide a clue to a tornado's existence or likelihood, even at longer ranges.

Typically, the TVS and even the mesocyclone are detectable within SW products as broadened widths. But these broad widths cannot be substituted as recognition criteria for tornadoes because there are many other causes of broad SW. In addition, at longer ranges, there is a general increase in SW owing to the shear of the horizontal winds with height and the broad beamwidth. In addition, the mesocyclone itself is typified by broad spectrum widths across the signature center.

A tornadic signature may be located at the periphery of the storm echo. This is especially true in low-levels on the edge of the storm echo itself or at the edge of the hook echo where weak power returns result in a low signal-to-noise ratio (where sidelobe contamination may also occur), thus hindering signature recognition. Portions of the supercell WER and BWER are also areas of weak signal return and the area where TVSs occasionally develop, making recognition of tornadic signatures difficult in these areas, as well.

The greatest potential for tornado development is indicated when a tightening/deepening mesocyclone circulation is noted on the SRM, a TVS is identified (operator), strong low-level convergence below a mesocyclone base is detected, a storm moving into a low LCL and/or strong low-level shear environment is seen, and when a storm is interacting with a boundary.

We have addressed here the TVS associated with the supercell because of the signatures overriding importance and because a TVS is usually associated with stronger or violent tornadoes. Weak tornadoes, those from F0 to, perhaps, F2 on the Fujita scale, are more often not associated with detectable TVSs. However, TVSs, manually or algorithm detected, also do occur with non-supercell storms, although rarely.

4.8 Hail. Thunderstorms with strong and extensive updrafts, high super-cooled liquid water content, and large, supercooled cloud drop sizes are favorable for hail formation. Essentially, the features important to large hail formation are: strong storm-relative flow, large CAPE in the hail growth region of the atmosphere (-20 to -40 deg C), strong, deep layer shear ($> 15.4 \text{ ms}^{-1}$ (30 kts) in the 0-6 km layer), a strong mesocyclone, a storm WER, a BWER, high reflectivity, and high VILs (and VIL density). The resulting hail can be spherical or irregular in shape and sometimes extremely large.

4.8.1 Recognition of Hail Potential. Historically, one of the first techniques used to identify storms producing hail was to identify storms that possessed high reflectivity $> \sim 55 \text{ dBZ}$. Subsequently, storms that possessed unusually high reflectivity at unusually high altitudes within the storm were found to produce hail, often large in size. An intense core in a hailstorm will usually begin developing at higher elevations in the storm and then descend toward the base of the storm cloud. Therefore, a quarter-screen display of successively higher heights may enable the detection of the descent. An RCS product accurately placed through the storm can aid in the identification of strong mid- or high-level reflectivity magnitude. In addition, the LRM product can be used to isolate those storms with abnormally high altitude and high magnitude reflectivity and likelihood for large hail. However, while LRM layer-heights are established, the altitude thresholds for this high reflectivity are variable and change with season and with airmass.

High values of VIL (Green and Clark 1972) and the related severe weather probability values have been used in the past as estimators of hail potential, as well as other forms of severe weather. In fact, VIL was one of the more reliable products. However, we also know that the critical VIL values signifying hail vary with season, with airmass, over the radar coverage area, and even as a function of the Volume Coverage Pattern. Additionally, a “critical VIL value” is normally needed to establish the threshold for hail, given an airmass or particular day. Therefore, at this time, use of VIL as a hail discriminator is not highly recommended although it can be somewhat useful.

A second related parameter has been developed, that of VIL Density (Amburn and Wolfe 1997; Cerniglia and Snyder 2002; Blaes et al. 1998). VIL Density is VIL normalized to storm depth. This was done in part to accommodate VIL values that are smaller simply because the storms in question are mini- or “moderate” supercells which are still very significant from a severe weather perspective, yet will have smaller VIL values by reason of their smaller stature. While certain values are indicative of hail, estimating hail size through the use of VIL Density shows very little skill according to Edwards and Thompson (1998).

The structure of convective storms in a sheared environment has been found to provide an excellent clue to the potential for intense updraft and large hail with a storm. For example, storms exhibiting an overhang, related WER, and maximum storm top located above the low-level, tight reflectivity gradient (or the WER itself) have been found to be large hail producers (Lemon 1978; Burgess and Lemon 1990). Generation of these same three-dimensional echo features is related to the abnormally large vertical mass transport and the intense divergence at updraft summit. In fact, Witt and Nelson (1991) have documented the direct relationship of hailstone size to divergence

strength (Figure 4-32).

Note that storms exhibiting this three-dimensional reflectivity structure are often supercells, as well. These same storms containing mesocyclones are often prolific producers of very large hail (> 5 cm (2 in) in diameter). Mesocyclonic storms seem to be associated with airflow (and liquid water concentrations) that favor long hailstone residence-times within the storm where very rapid wet hail growth occurs. Thus, detection of mesocyclones via V and DV products and, therefore, supercells, are strong indications of large or very large hail.

We now have an improved HI that uses the HDA output as explained in Part C, Chapter 3, of this Handbook (Witt et al. 1998). The algorithm output includes the POH and POSH, as well as MEHS with the storm cell in question. This algorithm, dependent on the current thermodynamic properties of the atmosphere within the County Warning Area (CWA) of the associated Weather Forecast Office and, as determined by a local, recent, atmospheric sounding, bases its output on the distribution of reflectivity relative to the environmental thermodynamic profiles. While subject to algorithm limitations, this algorithm has proven to function far better than the previous hail algorithm it replaces.

Products that can be used for large hail identification include the reflectivity and velocity products and the high resolution versions, displayed using the multi-panel methods with R, V, and DV. In addition, properly placed Vertical Cross Sections (RCS and VCS), as well as LRMs, VIL, and the output of the hail algorithm and product, HI (updated with the current sounding information) are effective products for hail detection.

Although divergence measurements are not provided directly by the WSR-88D, a VCS through the storm may provide information on the magnitude of the divergence at the storm summit, which may help assess the potential for hail. Vertical Cross Section placement is critical. However, use of high elevation angle velocity products may be superior to attempted use of the VCS product. The limitation of velocity product usage is that both the maximum outbound and inbound velocities may not be present in a single elevation angle velocity (or SRM and SWA) product.

Finally, the Three-Body Scatter Spike (TBSS) as occurs in the Mie scattering range of radars can be used (Figures 4-33 and 4-34). Use of this operational hail identification and related warning criteria was proposed by Lemon (1998). Lemon's work was based on Zrnice (1987) and Wilson and Reum (1986, 1988).

For operational application using the WSR-88D, Lemon (1998) recommended interpreting the signature as indicating hail greater than 2.5 cm in diameter is falling or will fall with the storm. The TBSS signature for large hail identification is a sufficient, but not necessary, condition. Further, because storms associated with the TBSS are also often high-end damaging wind storms, the user should anticipate the potential of winds up to 41 ms^{-1} (80 kts) or more with the signature-bearing storms.

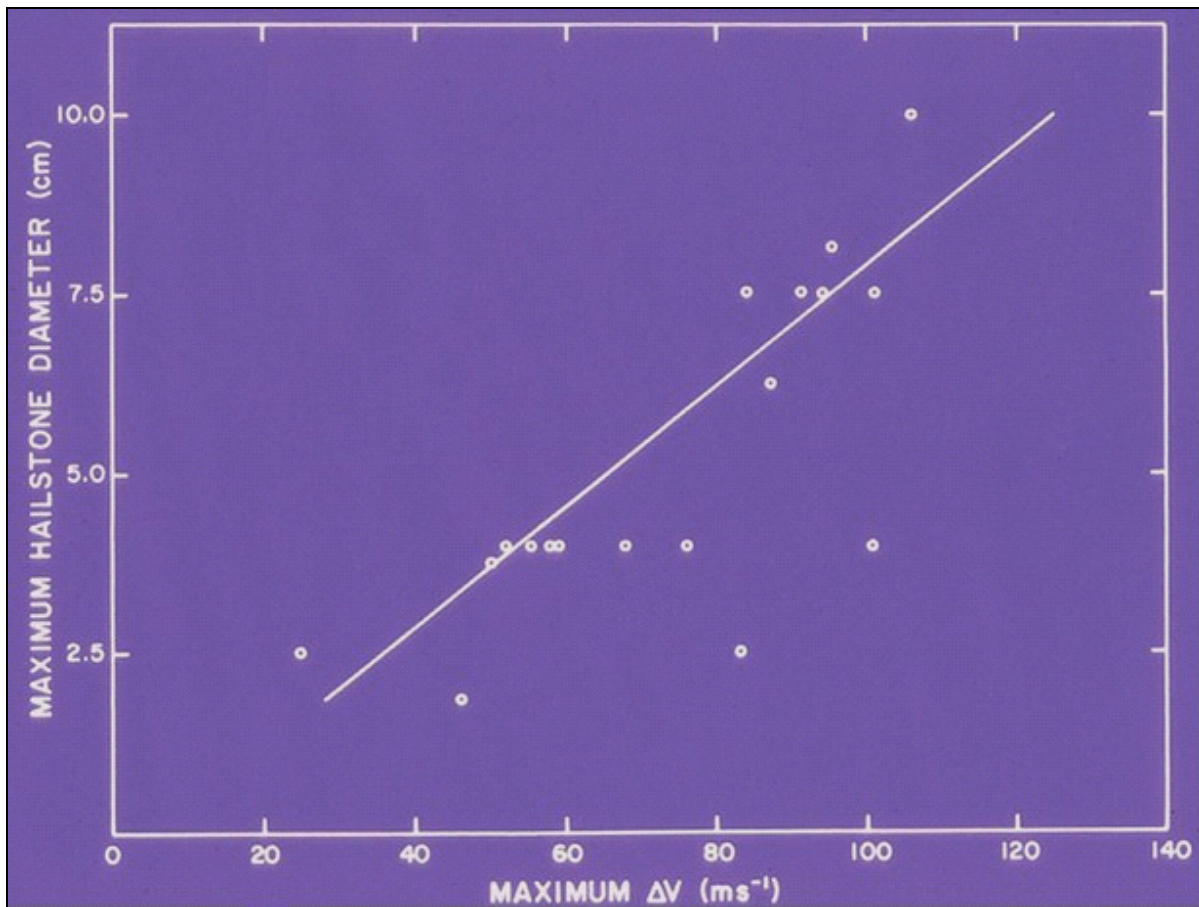


Figure 4-32
Storm Summit Divergence vs. Hailstone Size

Maximum hailstone diameter (vertical axis) as a function of the maximum measured storm summit divergence values (horizontal axis). Note the nearly direct relationship between the two quantities. From Witt and Nelson (1991).

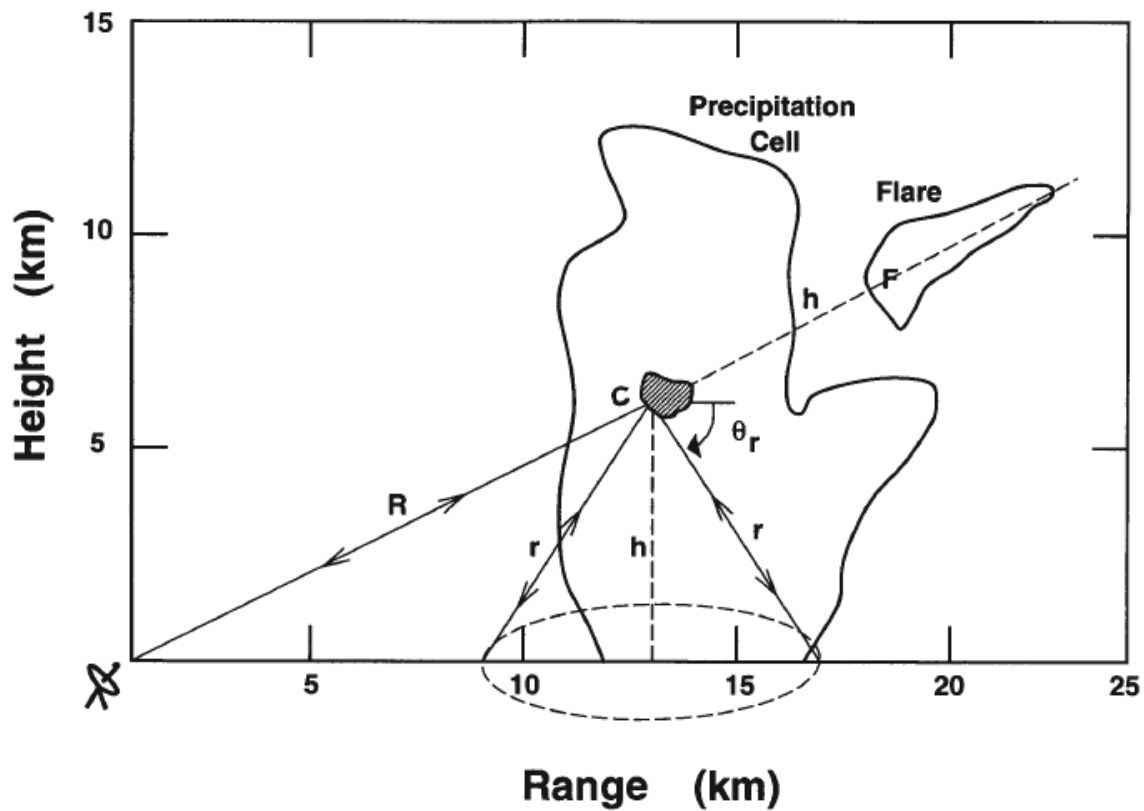


Figure 4-33
Radar Signal Path Schematic

Schematic of the radar signal path responsible for the TBSS (or flare echo). The dark shading near point C represents the 60+ dBZ core responsible for producing the artifact. From Wilson and Reum (1988).

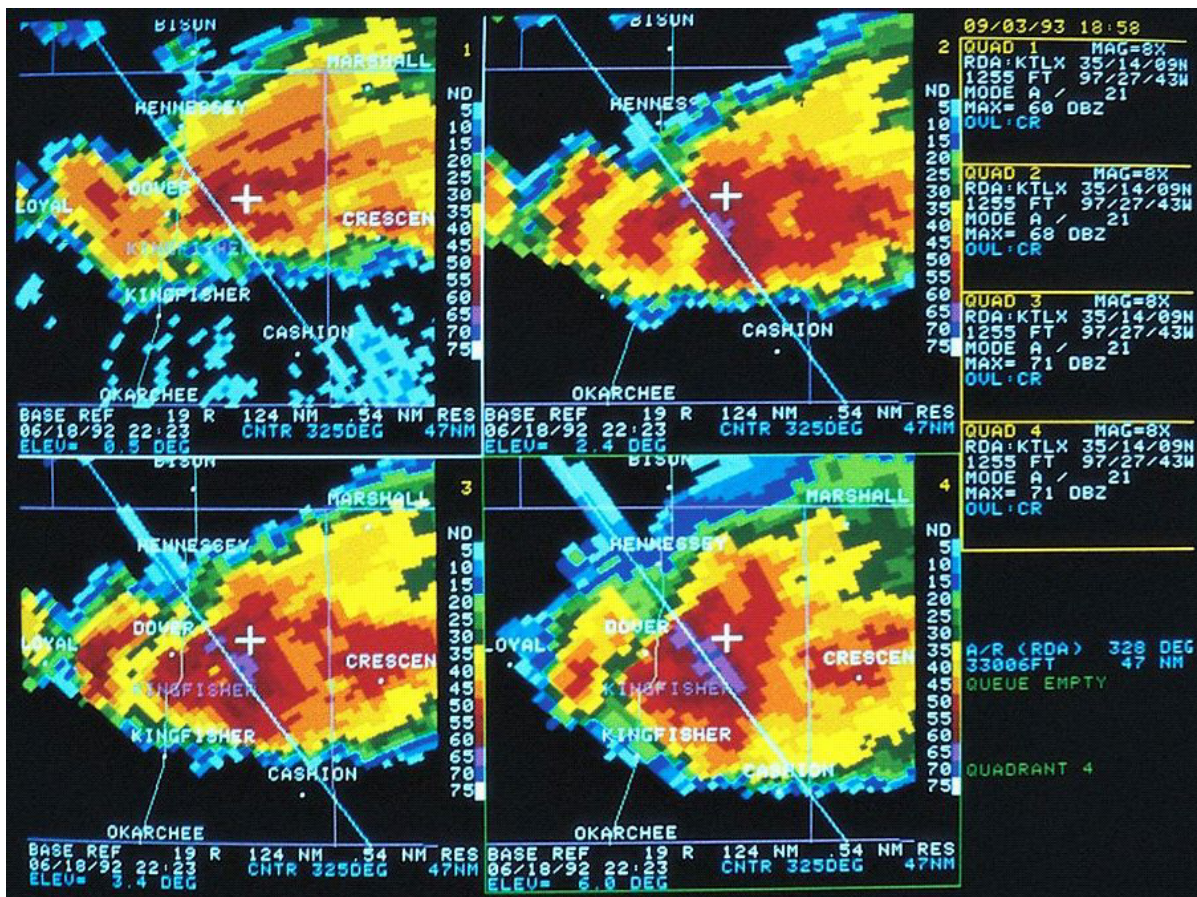


Figure 4-34
Three-Body Scatter Spike

Oklahoma City, OK WSR-88D 4-panel Reflectivity products at 22:23 UTC on 18 June 1992 (PUP display). The images were made at the same time a hailstorm was bearing down on Cashion, OK (bottom center of each panel). Images are magnified eight times; data resolution is 1 km (0.54 nm). Radar data elevation angles are: upper left, 0.5°; upper right, 2.4°; lower left, 3.4°; and lower right, 6.0°. The white cross is located on the reflectivity core responsible for TBSS and the cross section axis extends through the TBSS to the rear of the storm in 2.4°, 3.4°, and 6.0°. From Lemon (1998).

4.8.2 Considerations. High, near-surface reflectivity values (over ~ 60 dBZ_e) often indicate that the precipitation is in the form of hail and not rain. The existence of sidelobe contamination may also indicate the presence of hail.

Within about 93 km (50 nm), VCP 11 and 12 will provide better coverage for derived product estimates (such as VIL) and cross sections through storms than will VCP 21.

A combination of products should be used to assess the potential for hail, i.e., RCS, and VCS, VIL, LRM, the HI product, and R, V, and DV (especially for mesocyclone detection and storm summit divergence) products. Note that normally the radar is configured to measure velocities with 0.5 m s^{-1} resolution. This limits the velocity resolution of the system to $\pm 62 \text{ ms}^{-1}$ or ± 123 kts. However, because of the intense storm summit divergence within very large hail producing storms, the velocity resolution of the system should be changed to 1 ms^{-1} before these measurements are made. This increases these system velocity measurement limits by a factor of 2.

In order to process the necessary information, the Hail algorithm needs to sample the full volume and depth of the storm. This seriously limits the HDA output when the storm is located within the radar “cone of silence.”

As a review, for ordinary storms, the user will mostly be evaluating updraft strength. They will need to determine updraft location, via the mid-level reflectivity core. Hydrometeor growth is most rapid as these hydrometeors pass through the most intense part of the updraft and through the -20° C to about -40° C layer. The intensity and elevation of the core increase as the updraft intensity increases. So, for severe hail (and potential damaging winds and microbursts), the maximum heights of the 45, 50, or 55 dBZ reflectivity core (this may vary by season and airmass) should be monitored. For the vast majority of pulse storms, a warning forecaster must infer the presence of large hail using a variety of techniques including a higher than normal elevated reflectivity core, high VIL and VIL density, the presence of low-level reflectivity > 60 dBZ, and high values of the POSH. This does not include large hail signatures for storms within a moderately to strongly sheared environment associated with supercells including a Mesocyclone, a WER, and a BWER. There is a direct observation of large hail within the beam when a WSR-88D or S-band weather radar detects the TBSS signature.

The types of radar products useful for analyzing potential hail-producing storms are: R/SRM combinations using multi-panel displays, high resolution Reflectivity and Velocity products and LRM, CR, VIL, and HI products. In some situations, the user can evaluate hail potential at the same time they are evaluating its tornado threat as some of the features looked for are the same (e.g., WER, BWER, a strong mesocyclone) for both threats. Time-lapse loops using 6 to 10 frames can be useful to monitor motion and development.

4.9 Extratropical Cyclones. In mid-latitudes, upper level, long wave troughs, and short-waves generate low pressure systems with a characteristically well-defined region of warm air advection

ahead of the disturbance and cold air advection to the rear. Extratropical cyclones (ETCs) typically have a diameter exceeding 500 km (270 nm) which, if centered on a radar, more than encompasses the area of radar coverage. This means that, most of the time, only a partial picture of an extratropical cyclone is obtained from a single radar. Thus, use of regional or national mosaics generated from the radar network as a whole are normally essential in order to obtain the full picture of an extratropical system (Figures 4-35 and 4-36). However, at times, a single radar may detect a circulation pattern associated with the cyclone.

4.9.1 Evolution of Stratiform Clouds and Precipitation. The evolution of cloud and precipitation layers can be monitored as described previously in Section 4.5. In addition, the VWP is useful in determining the formation of stratus clouds, as well as monitoring advection patterns. For example, with the derived wind information and use of upper air charts the user can monitor moisture and thermal advection with time. Moreover, the VWP can be used to evaluate numerical model performance.

The ET can be used to aid in monitoring the development of precipitation over time. Increased returns and identification of cloud layers and cloud tops in Reflectivity data (best in Clear Air Mode) can be expected. Otherwise, the user can monitor trends in precipitation development in mid-levels via mid-level Reflectivity products.

4.9.1.1 Recognition of Precipitation Trends. A time lapse sequence of Reflectivity and Precipitation Accumulation products, as well as the CR products (Figures 4-35 and 4-36), can be used to provide information on the extent of coverage, intensity, and trend of the system and associated precipitation. The local radar CR provides trend information via changes in maximum reflectivity throughout the volume, and the associated Combined Attribute Table provides output from the majority of algorithms. Of course, some of the reflectivity in the CR products may be thunderstorm anvils or precipitation aloft not yet reaching the surface (virga). Reflectivity Cross Section products can also be helpful in determining the depth of a layer of precipitation and the change in this layer over time.

Much of the precipitation in these ETC systems is stratiform precipitation characterized by growth through collisions and coalescence. Precipitation of that character is most intense at or very near the surface and, therefore, reflectivity is strongest at the lowest levels scanned. Because of the improved low-level scanning provided by VCP 12, this is the preferred VCP in extratropical systems. Reflectivity data is used in much the same way as it is used in convective storm events (i.e., the base data is used primarily in 4-panel reflectivity and velocity mode). This is done to obtain the best four-dimensional picture of the evolving precipitation areas, and embedded heavier precipitation bands caused by frontogenesis, isentropic lift, gravity waves, and/or slantwise convection (Shields et al. 1991; Moore and Kaster 1993).

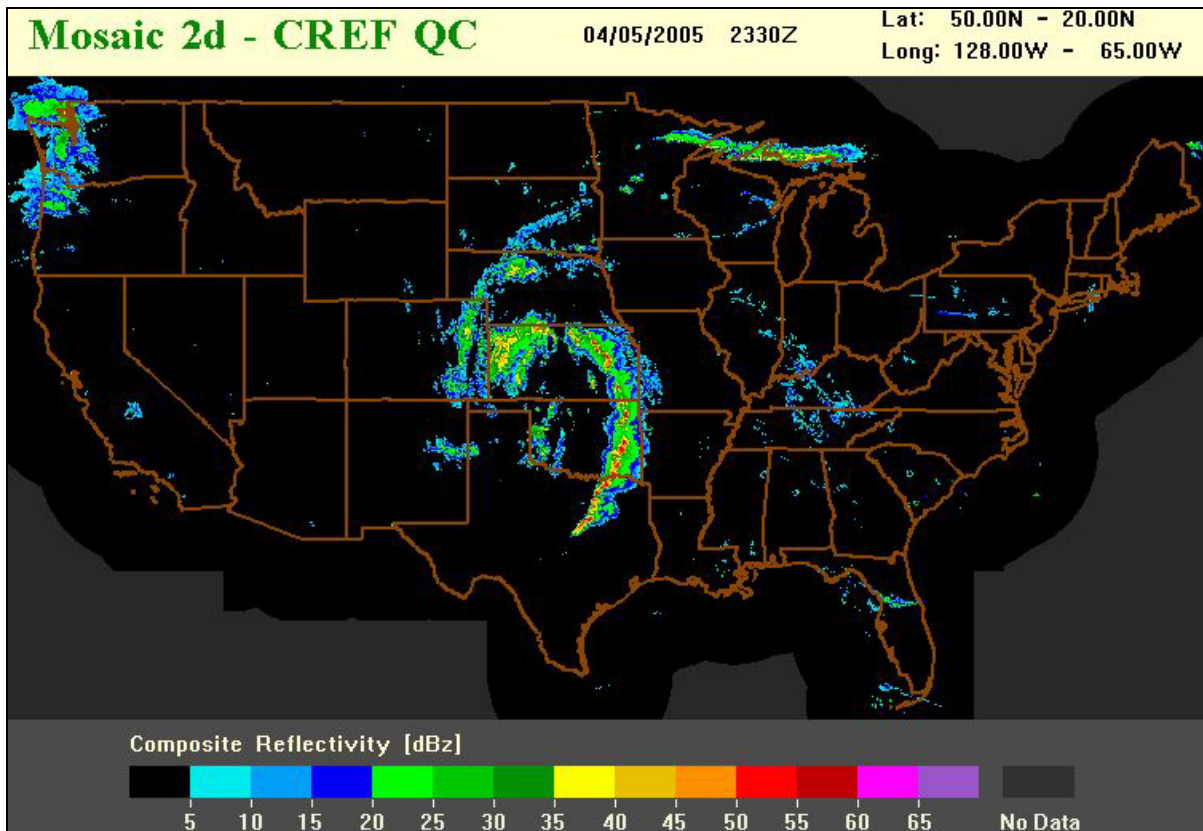


Figure 4-35
National Mosaic of Base Reflectivity of an Extratropical Cyclone

A national mosaic of Composite Reflectivity products obtained from WSR-88D radars at 23:30 UTC on 5 April 2005. The precipitation shield and convection centered over Kansas was created by an extratropical cyclone. The cyclone with a deep upper low pressure and surface system is centered over southwest Kansas. A frontal line of thunderstorms is over east Oklahoma and northeast Texas while a more stratiform area of rain is centered over western Kansas. (Courtesy, National Severe Storms Laboratory).

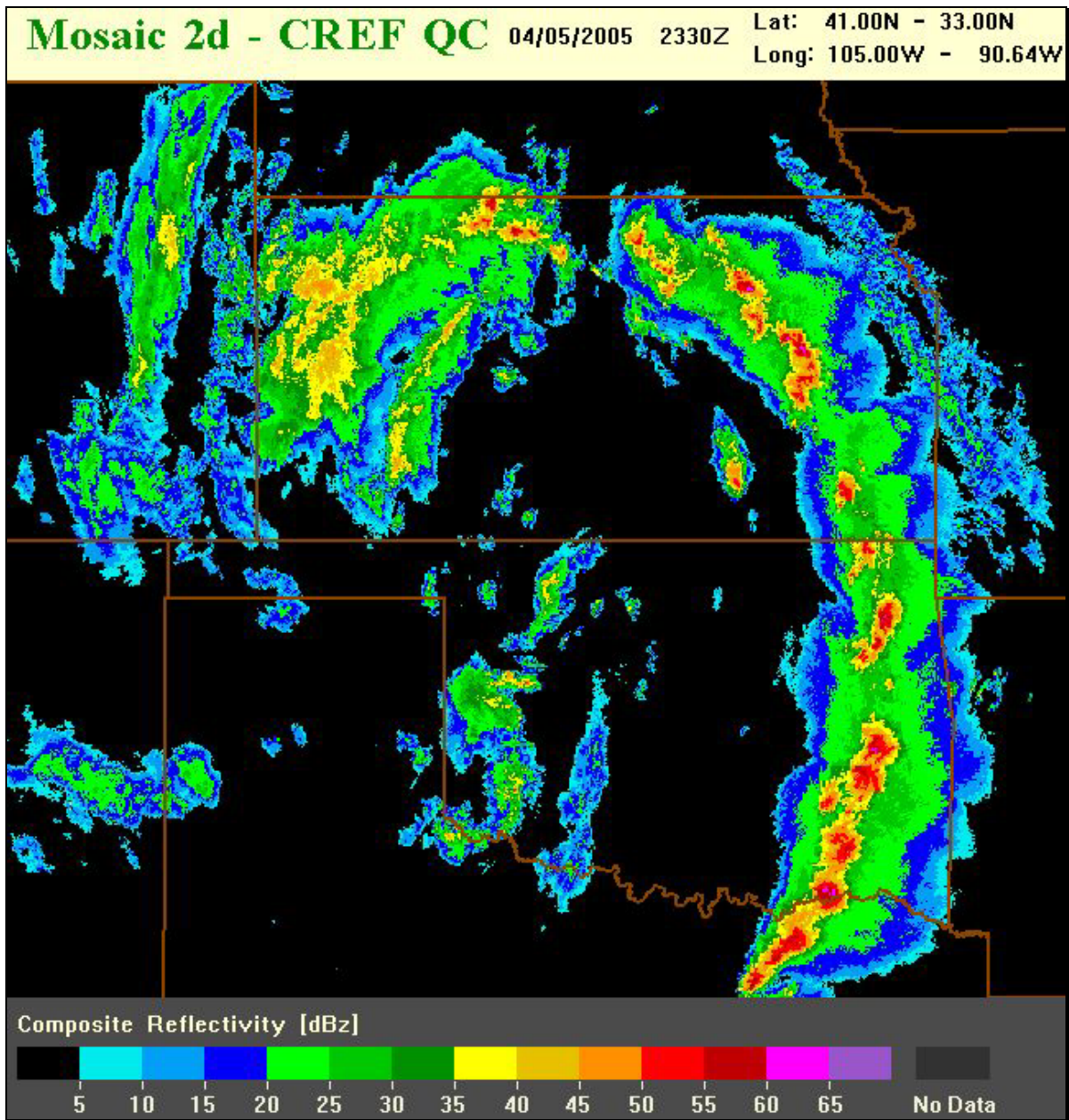


Figure 4-36
Regional Mosaic of Base Reflectivity of an Extratropical Cyclone

Same as Figure 4-35, except as a regional view of the central Great Plains. (Courtesy, National Severe Storms Laboratory).

4.9.1.2 Considerations. The ET is limited due to its reflectivity threshold (18 dBZ_e) in its ability to effectively monitor precipitation development and trend. This threshold will need to be lowered for stratiform and other events. Determining necessary changes to threshold levels may require on-site directives and operational experience.

During stratiform events, since the main concern is usually the weather in the lower two or three elevation angles, operating the radar using VCP 12 or 121 will often provide adequate vertical resolution. Moreover, the extent of range-overlaid echo can be significantly mitigated through the use of VCP 121. This is especially important because of the likelihood of widespread precipitation and range-overlaid echo.

4.9.2 System Movement. Within range of the radar, a closed circulation around the center of an ETC is normally not observed unless, perhaps, the system is deep and intense. Normally, only a portion of the circulation is evident. Rather, only a portion of the wind field can be observed by individual radars. However, cyclone-associated low-level jets are often observed in the radar-centered velocity products with modest elevation angles. The VWP may be used in conjunction with these products as well. Moreover, in the velocity and Reflectivity products, fronts and other discontinuities associated with these circulations are often detectable as they near individual radars. This has allowed much more accurate frontal placement than in the past.

4.9.2.1 System Movement Recognition. Using individual rain shower or thunderstorm cell motion to determine overall cyclone movement is not recommended since cell movement does not match total system movement. The SCIT and its STI product should also not be used in attempting to determine (MCS/Mesoscale Convective Complex (MCC)) motion within the overall ETC. The algorithms will track individual cells, but these storms move with the local wind-field -- not with the larger-scale system.

Unless the ETC center is strong and small, a single radar cannot observe its center. Rather, a mosaic of the lowest level reflectivity data is needed and used with time-lapse. Sometimes the CR product can better portray circulation about the storm center. But even when using mosaic products, a closed circulation is rarely seen. Somewhat smaller scale convective systems within the ETC have resolvable vortex centers. The Mesoscale Convective Vortices (MCVs) are often associated with MCSs which, in turn, may be associated with the ETC. These MCVs are detected within mid-levels and the residual mid-level cloud, virga, and rainfall. Within the context of the extratropical cyclone, centers of these MCV systems and their tracks are often critical for later thunderstorm and MCC re-initiation. The feature tracking capability can be used for tracking these MCVs.

4.9.2.2 Considerations. Often, synoptic systems in their more mature stages of development are characterized by comma-shaped cloud and precipitation systems. Typically, there is not sufficient return from all sectors of the cyclone to detect and track the complete circulation. However, when there is widespread precipitation along the cold front, extensive warm-frontal precipitation, and precipitation within the cloud head, then it is

possible that the entire cyclone system (with the exception of the dryer air sector to the rear) may be tracked via the radar network mosaics. Thus, the network reflectivity mosaic capability provides an excellent comparison with numerical model forecasts.

4.9.3 Cell Movement. A characteristic feature of ETCs is the presence of narrow convective precipitation bands in both the warm and cold sectors of the cyclone. Within these bands, embedded cells with high values of reflectivity are not uncommon.

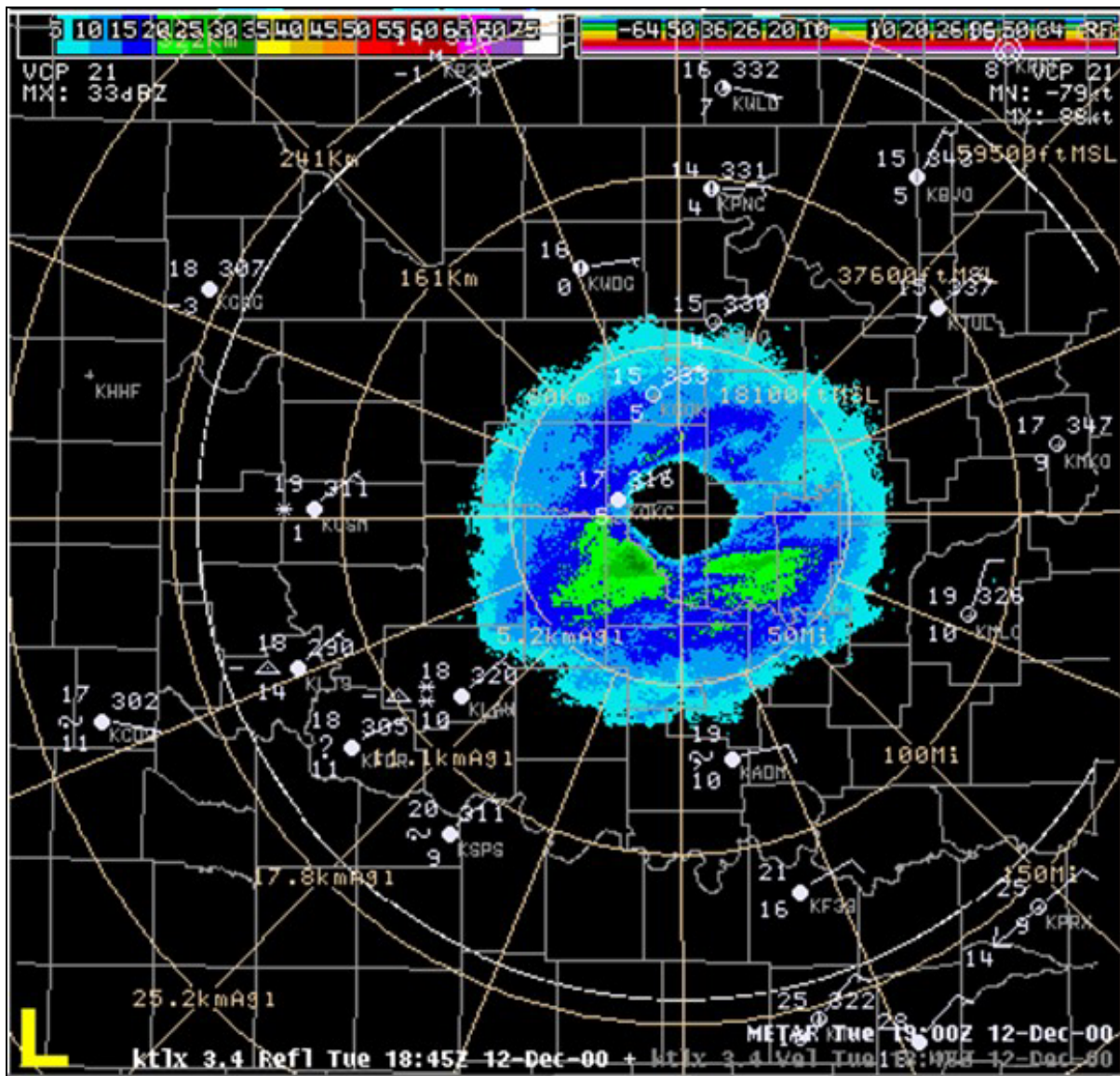
4.9.3.1 Cell Movement Recognition. Embedded cells can be easily identified and tracked by the SCIT algorithm from any individual radar. Generally, these cells move faster than the precipitation bands and to the left of the mean band motion.

4.9.3.2 Considerations. In cold ETCs, reflectivity values of individual cells rarely exceed about 45 dBZ_e. Higher reflectivity values, sometimes ranging from 50 dBZ_e to 60 dBZ_e, in precipitation bands, may be the result of large, wet, snowflakes and/or ice pellets within the melting level. Much of the reflectivity remains at or below 30 dBZ_e, but these will probably be tracked by the SCIT algorithm. Precipitation bands, like convective squall lines, are generally not tracked by the SCIT algorithm since it isolates individual reflectivity cores. Therefore, a time lapse of the Reflectivity product should be used to deduce overall complex or line motion.

4.10 Winter Storms. The WSR-88D provides data useful in monitoring the increase and lowering of ice crystal-laden clouds, in estimating precipitation onset at the surface, the height of the melting level, in tracking and predicting the motion of precipitation regions, mesolows, high wind areas, and heavy snow. Snow is generally more effectively detected by the WSR-88D, in contrast to past radars, but snow will be more difficult to identify than liquid precipitation. The dielectric constant of water is nearly 1.0, while that of snow is only ~0.20; thus, snow is a much less efficient reflector of microwave radar energy. Additionally, the small particle size and a more complex pattern and geometry of snowflakes further reduce microwave backscattering.

4.10.1 Onset of Surface Precipitation. With the WSR-88D, it is possible to monitor the development, advancement, and/or presence of cloud, inversions, or descending or evaporating precipitation layers, and infer height estimates from cursor readout information.

Cloud layers, inversions, and virga result in radar echo (reflectivity, velocity, and spectrum width) signatures best described as radar-centered "donuts" (Figures 4-10 and 4-37). Considerable information, produced from a variety of meteorological situations, can be derived from these signatures (Lemon and Quetone 1994). Examples include base and top heights of cloud layers, slope of a layer, estimation of precipitation onset, freezing level heights and descent rates, timing of precipitation phase change, and perhaps even strength of thermal gradients. The VWP is also a very useful tool for application to these same storms and situations. As mentioned earlier, it is possible to monitor the winds aloft and to compare them to numerical guidance. It is also possible to monitor the base of virga aloft and its rate of descent (Figure 4-37).



Oklahoma City, OK WSR-88D Reflectivity product at 18:45 UTC on 12 December 2000 (AWIPS display). This is a radar-centered “donut” echo created by virga aloft, with the inner edge of the donut at the base of the echo and the outer edge being the top of the detectable return of the precipitation. The surface observations are overlaid.

It is possible to estimate the onset of precipitation as it develops toward the surface. For example, the radar is located north and east of an eastward-moving mid-latitude cyclone with the associated frontal system south of the area. Commonly, these storms begin by a gradual increase in high and mid-level cloudiness, the formation of multiple cloud layers that advance progressively from the southwest or west, and a corresponding lowering in cloud bases. "Overrunning" has often been used to describe these events, owing to the presence of a surface warm front upstream (relative to mid-tropospheric flow). Echo monitoring can be done using R and V products in a multi-panel display and in time-lapse mode. Echo Tops can also be used in this process but again, the reflectivity threshold is ~ 18 dBZ_e. Reflectivity aloft near cloud and precipitation tops is often low, ranging from -10 to +15 dBZ early in the process. Especially in higher latitudes during the fall and winter months, precipitation aloft gradually develops from these advancing cloud layers but falls into dryer air and evaporates. This process both cools and moistens the troposphere at progressively lower levels until rain or snowfall reaches the surface. This, in turn, is often well observed by the WSR-88D. In the absence of algorithms, the operator can manually estimate the base descent rate and arrive at an estimated time of the onset of surface precipitation at the radar and other locations. The base of the descending precipitation will usually be lower toward the direction from which the clouds advance. The freezing level, if aloft, will also often slope in the same sense.

4.10.2 Cold Air Depth, Freezing Level. When, within the precipitation-filled volume, precipitation changes from snow to rain during its descent, and convection is neither vigorous nor widespread, there is also frequently a radar detected "bright band" (Figure 4-39). This relatively highly reflective freezing/melting layer is known as the bright band from observations made using range-height scanning and display early in weather radar history (Battan 1959). As in the detection of inversions, cloud layers, or precipitation aloft, and owing to the geometry of using an elevated scanning beam, this confined phase-transition layer is detectable as a ring of enhanced reflectivity of finite depth centered about the RDA (Lemon and Quotone, 1994).

As explained, the melting level of uniform height can be identified as a ring, or partial ring, of higher reflectivity values in the Reflectivity product (Figure 4-39). If the height of the melting level varies or slopes within the range of the radar, the ring will be asymmetric (closer to the radar on one side than on the other), or the bright band may appear as an arc or as an irregular band. The signature will coincide with one of slightly higher spectrum width values (perhaps of ~ 8 knots). The increase or decrease in altitude of this feature can be monitored.

Reflectivity Cross Section products can be useful in identifying the melting level. An exact base and top cannot be obtained due to the variance within the melting level of frozen versus liquid water droplets, distance of the phenomenon from the radar, thickness of the layer itself, and the ambiguity of radar height measurements due to beam width and refraction index variation.

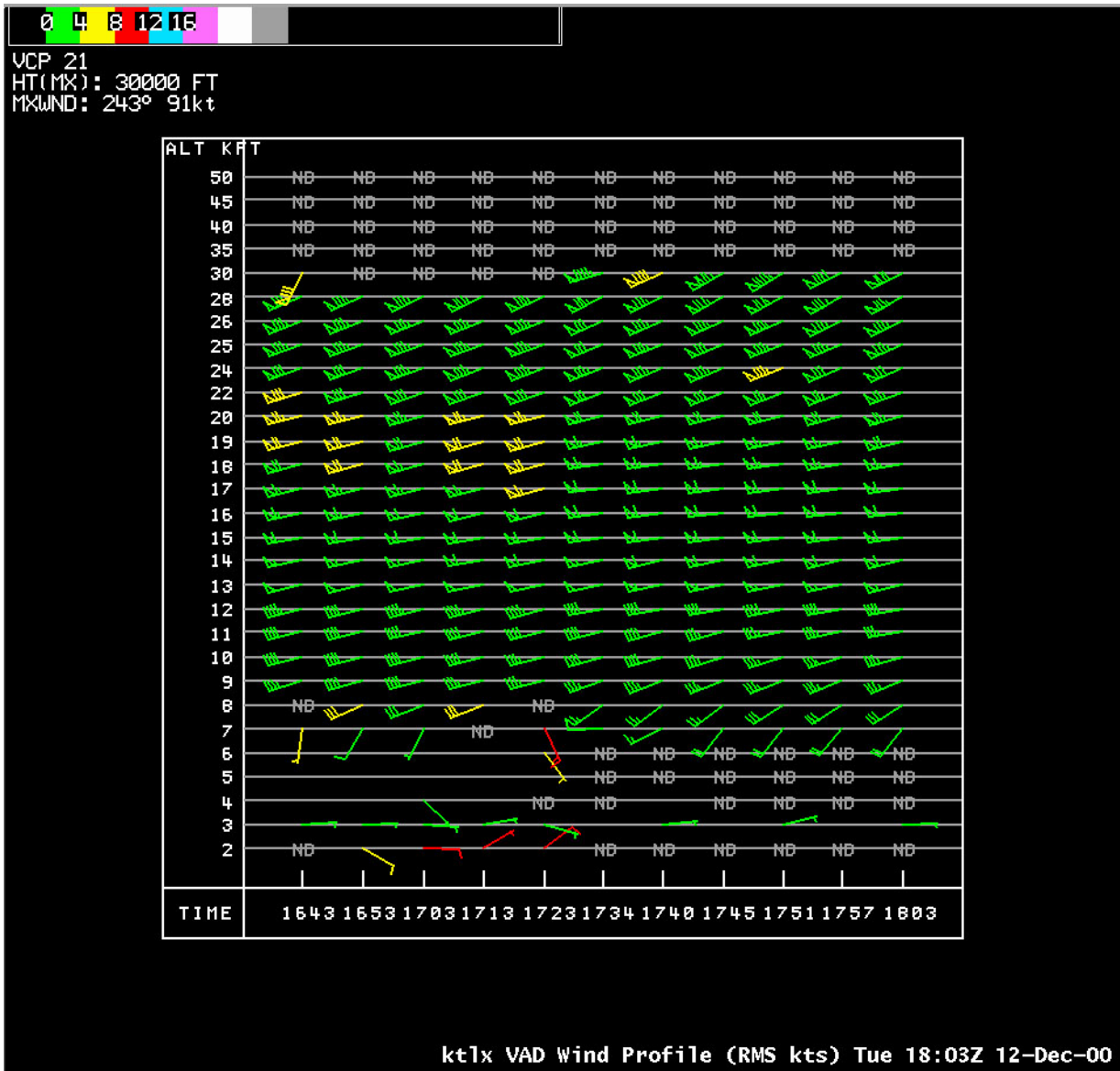


Figure 4-38
VAD Wind Profile Product

Oklahoma City, OK WSR-88D Velocity Azimuth Display (VAD) Wind Profile product at 18:03 UTC on 12 December 2000 (AWIPS display). The base of the virga aloft is about 7,000 ft and the wind profile shows west-southwest winds above the low-level easterlies in the colder air below the frontal inversion.

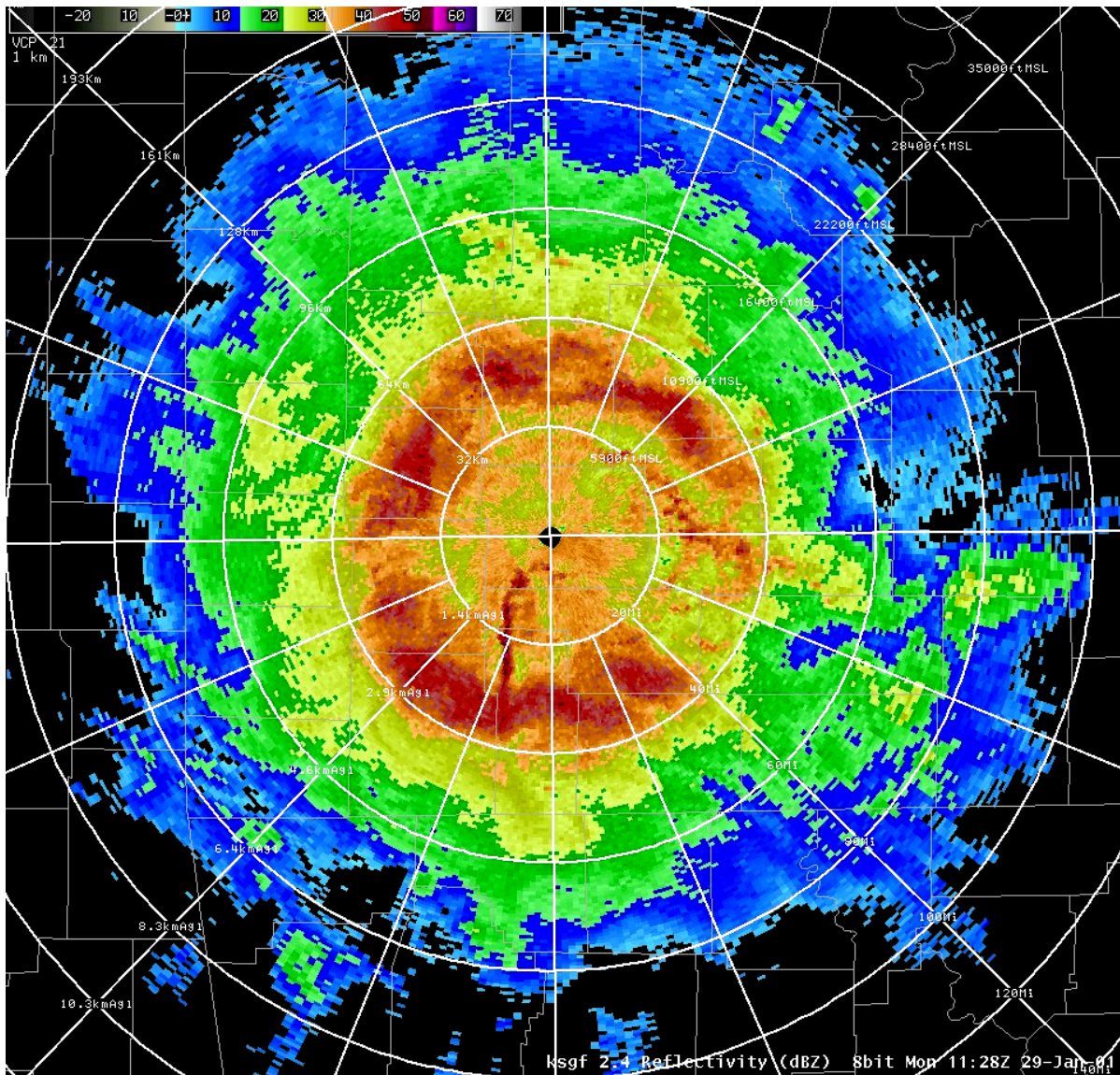


Figure 4-39
Bright Band

Springfield, MO WSR-88D Reflectivity product at 11:28 UTC on 29 January 2001 (AWIPS display). This product, 2.4° elevation angle, shows a bright band (dark red ring of 40 dBZ to 50 dBZ) surrounding the radar.

The observation of the band is useful because it denotes the environmental freezing level and a region of precipitation phase transition from frozen to liquid. It is also usually a region of abundant cloud water. Cursor-indicated height, when placed on the outer ring edge, suggests the transition height from dry snowflakes to moist snowflakes. (The dendritic snow crystal growth zone is above this region where temperatures are nearer -12° to -15° C). Inner ring height locates the transition altitude from wet snow to rain.

There is also the ability to monitor the critical depth of the cold air as is illustrated in Figure 4-38. In this case the cold air (with easterly winds) appears to be very shallow, although from 1.2 km to 2.1 km (4,000 ft to 7,000 feet) there is no data displayed. This, in part, may be due to the lack of tracers, yet there is also the likelihood of asymmetric flow due to the frontal surface itself. Cold air depth will often dictate if the precipitation is liquid or solid when it reaches the surface.

Through the use of multiple radars and/or use of a single radar over time, the slope of the bright band (and the freezing level) can be mapped. Identification of the freezing level and areas of mixed precipitation will permit specificity in nowcasting and short term forecasting. Additionally, within mountainous areas it is possible to accurately estimate the rain and snow levels and areas of mixed precipitation. At times, a time-lapse loop may be needed to reveal a bright band rather than passing shower cells if it is present.

4.10.3 Snowfall Estimation. Algorithms have been added to the WSR-88D that estimate both snowfall accumulation (Snow Depth, SD) and liquid water equivalent (Snow Water Equivalent, SWE) with that snowfall. Six new products are used. Those products are very similar to the rainfall products because they cover the same time-periods. When the user is within the snowfall portion of the storm, north of the surface low track, these products are very useful. In order to estimate snowfall and the water equivalent over a one-hour running period, the user requests the One-Hour Snow Depth (OSD) product (Figure 4-40).

The OSD is used on a continuous basis during significant snowfall. In order to maintain a record of the water equivalent of this snowfall, the Snow Water Equivalent (OSW) is requested (Figure 4-41).

When snowfall accumulations are expected to occur over an extended period and to be significant, then the Storm-Total Snow Depth (SSD) product can be requested (Figure 4-42). Like the OSW, there is also the water equivalent product (not shown), the Storm Total Snow Water Equivalent (SSW) product. This measure of snow water increases in importance as the weather warms after an extended period of snow and rains fall on significant snow packs with considerable melting. Floods frequently result. Thus, the amount of stored snow water becomes very important in estimating potential runoff and potential flooding, sometimes the sole source of runoff. Of course, periods of sublimation may deplete the snow water significantly.

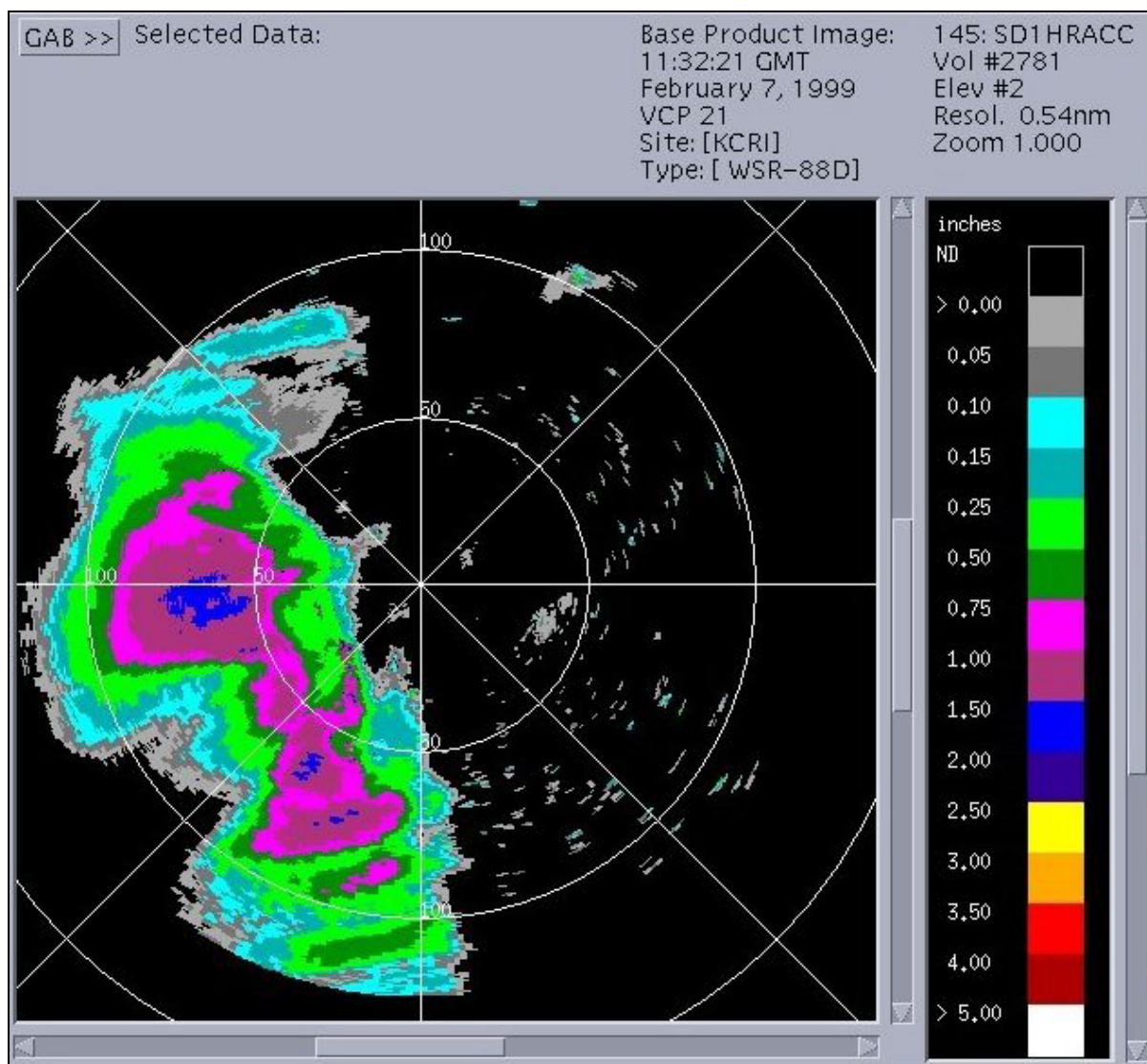


Figure 4-40
One-Hour Snow Depth Accumulation Product

Norman, OK WSR-88D (test bed radar) One-Hour Snow Depth Accumulation product (OSD) at 11:32 UTC on 7 February 1999 (CODEview graphic). The radar-estimated snow accumulation, snow depth that occurred over the last one hour period is included.

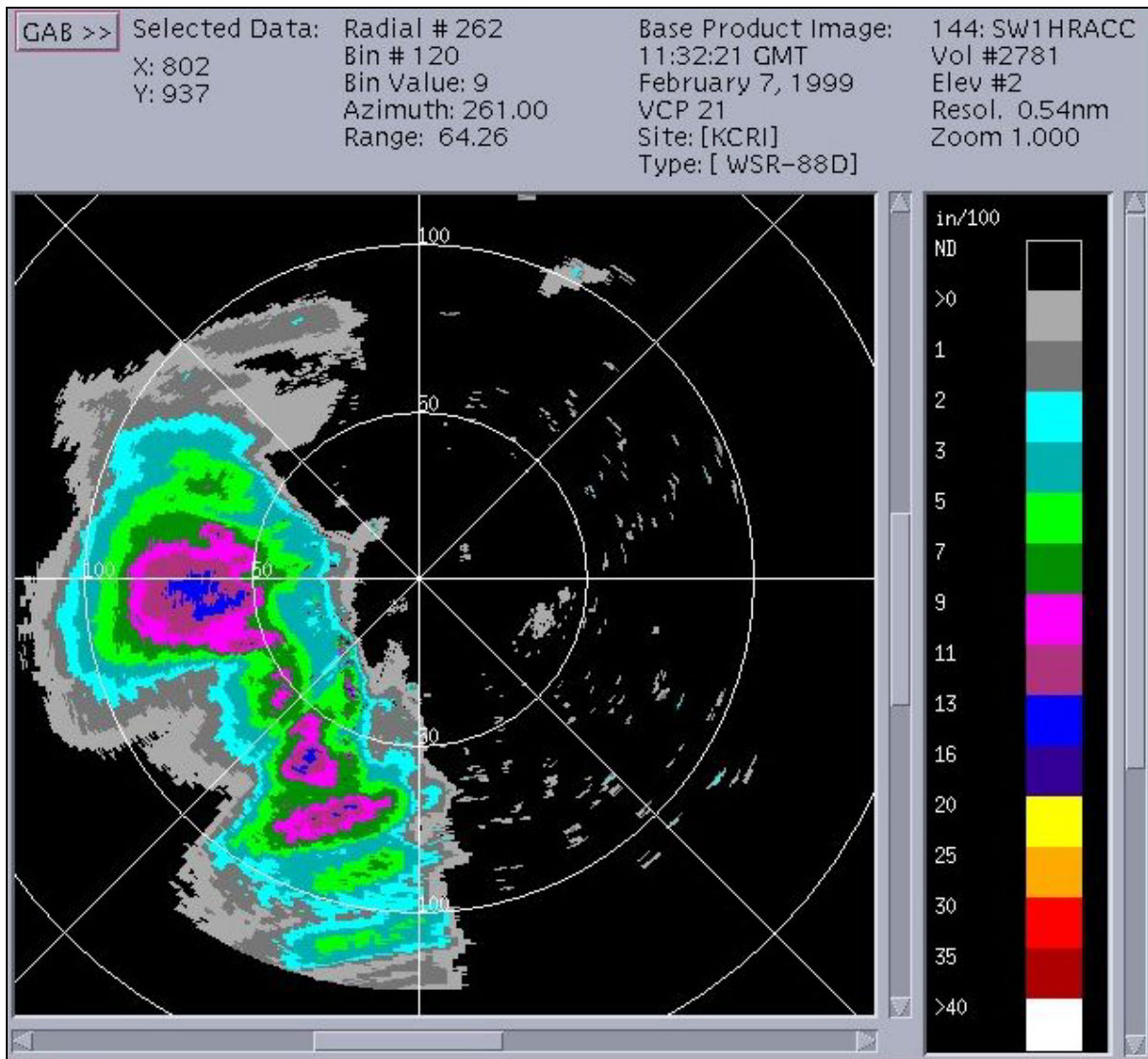


Figure 4-41
One-Hour Snow Water Equivalent Accumulation Product

Norman, OK WSR-88D (test bed radar) One-Hour Snow Water Equivalent Accumulation product (OSW) at 11:32 UTC on 7 February 1999 (CODEview graphic). The liquid water content of Figure 4-40 is shown here.

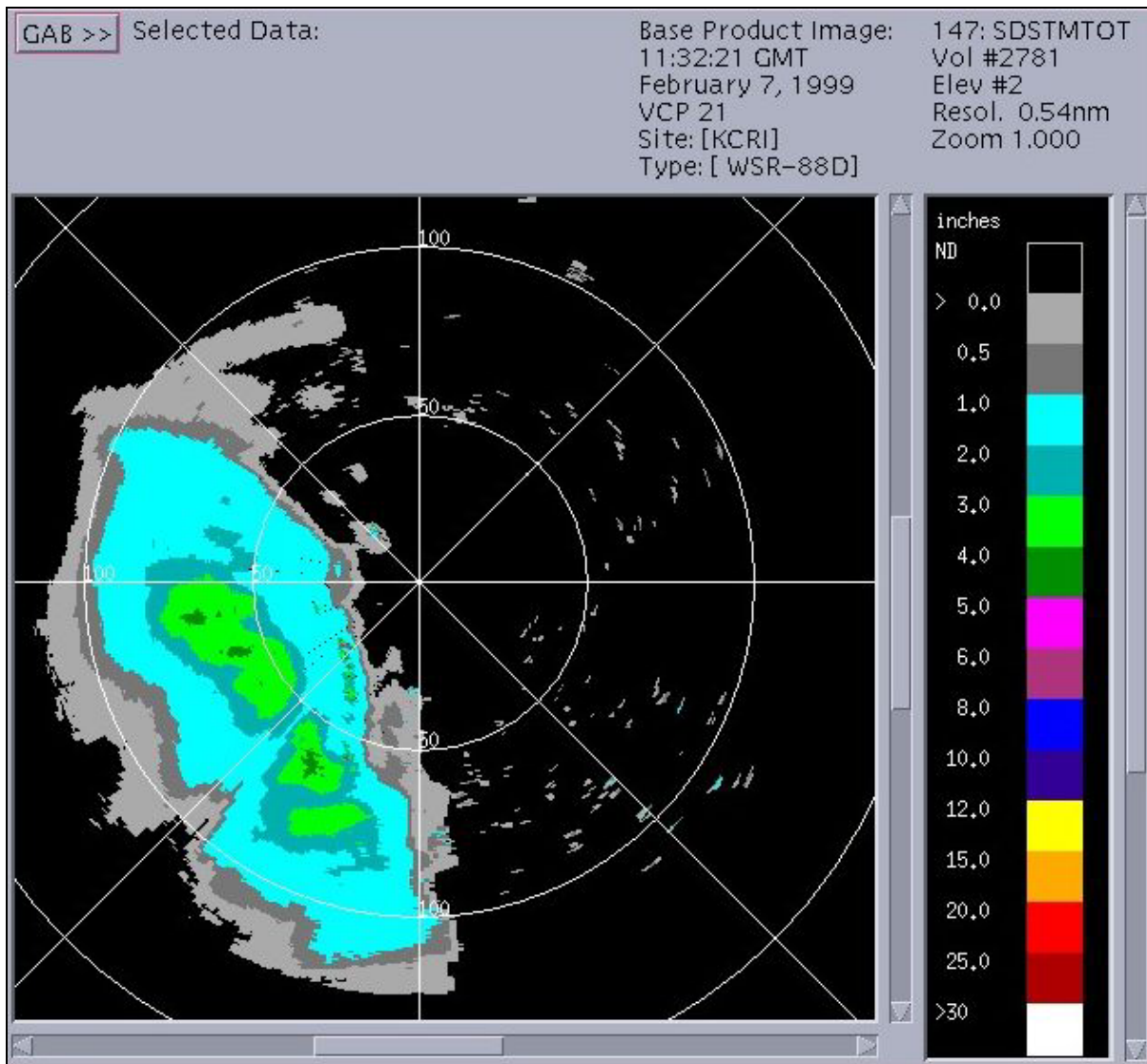


Figure 4-42
Storm Total Snow Depth Accumulation Product

Norman, OK WSR-88D (test bed radar) Storm Total Snow Depth Accumulation product (SSD) at 11:32 UTC on 7 February 1999 (CODEview graphic).

At times, the user wants to select a specific period of snowfall accumulation such as from 0000 UTC to 2400 UTC. The User Selectable Snow Accumulation (Depth) product, USD, is used for such a purpose (Figure 4-43). The accompanying product used to estimate the snow water equivalent for a user selectable interval is the User Selectable Snow Water Equivalent (USW) product (Figure 4-44).

Mesoscale snowbands, perhaps only a few miles in width, but producing heavy snow, are common in winter cyclones (Figure 4-45). These bands are typically 90 km to 160 km (50 to 100 nm) to the left of the surface low's track. Intense wind shears and strong frontal zones, also found in these mid-latitude winter storms, often result in significant mesoscale vertical motions and corresponding slantwise convection (sometimes accompanied by lightning). These snowfall products will be quite helpful for monitoring the type of snowfall.

4.10.4 Recognition of Heavy Snow and Snow Showers. During snowfall situations, it is not unusual to see narrow bands of higher reflectivity values in a Reflectivity product that often indicate areas of heavier snowfall. This banding, often related to slantwise convection, may also be identified occasionally in the velocity field. The 4-panel or multi-panel Reflectivity products are the best way to monitor these bands.

In the case of both sleet and rain occurring within the sampling area of the radar, embedded areas of higher reflectivity will often appear (40 to 50 dBZ_e may be common) as a result. A linear discontinuity in reflectivity returns will sometimes be seen along the rain/snow line. Spectrum widths will again be enhanced along this line.

Often found embedded within areas of snow are slantwise convective cells producing moderate to heavy snowfall at the surface. Sometimes these heavy convective snow regions will be associated with lightning. These cells generally move faster and to the left of the mean band motion. With reflectivity values often exceeding 40 dBZ_e in these convective cells, they will be tracked well unless segments from adjacent cells overlap.

4.10.4.1 Considerations. The OSD and the USD can support nowcasts by quantifying snow rates, highlighting areas of higher and lower rates, and showing movement and trends of these areas. The SSD and longer-term USD products can support updates to forecasts of total accumulations and verification of snow amounts, especially where there are gaps in snow spotter coverage. Time lapse loops of these snowfall and water equivalent products will also better highlight motion and tracks of greater accumulation.

These products suffer less from blowing and drifting snow (most of the blowing snow is below radar horizon) that plagues spotter surface measurements. However, below beam effects such as low boundary layer humidity, can lead to overestimation of snowfall.

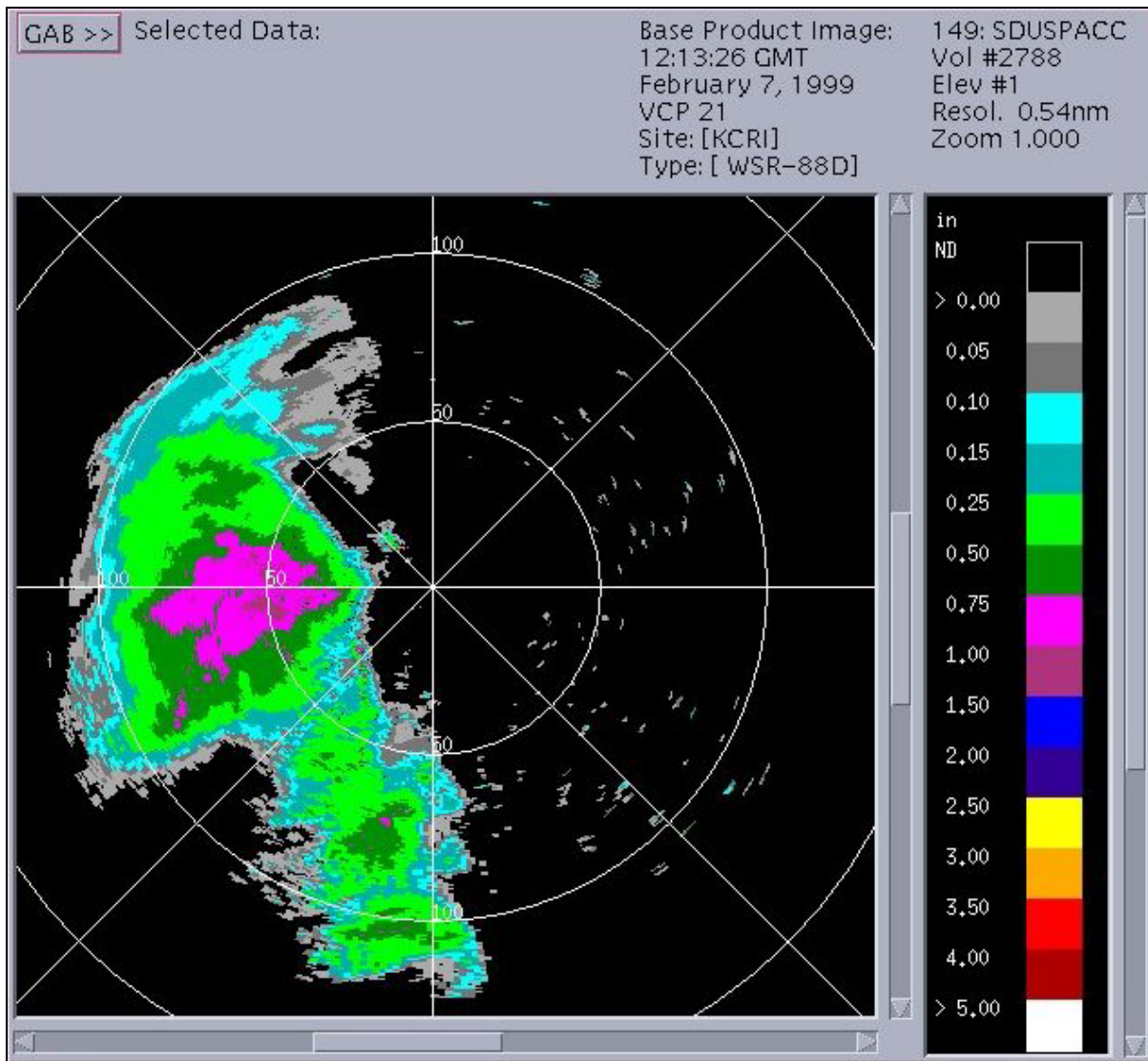


Figure 4-43
User Selectable Snow Depth Accumulation Product

Norman, OK WSR-88D (test bed radar) User Selectable Snow Depth Accumulation product (USD) at 12:13 UTC on 7 February 1999 (CODEview graphic).

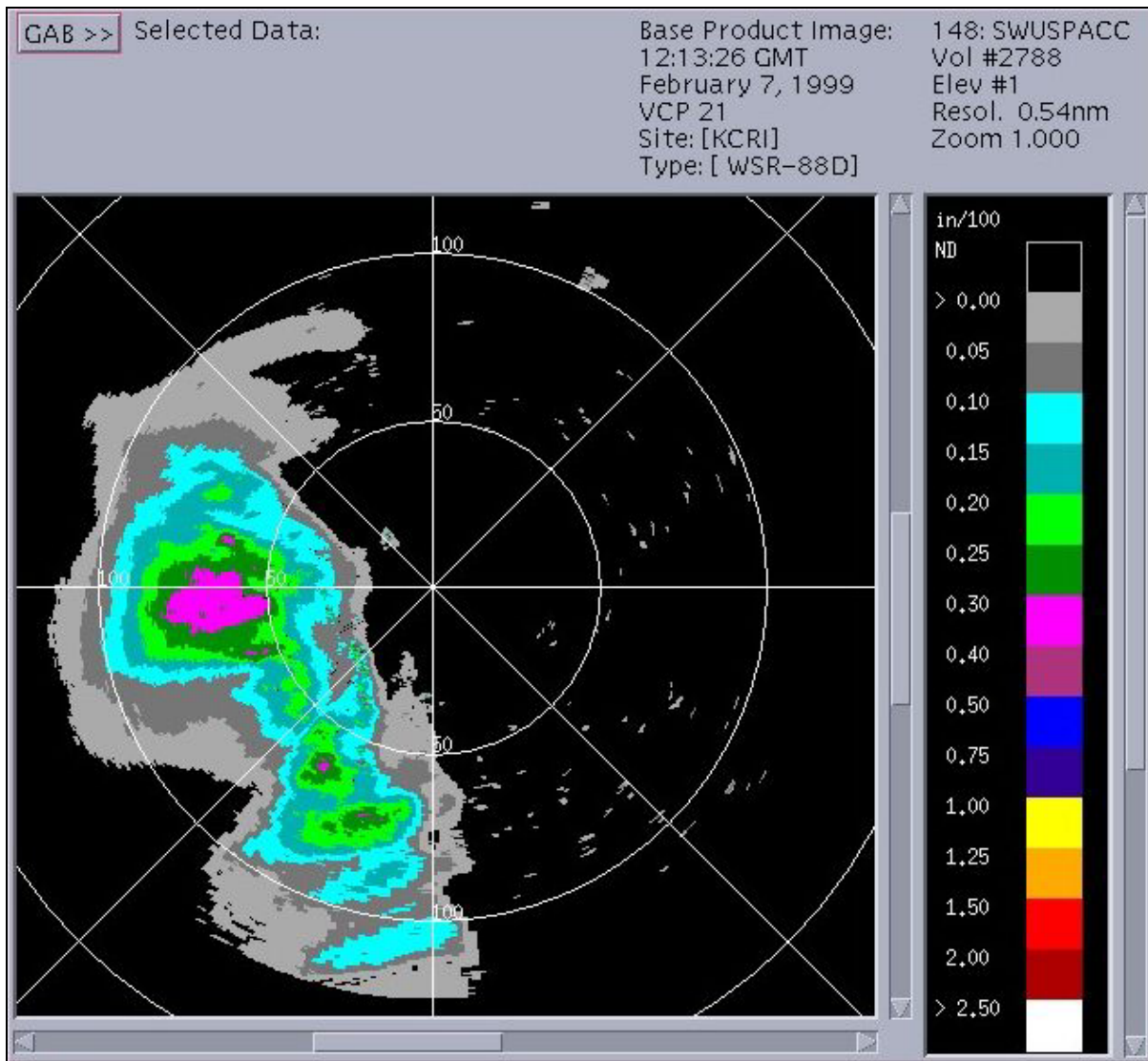


Figure 4-44
User Selectable Snow Water Equivalent Accumulation Product

Norman, OK WSR-88D (test bed radar) User Selectable Snow Water Equivalent Accumulation product (USW) at 12:13 UTC on 7 February 1999 (CODEview graphic).

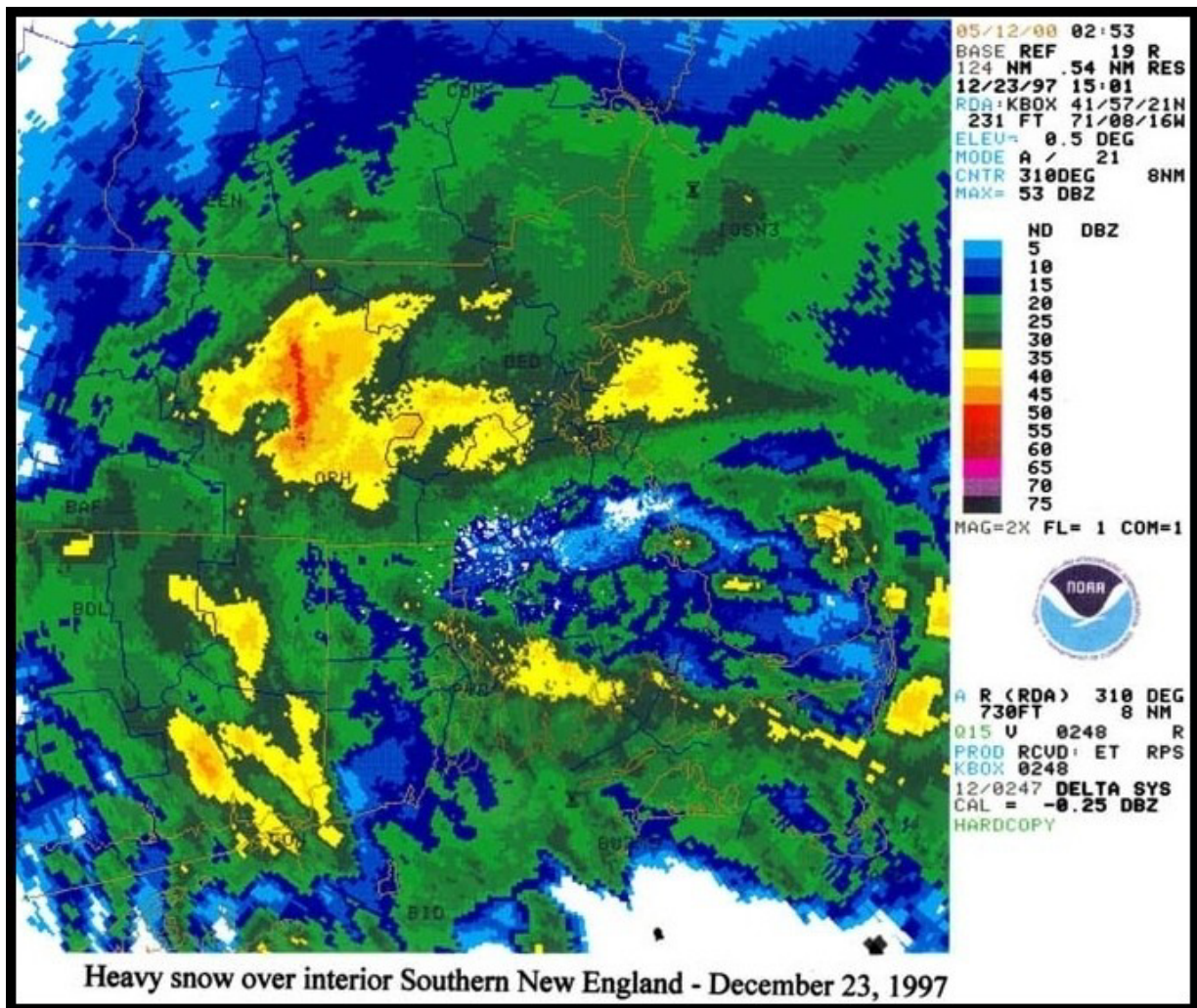


Figure 4-45
Convective Snowfall Reflectivity

Boston, MA WSR-88D Reflectivity product at 15:01 UTC on 23 December 1997 (legacy PUP display). The embedded heavy (yellows) and very heavy (red) areas depict convective snow.

Moreover, variable Z-S (Reflectivity – Snowfall rate) relationships will also significantly contribute to snowfall and water equivalent inaccuracies. For example, air temperature contributes to the amount of liquid water that is contained in the snow, and more importantly, its reflectivity. For comparable snowfall rates the reflectivity can vary appreciably. Thus, one of the most significant limiting factors in snowfall estimation is the Z-S relationship.

User selectable products can be requested to coincide with other regular operational products (e.g. 24-hour totals to coincide with daily climate summaries). Reliable snow measurements (such as trained spotter reports), if available, should be used in conjunction with Snow Accumulation Algorithm (SAA) products to validate and calibrate the algorithm estimates. However, if no reliable and timely snow measurements are available, WSR-88D snow products may be the only or best source of snow estimates. For example, during severe snow storms with strong winds, spotters may be unable to make accurate, or even regular, measurements and report them in a timely manner, or spotters may not be directly under the echoes of interest (such as the heaviest snow bands).

The SAA products will have limited range, perhaps out to about 75 to 90 km (40 to 50 nm) owing to overshooting the dendritic snowflake formation zone and overshooting the convective cloud layer. This is the result of the relatively shallow cloud layers characterizing many snow storms. This will especially be the case with the very shallow lake-effect storms. Other complicating features include contamination due to the bright band and evaporation below the radar horizon which can't be compensated for. Additionally, in the cases of strong low-level winds, there is the problem of horizontal drift of falling snow. Depending on conditions and radar sampling depths, falling snow may be carried up to a few kilometers before reaching the surface while below the radar horizon. Finally, irregular precipitation particle shapes will not fit well with the Z-S fundamental assumptions.

The above-mentioned lake-effect snow storms occur in the form of shallow convective bands that nearly parallel low level winds. At times, they may be only a few thousand feet in depth, yet can produce extremely heavy snow with near-zero visibilities. Occasionally, strong winds and lightning will also accompany these occurrences. Sampling these events using the Clear Air scan strategies is often effective as is the case with many non-lake effect snow situations. However, owing to the shallow nature of these events, radar is effective at times only to about 35 to 50 km ranges.

Movement of snow bands may be deduced by a time lapse of the Reflectivity and the SSD, the storm total snowfall product. The SCIT algorithm may not provide adequate information if these snow bands lack a cellular nature and overlap. Lake-effect snow bands may remain nearly stationary over prolonged periods.

Embedded higher reflectivity may be the result of the melting level and not heavier snow, sleet, or convective cells. On the other hand, they may be convective in nature (Figure 4-45) and may even be associated with lightning. Surface conditions and surface reports are invaluable in these

cases. Additionally, examining somewhat higher elevation angles may reveal the bright band and its location relative to the embedded higher reflectivity and may provide an indication of their relationship.

4.10.5 Rain/Snow Line. Determining the location of the rain/snow line is often difficult. The base data products from the WSR-88D may prove somewhat useful in this, but integration of all types of data are usually needed to locate this change. But, when present, the bright band can assist, especially when one side of the ring is much closer to the radar than the other, indicating a sloping freezing level. Additionally, the area of transition in low-level Reflectivity products is often marked by higher reflectivity values, whether cellular or stratiform, where there are large, wet snowflakes falling in a mixture with rain, or where rain, sleet, and snow are mixed. In these regions reflectivity may even exceed 60 dBZ_e. Additionally, areas of rain are often more cellular in nature with higher reflectivity gradients. This can help in identifying regions that are only rain or only snow.

4.10.5.1 Recognition of a Rain/Snow Line. It might be possible to determine the rain/snow line through use of the Spectrum Width products. These products may provide a means to help identify temperature discontinuities. Used in conjunction with the Reflectivity product, Spectrum Width products might be used in certain situations to estimate where, within the reflectivity field, the rain/ snow line is located. The transition region is often characterized by somewhat higher SW values. But, there are a variety of reasons for broadened spectrum widths, so caution must be exercised and SW should never be used alone. Integration of all observations is needed.

4.10.5.2 Considerations. Cross sections of base data products may provide an indication of frontal position. However, the VWP is most effective in identifying the frontal surface aloft above the radar and changes in the cold-air depth. In most situations, surface reports will be most useful in locating the rain/snow line.

4.11 Tropical Cyclones. In the fully developed stage, a tropical cyclone is a nearly circular, warm core vortex that extends throughout the depth of the troposphere and has a typical horizontal scale of hundreds of miles. Maximum horizontal winds occur 10 to 55 km (5 to 30 nm) from the center and 0.5 km to 1 km (1,600 to 3,300 ft) above the surface (Willoughby et al. 1984) (Figure 4-46).

The WSR-88D provides Velocity and Reflectivity products allow the tracking and anticipation of wind and precipitation patterns associated with tropical cyclones before during and after they make landfall. As these destructive phenomena come within range of coastal radars, information on system center, spiral rain bands, and wind distribution will increase. In mature tropical cyclones, eye-wall diameter and quantitative estimates of intensities are available.

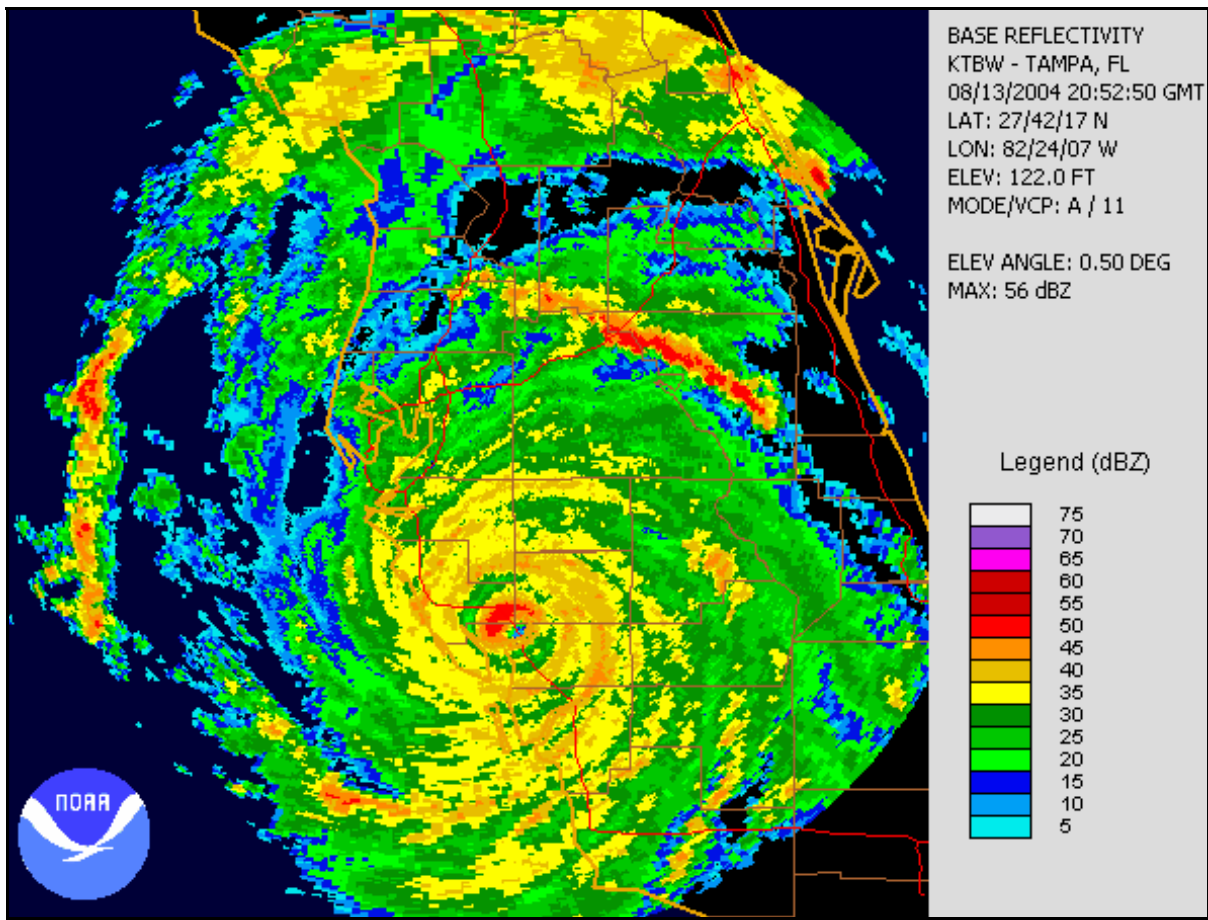


Figure 4-46
Hurricane Charley Reflectivity

Tampa, FL WSR-88D Reflectivity product at 20:52 UTC on 13 August 2004 (NCDC NEXRAD viewer). This image was taken as Hurricane Charley made landfall. The eye diameter is about 11 km (6 nm).

The effects of the Doppler velocity-range ambiguity (Part B of this Handbook) are especially critical during the observation of tropical cyclones. The legacy WSR-88D scan strategies (without VCPs 12 and 121) allow the unambiguous measurement of Doppler velocities out to a range of only 150 km (81 nm) (Nyquist co-interval of $\pm 25 \text{ ms}^{-1}$ (49 kts)). To raise the Nyquist co-interval to $\pm 31 \text{ ms}^{-1}$ (60 kts), the radar is only able to unambiguously measure Doppler velocities out to 120 km (65 nm).

Thus, tropical cyclones offer the combined problems of extensive precipitation areas with diameters often exceeding 300 km (160 nm) and wind speeds often exceeding 51 ms^{-1} (100 kts). In order to minimize regions of range-folded Doppler velocities, it is necessary to operate with a low Nyquist velocity. However, the new VCP, 121, greatly aids in reducing range-overlaid data, as well as simultaneously increasing the measurement of high velocities.

The MPDA, as part of VCP 121, is well suited for tropical cyclone observations. The purpose for this VCP is to enable a WSR-88D unit to optimize scanning and the volume sampling interval for changing radar echo patterns while, at the same time, permitting a large decrease in range-overlaid echo and in incorrectly dealiased velocities. It was designed to mitigate range folding and improperly dealiased velocities. Thus, this is ideal for the purpose of tropical cyclone observations. For example, VCP 121 decreases the amount of overlaid echo by 50% to 70% over that with VCP 21.

It is important for most tropical cyclone-affected weather forecast offices to change the velocity measurement increment value for the WSR-88D system from the default setting of 0.5 ms^{-1} to 1.0 ms^{-1} . This allows the system hardware to measure velocities of $\pm 124 \text{ ms}^{-1}$ or $\pm \sim 248$ kts rather than ± 122 kts. More information on WSR-88D operations during tropical cyclones can be found in the National Hurricane Operations Plan; Chapter 7 – Surface Radar Reporting; and Appendix H – WSR-88D Operations Plan for Tropical Cyclone Events (<http://www.ofcm.noaa.gov/>).

4.11.1 Embedded Convective Storms and Tornadoes. Precipitation in tropical cyclones is organized in rain bands that may not completely encircle the storm center. While extensive areas of stratiform rain exist in a tropical cyclone, embedded areas of deep convection are often present. Most tropical cyclone-associated tornadoes develop near areas of intense convection in the outer spiral rain bands, and are generally weaker than those observed in the Midwestern United States. However, mesocyclones can occasionally be found in the eyewall, and strong tornadoes can, and do, occur anywhere within tropical systems. As the storm makes landfall, the right-front quadrant of the storm is the area most prone to these tornadoes.

4.11.1.1 Recognition of Embedded Convection and Tornadoes. As the first and subsequent spiral rain bands move toward the shoreline, interest will be in locating the strongest convective activity embedded in the bands, and any mesocyclones and tornadoes located at the fringes of the bands. The R, VIL, and ET products can provide an indication as to the intensity of the convection. However, when examining these rain bands for supercells (often

mini-supercells), the multi-panel high resolution reflectivity (DR), and velocity (DV) products are most useful. Because these storms can move very rapidly, SRR products for particular rain bands can be used. But this is also made difficult because of the almost continuous change in direction of motion. (Spratt et al. 1997).

Maximum reflectivity in the eye wall is typically 45 to 50 dBZ_e (Part B of this Handbook), a lower value than mid-latitude extratropical thunderstorms. The lower reflectivity is due to smaller drop sizes and to the lack of hail in tropical cyclones. Outside the eye wall, there are usually several rain bands that have isolated areas of deep convection and extensive areas of stratiform rain. These rain bands have fewer vertically-oriented reflectivity cores than the eye wall. However, it is not unusual for cells in the outer rain bands to exceed the reflectivity of the eye wall itself.

The favored location for tornado development is either the right front or right quadrants of the storm at landfall or in any quadrant within 25 nm of the center. Small scale (mini) supercells even with BWERs and hook echoes are detectable using R, V, and SRR products (Figure 4-47). Low-level convergence, when the radar is near one of these storms, can also be detected. This, too, is substantially weaker than that typical of extratropical severe convection. As before, multi-panel base product display is preferred for the lowest 4 elevation angles in order to monitor storm structure and mesocyclone development and strength. Vertically Integrated Liquid (VIL), ET, and LRM may also be used to monitor cell significance, but these are of relatively degraded resolution and value as compared to base products. Time-lapse loops of 6 to 10 frames are useful.

4.11.1.2 Considerations. Tropical cyclone-induced tornadoes typically form very rapidly, are weak, and have a short life span, much like gust front tornadoes. As seen in Figure 4-47, these are mini-supercells with small scales in reflectivity and velocities, but with the supercell features including the mesocyclone. Thus, they are supercells of the mini variety. The observer should be mindful that these storms and associated mesocyclones can, although rarely, become quite strong.

4.11.2 Heavy Rainfall. One of the most devastating aspects of tropical systems can be the very heavy rainfall. Thus, continuous use of the system rainfall products, especially the STP/DSP is extremely important in these cases (Figure 4-48). Flooding caused by heavy rainfall from a tropical cyclone making landfall is common. Both extensive areas of stratiform precipitation and intense rain-bands are responsible for this phenomenon. Climatologically, much of this rainfall can, at the same time, be very beneficial.

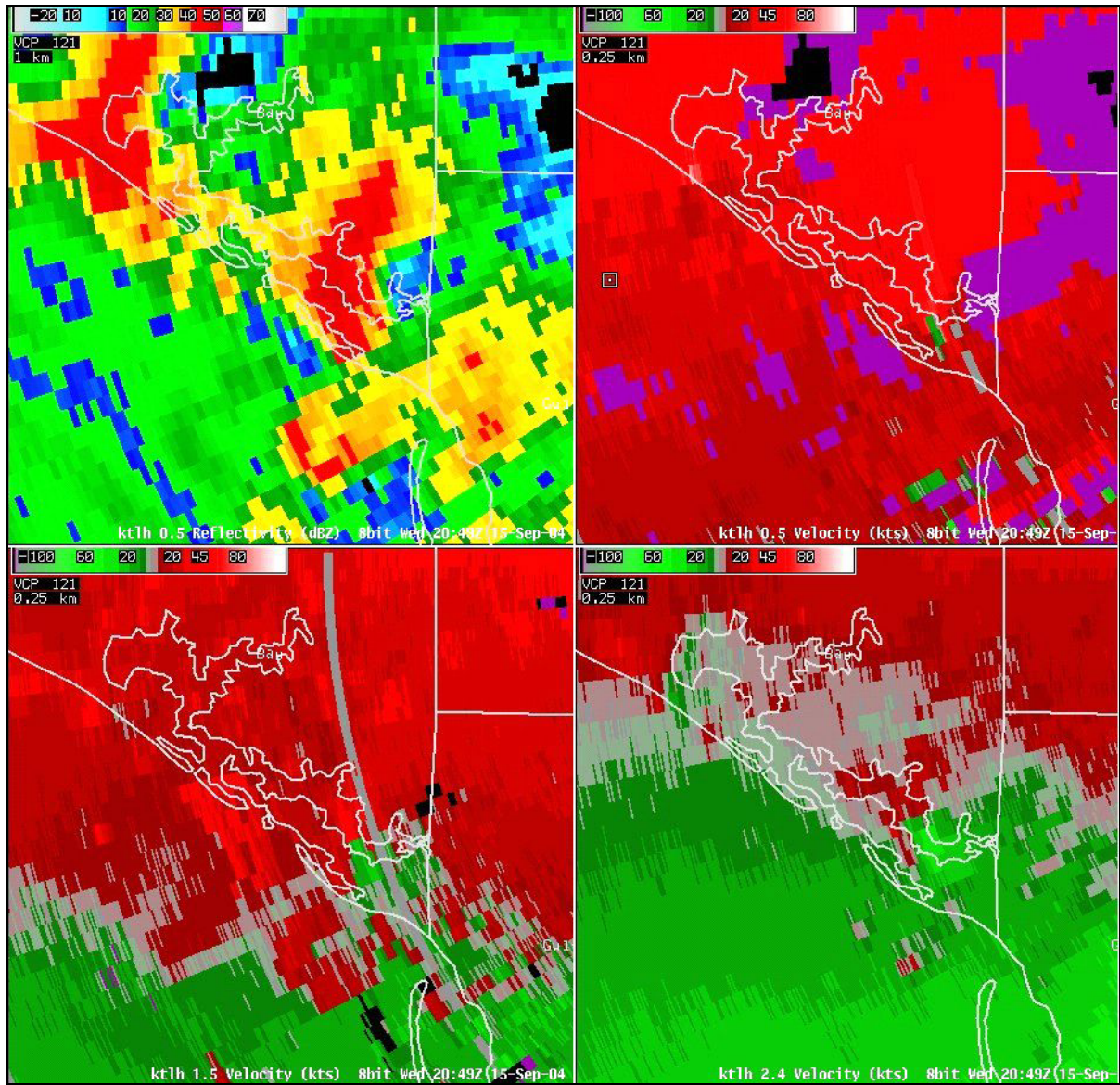


Figure 4-47
Mini-Supercell and Mesocyclones Associated with Hurricane Ivan

Tallahassee, FL, WSR-88D 4-panel of products at 20:49 UTC on 15 September 2004 (AWIPS display). A mini-supercell associated with Hurricane Ivan is shown. Top left is a 0.5° Base Reflectivity Data Array product, top right is a 0.5° Base Velocity Data Array product, bottom left is a 1.5° DV, and bottom right is a 2.4° DV. The mesocyclone is very small and can be seen in the DV products (red and green associated) with the southern portion of the storm. This was one of several supercells in the outer band of Ivan, which moved onshore and produced up to F2 tornadoes.

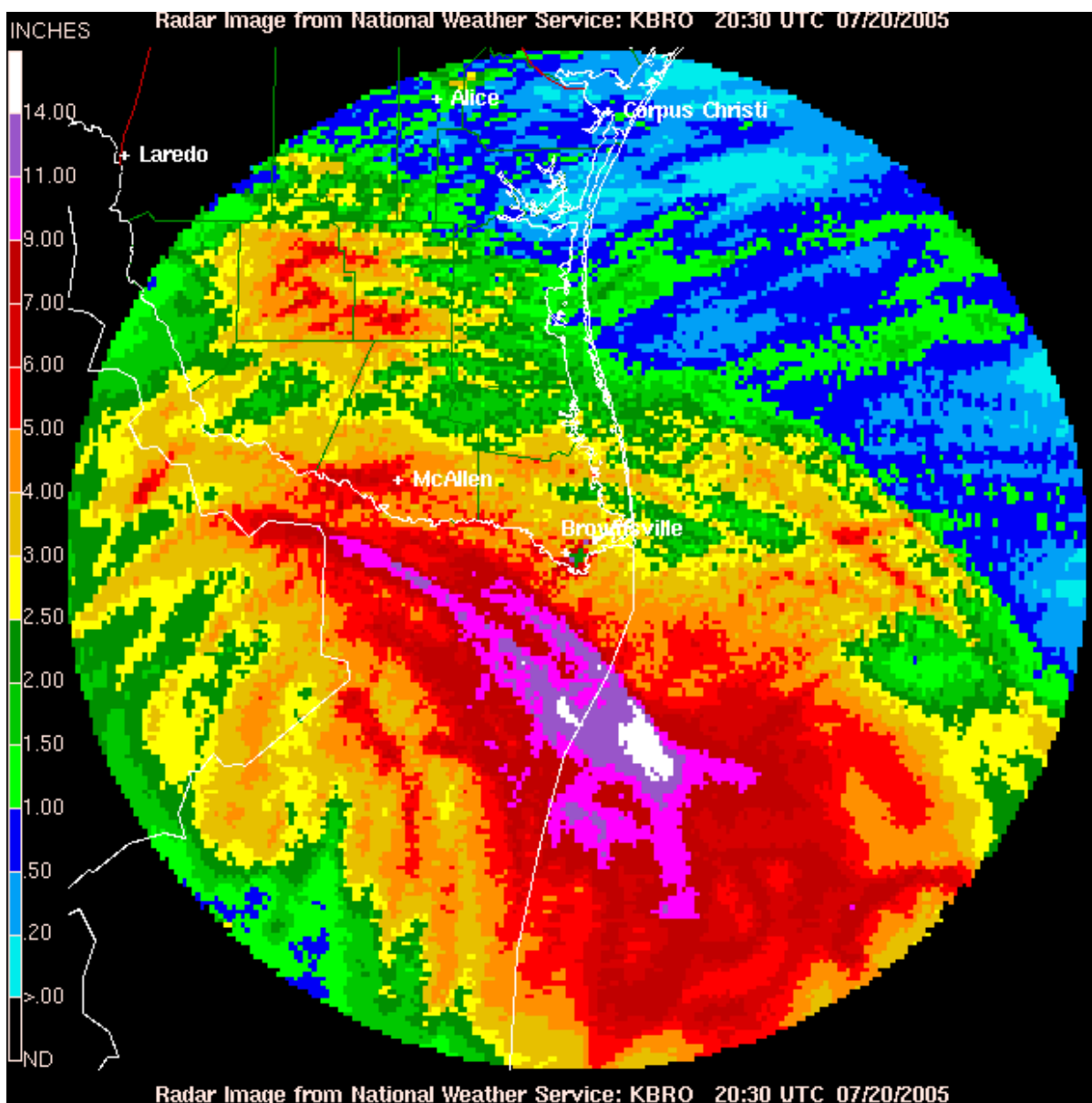


Figure 4-48
Storm Total Rainfall Accumulation Product of Hurricane Emily

Brownsville, TX WSR-88D Storm Total Rainfall Accumulation product for the period ending 20:30 UTC, 20 July 2005, TX (National Weather Service Radar Web page). The rainfall was due to Hurricane Emily which made landfall about this time 75 miles south of the Texas border about 12 hours earlier.

4.11.2.2 Considerations. Effectiveness of the SCIT algorithm to accurately identify and track movement of convective cells in tropical cyclones is limited. Because of the rapid changes in cell character, intersecting storms, or storms in close proximity to each other, their rapid and curvilinear motion, storm cells, and tracks are frequently reinitialized. However, the SCIT algorithm, when applied outside of strong tropical cyclones, can be effective in many other convective situations, such as echo training.

4.11.3 Convective Scale and Straight Line Winds. Common to tropical cyclones making landfall is widespread damage from strong winds (Figures 4-49, 4-50, and 4-51). The potential for convective downdraft occurrences with individual cells is limited owing to the nearly saturated deep layers within the storm environment, but the mesocyclonic winds with mini-supercells are a threat, as are the locally “straight-line” winds associated with tropical cyclones moving inland.

4.11.3.1 Recognition of Potential Damage from Embedded Convective Cells and Straight Line Winds. The high-resolution Base Velocity, DV, is the primary product to assess these velocities and winds because these winds are ground relative and they are the winds that do the damage. However, Mean Radial Velocity is also useful (Figure 4-49). (But note that monitoring these velocities is best done when the velocity product color levels have been adjusted for the stronger velocities.) The SRM and SRR can be attempted in evaluating storm relative flow and mesocyclone presence and strength but are not appropriate for evaluating ground relative damaging winds. (However, SRM and SRR are of limited use with the generally curvilinear and rapid motion of all cells.) The strongest winds are nearly always associated with the higher reflectivity rain-bands and the eye wall (Figures 4-46 and 4-49). Multi-panel R, DR, V, and DV products will be most useful in determination of the wind field characteristics and wind speeds. Through use of time sequenced velocity and Reflectivity products, wind field motion, and changes can be tracked. This is useful in assessing regions of greatest damaging wind threat from hurricane winds (Figure 4-50).

An important source for damaging wind enhancement with tropical cyclones that is often overlooked is the embedded mesocyclone (Spratt et al. 1997). These circulations are often emphasized as potential tornado producers but can be overlooked as sources for enhanced ground relative winds. But these mesocyclones do, in fact, pose an enhanced threat for damaging surface winds above that of the tropical cyclone itself.

For indications of vertical shear associated with surface frictional affects and the typical wind-field, irregularities and distribution, the multi-panel high-resolution DV and DR products may be used. These shears are important because it is believed that they contribute to the low-level shear favorable to the production of mini-supercells and associated tornadoes. But, for the most part, this friction induced shear must simply be inferred rather than actually observed owing to radar horizon. The same is true for the actual tornadoes themselves. Tornado Vortex Signatures are rare with these mini-supercells because most associated tornadoes are small and relatively weak.

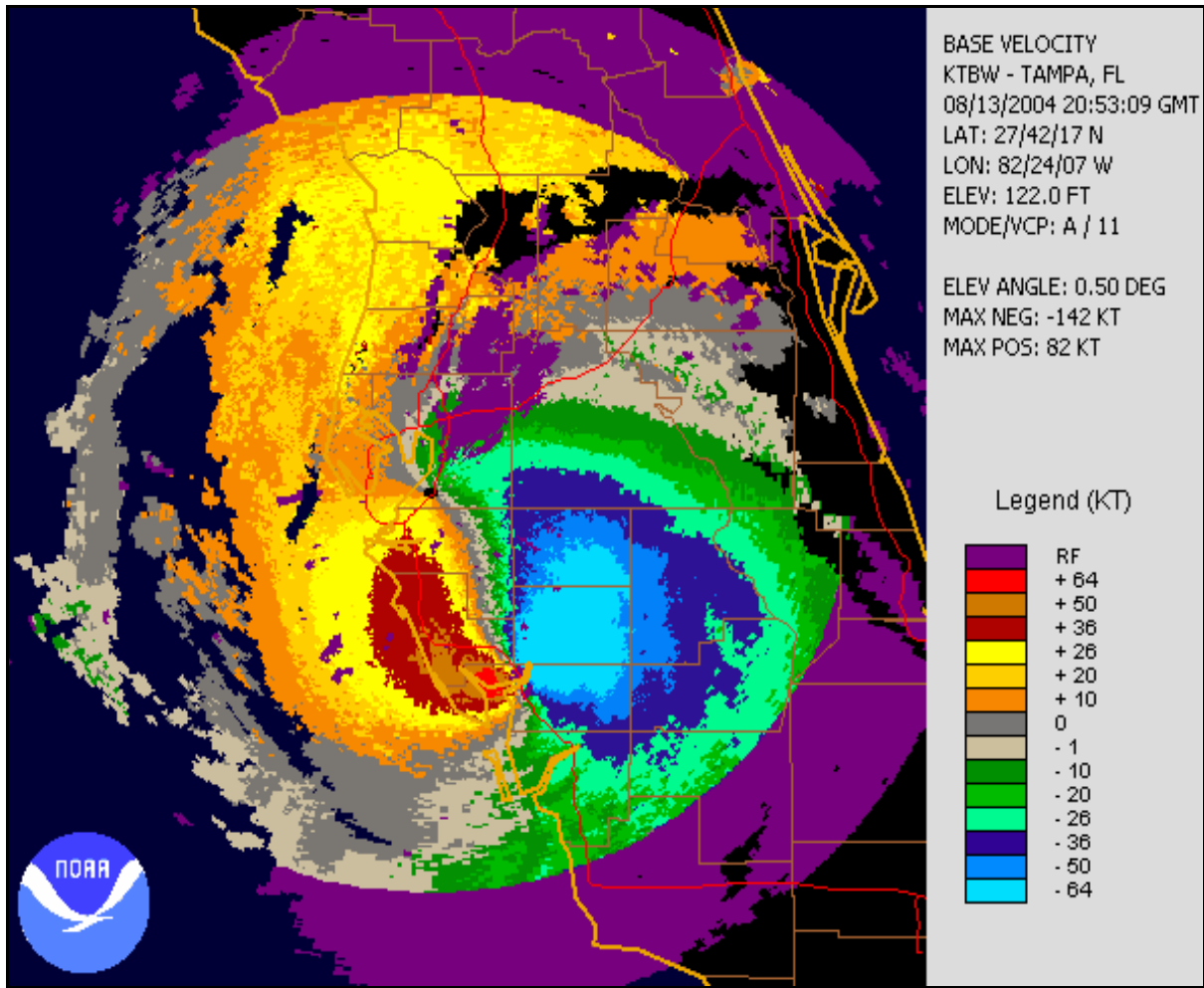


Figure 4-49
Mean Radial Velocity Product of Hurricane Charley

Tampa Bay, FL WSR-88D Mean Radial Velocity product at 20:53 UTC on 13 August 2004 (NCDC graphics). This 0.54 nm resolution at 0.5° elevation product was made as Hurricane Charley was making landfall. At this time, radar indicated velocities were up to 263 kmhr^{-1} (142 kts).

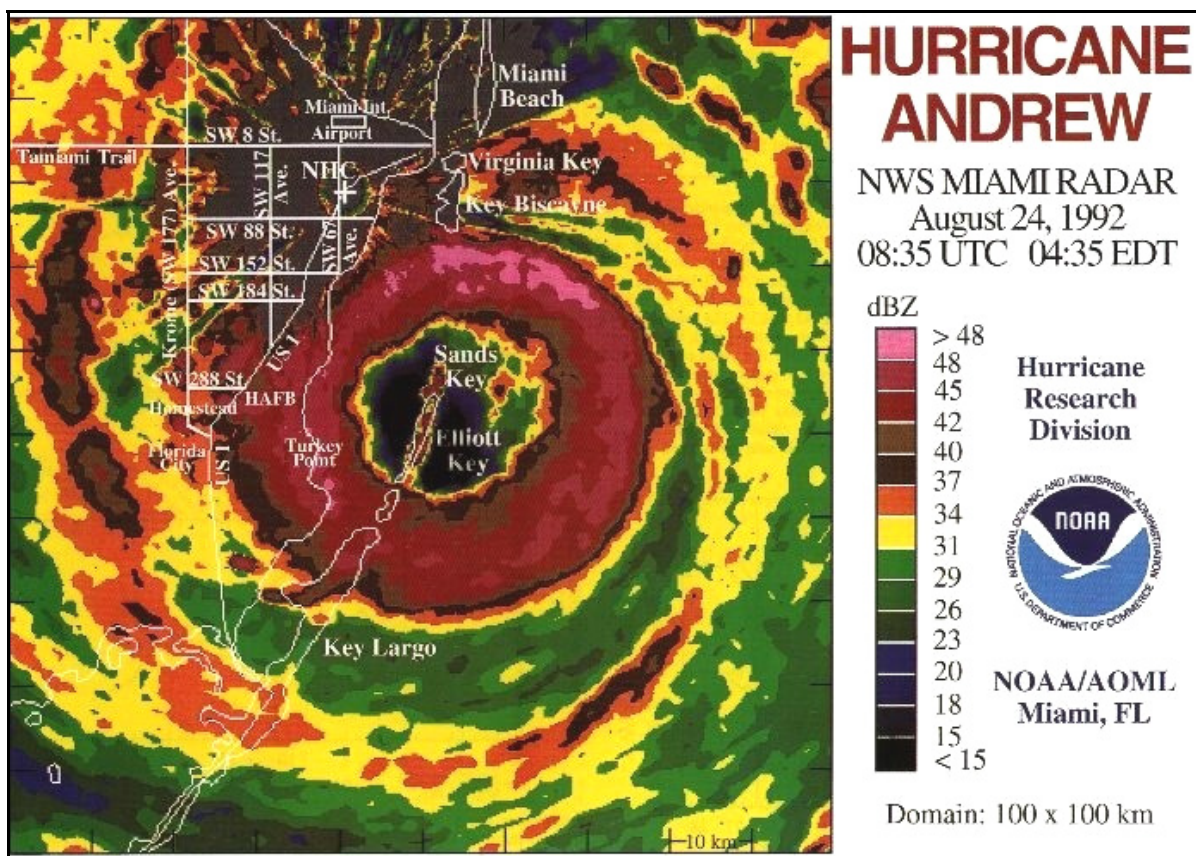


Figure 4-50
WSR-57 Radar Reflectivity of Hurricane Andrew

Miami, FL WSR-57 radar reflectivity eye wall (0.5° radar elevation angle) of Hurricane Andrew at 08:35 UTC on 24 August 1992 as the storm moved inland. The hurricane is virtually centered on the shoreline. This is shortly before the WSR-57 was destroyed by hurricane wind gusts. Source: NOAA Hurricane Research Laboratory.

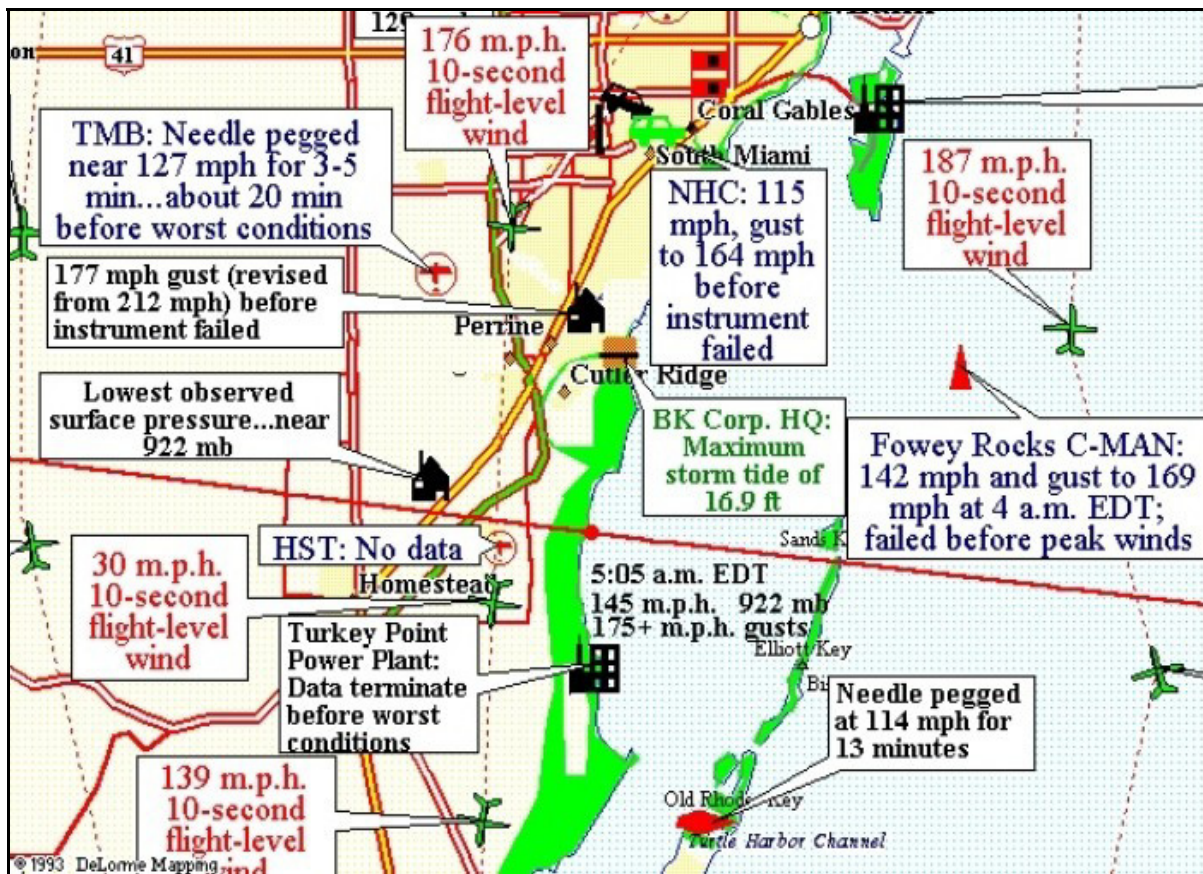


Figure 4-51
Surface Observations of Hurricane Andrew

Surface observations as the Hurricane Andrew eye-wall (shown in Figure 4-50) moved inland near Miami, FL. Source: NOAA Hurricane Research Laboratory.

Areas of high reflectivity and precipitation rates can be monitored for correlation with the occurrence of significant winds and damage. This will best be monitored through the use of time lapse and the multi-panel R, DR, V, and DV products. In addition, use of the VWP product can be used to monitor velocities and the shear profiles.

4.12 Flash Floods. Flash floods typically result from locally excessive rainfall, nearly stationary thunderstorm cells, or repeated thunderstorm cells that "train," passing over the same area. Flash floods may also be caused by a dam or levee failure, or from a sudden release of water by an ice jam. In some instances, rainfall may augment rapidly melting snow and ice and cause flash flooding.

Factors such as storm movement with respect to a river basin's shape and orientation, terrain, and soil moisture conditions must also be considered when assessing the potential for flash flooding. In many flash flooding instances it is local hydrological factors that dictate and actually create flood occurrence. The WSR-88D user must be cognizant of these local affects.

4.12.1 Recognition of a Flash Flood Event. The WSR-88D provides access to several products that will be helpful in determining the potential for a flash flood event. The most important products are the Precipitation Accumulation products, especially the OHP and the STP products (Figures 4-52 and 4-53), as well as Reflectivity products.

Other meteorological dependencies may contribute to flash flooding, such as:

- Storm (system) motion
- Strength of inflow
- Instability of inflow
- Mixing ratio of inflow layer
- Storm-relative flow (mid-upper)
- Seeding efficiencies (line and interstorm)
- Depth of warm cloud layer

These are just some of the meteorological considerations involved in evaluating convective flash flood threat potential. Thus, combining these parameters with basin characteristics indicate many of the various considerations outside of radar that must be considered when evaluating flash flood potential.

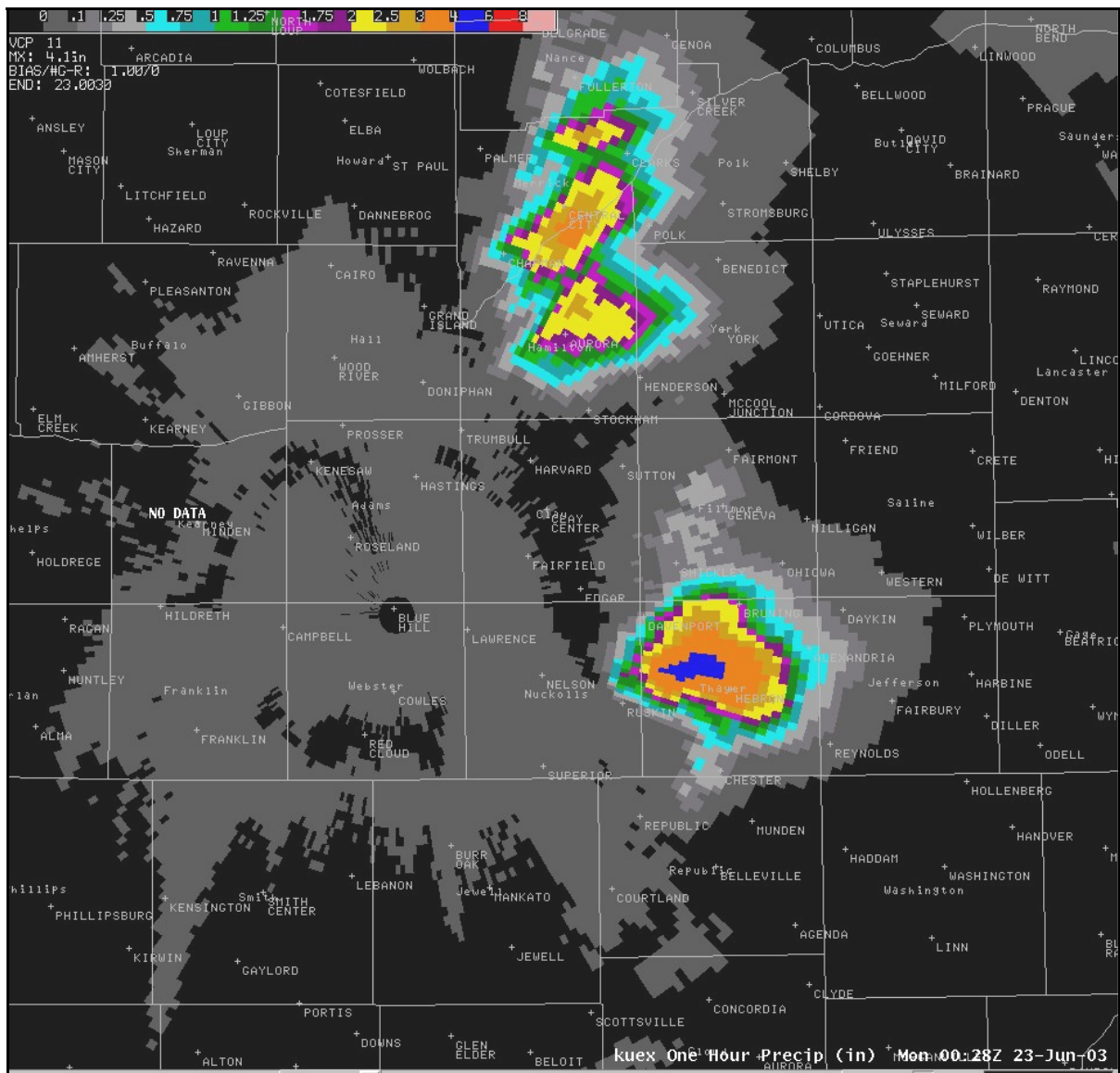


Figure 4-52
One-Hour Rainfall Accumulation Product

Hastings, NE WSR-88D One-Hour Rainfall Accumulation product (OHP) at 00:28 UTC on 23 June 2003 (AWIPS display). The storm was nearly stationary and very severe.

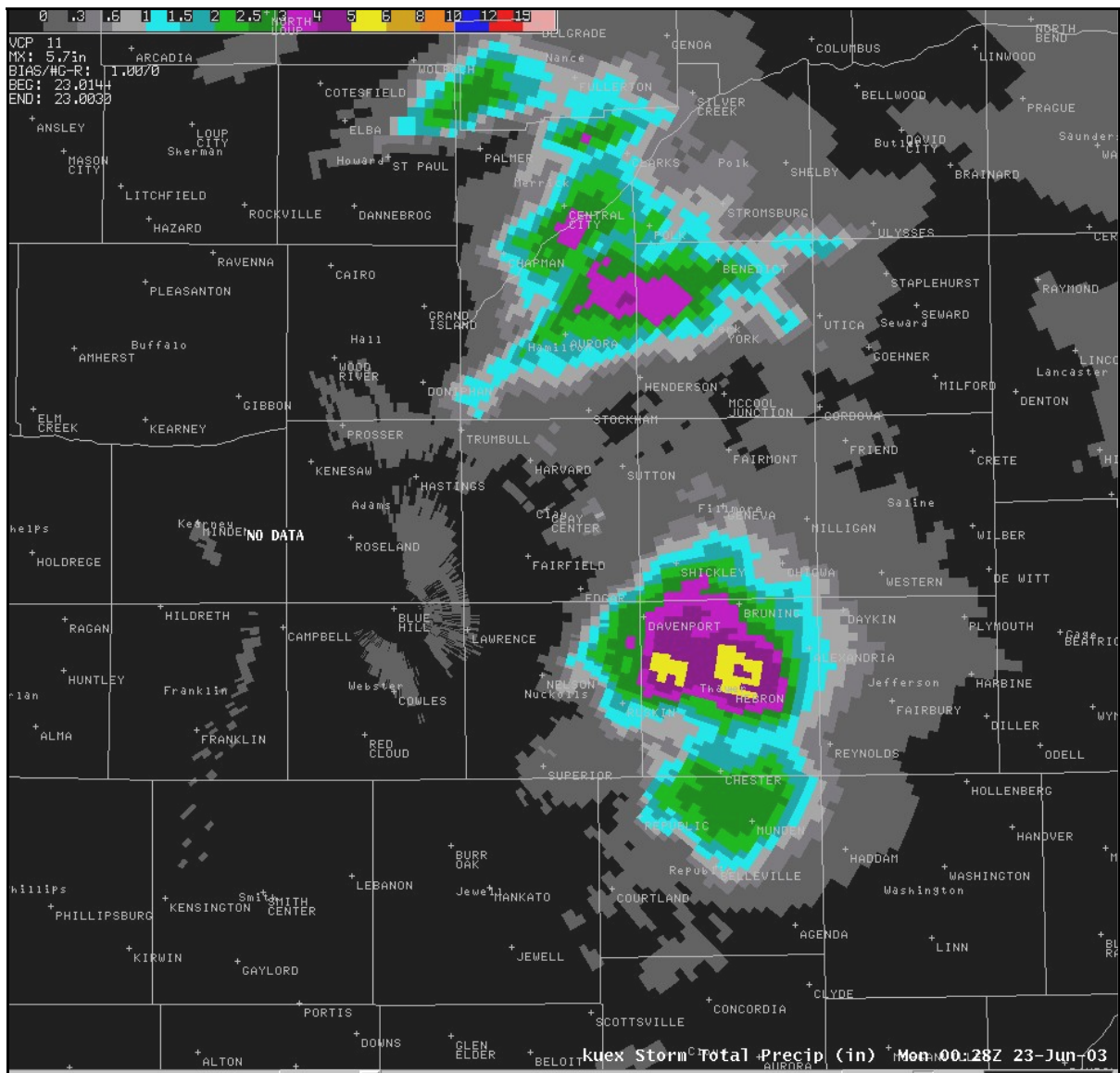


Figure 4-53
Storm Total Rainfall Accumulation Product

Hastings, NE WSR-88D Storm Total Rainfall Accumulation product (STP) at 00:28 UTC on 23 June 2003 (AWIPS display). The storm was nearly stationary and very severe.

Individual cell motion is often handled well by the STI product. However, evaluating system motion is much more difficult, being based on factors that control propagation. The mixing ratio in the inflow layer is one of those and is related to vertical water vapor flux. Storm-relative mid- and upper-level flow is important for single cell considerations. Can these winds allow recycling of hydrometeors back into the updraft? Weaker storm relative flow allows a greater chance of hydrometeor recycling into the updraft which, in turn, increases precipitation efficiency of single cell events. Interstorm seeding can help increase precipitation efficiencies in those situations where individual updrafts are inefficient at recycling their own hydrometeors. Look for connected regions of 30 dBZ or larger reflectivity between individual convective cores. Also, look for sustained flanking convection moving into, merging, or developing with slow moving storms.

The depth of the warm cloud layer is important. This is the saturated layer that is above freezing and is the area where collision coalescence of liquid precipitation occurs. If this layer is deep, then there is a greater hydrometeor residence time for this process to occur and, therefore, result in a high precipitation rate, even from relatively innocuous convection. Awareness of this process is most important if convective cells appear deceptively weak, that is, if they have warm cloud tops, little lightning, and unimpressive reflectivity. If weak convection is occurring in a nearly saturated environment with weak CAPE and a high freezing level and low LCL, then it is likely that this convection is characterized by high precipitation efficiencies along with rain drop distributions that favor the use of the tropical Z-R relationship. See Petersen et al. (1999) for more details on excessive rainfall from warm clouds.

In addition to the precipitation accumulation products, other useful products include reflectivity (multi-panels) and cross sections. In addition, VIL, LRM, and ET products can be used to monitor storm size, strength, and trends. Moreover, the STI products can be useful in recognizing a developing or ongoing flash flood situation. The location of boundaries and the low-level jet are very important in creating and sustaining precipitation and flooding. The VWP product can be very important in detecting and monitoring this process.

4.12.2 Precipitation Accumulation. The Precipitation Accumulation products provide estimates of precipitation accumulations for OHP, STP/DSP, THP, and USP (Figures 4-52, 4-53, 4-54, and 4-55). These quantitative precipitation estimates can be compared with Flash Flood Guidance values provided by the River Forecast Centers (RFCs) to determine flash flood potential.

Time lapse sequences of the OHP, STP, and USP will prove to be extremely valuable in some situations. The time lapse sequences will aid in identifying stationary storm complexes or a train of cells with intense precipitation. A time lapse will also aid in the determination of precipitation patterns within a basin and, potentially, a basin's response.

Used in conjunction with one another, the Precipitation Accumulation products provide information about the potential for flooding. For example, the THP (Figure 4-54) used with a later OHP can help in the identification of areas where basin saturation has occurred.

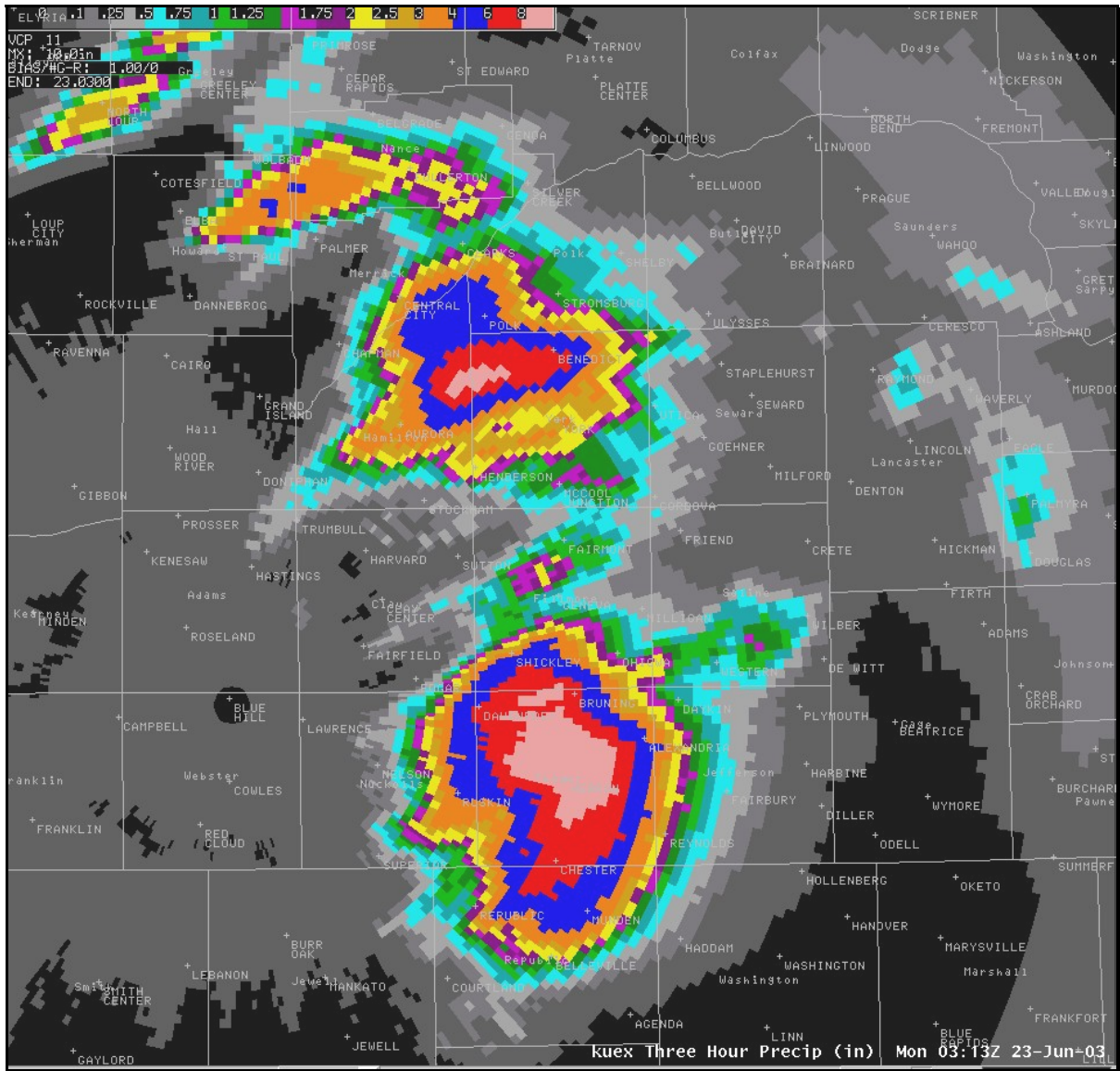


Figure 4-54
Three-Hour Rainfall Accumulation Product

Hastings, NE WSR-88D Three-Hour Rainfall Accumulation product (THP) at 03:13 UTC on 23 June 2003 (AWIPS display). The storm was nearly stationary and very severe.

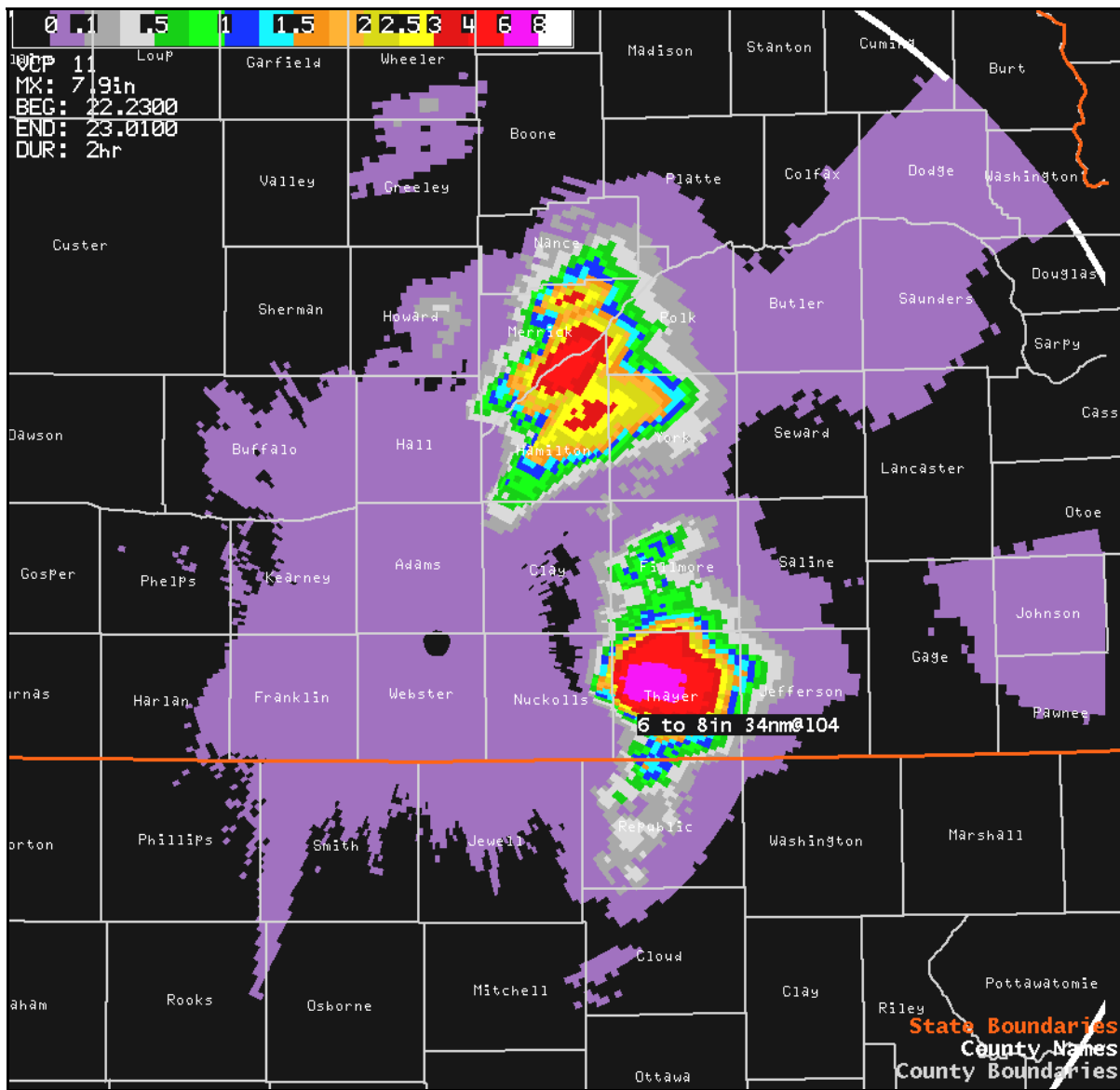


Figure 4-55
User Selectable Rainfall Accumulation Product

Same as Figure 4-52, except it is a User Selectable Rainfall Accumulation product (USP) and only a 2-hour duration beginning at 23:00 UTC on 22 June 2003 and ending at 01:00 UTC on 23 June 2003 (AWIPS display).

In severe convection-related rainfall estimation, one note of caution is worthwhile. In some cases such as that illustrated in Figures 4-52 through 4-55, hail contamination may affect radar rainfall estimates. That is, when significant hail fall accompanies a storm this will tend to artificially enhance rainfall estimates above that which actually occurs. While certain adaptable parameters are included to mitigate the rainfall accumulation hail bias, it cannot be concluded that all the bias is eliminated (Fulton et al. 1998).

4.12.2.1 Reflectivity. Reflectivity time lapse is a method to identify a train of cells passing over the same area, stationary cells, or merging cells. Often, with the merger of cells, precipitation rates associated with collision and coalescence will markedly increase.

4.12.2.2 Vertically Integrated Liquid Water. Monitoring the updated VIL product not only provides information about water content within a storm (not precipitable water), but a diminishing of the VIL values that might be indicative of a weakening trend. A time lapse sequence of this product may provide this indication.

4.12.2.3 Echo Tops. Echo Tops, especially the high-resolution version, EET, can provide information on trends in overall precipitation intensity. Increasing precipitation tops may signal increases in updraft strength, CAPE, and/or the depth of the collision and coalescence process. All are important to the flooding potential.

4.12.2.4 Storm Tracking Information. Movement of an intense storm or region of storms is likely the most important factor of flash flood events. A storm with a high rainfall rate may be moving too fast to produce a flash flood in any one location. On the other hand, a storm with a moderate rainfall rate could cause a flash flood if it is persistent over one location or moves along a stream or river basin. The STI product can be helpful highlighting a region of excessive rainfall and current flooding, or in determining future areas of threat from flash flooding. If movement is not erratic, strong individual storm cells should be adequately tracked by the product.

4.12.3 Considerations. As pointed out in the above discussion, flash flooding and flood warnings are dependent on many factors; meteorological, radar (e.g., Z-R relationship used), and otherwise. Thus, as is the case with all other warning types, integration of all available information is essential for an effective flood and flash flood warning program.

Stationary cells will be easily identified with time lapses of Reflectivity and Precipitation Accumulation products. The STI product may indicate a continuous storm cell motion but the upstream edge of the storm complex, where cell development occurs, may be nearly stationary. Thus, a succession of cells within the storm complex will pass over the same location, while the complex itself is nearly stationary.

The precipitable water content of the inflow to a region of convection and heavy rain (or potentially heavy rain) is very important. But the user must understand that VIL is a radar-

derived estimate of the liquid water content within existing storm cells or storms, but it is not an estimate of precipitable water values.

The presence of hail in storms can enhance the reflectivity values. The Precipitation Processing software contains logic and adaptable parameters that are designed to minimize the effects on the estimation of precipitation amounts. However, if these parameters are not properly adjusted, hail may cause considerable overestimation of rainfall accumulation. Other factors within the Precipitation Processing software, such as use of the proper Z-R relationship will also affect flood warning accuracy.

Precipitation estimates are the most critical element in making daily river forecasts to support a multitude of hydrological decisions. These include decisions pertaining to reservoir operations for flood control, hydropower generation, navigation, and industrial and municipal water supply decisions. The Precipitation Accumulation products, especially the Hourly Digital Precipitation Array (DPA), are used as input to river forecasting models. Instead of the accumulation products' 2 km (1.1 nm) x 1° polar grid, the DPA has a rectangular grid of about 4 x 4 km (2.2 x 2.2 nm). Instead of the accumulation products' 16 data levels, the DPA has 256 data levels. Similar to the OHP, the DPA has a moving one-hour accumulation (scan-to-scan accumulations). The product is used by the NWS RFCs to generate precipitation input for the NWS River Forecast System, and the AWIPS Multisensor Precipitation Estimator (MPE) used for the bias calculation. The rectangular grid allows for mosaicing the numerous WSR-88Ds within the RFC's area of responsibility.

The models run by the RFCs produce numerical mosaics of precipitation accumulation that are intended to alert the RFC forecasters to those basin areas demanding immediate attention. These models estimate soil moisture and runoff, important to river and flood forecasting.

4.13 Non-Convective High Wind Events. The Doppler capability of the WSR-88D has proven useful in the detection of high wind events. These events include strong gradient winds that are the result of a deepening or a strong extratropical cyclone. Some hazards that may result from high winds include dust storms, blowing snow, and dangerous wind-chills. Certain types of windstorms are more terrain enhanced and are inherent to particular geographical locations, such as the Santa Anna and the Chinook winds. Two products that can be very useful for observing and forecasting wind speed and direction are the V and VWP.

4.13.1 Recognition of High Wind Events. The V and DV products can be used to determine wind field characteristics when sufficient tracers are available. The speed of the winds can be deduced by observation of the strength of the velocity field depending on tracers and the viewing angle and, if the radar is within those winds, the VWP. Prior to the onset of a high wind event, the velocity field may indicate stronger winds at mid-levels or lower mid-levels that could possibly mix downward to the surface. Deep environmental lapse rates and identifying the mixed layer are important in this regard. These higher velocities may also be evident in the VWP product, again, depending on tracers and the wind location relative to the radar.

4.13.2 Considerations. Depending on the amount of sufficiently large scatterers or sufficiently strong refractive index gradients in the atmosphere, the velocity field may or may not reflect high wind events. On the average, clear air returns extend to ~30 nm in horizontal range and ~3,000 feet in height depending on site, season, time of day, and airmass. If operating in Clear Air Mode, and the interest is in the most accurate velocity estimates possible, selection of the short pulse may be preferable. However, the long-pulse mode uses as many as 250 pulses per pulse volume and is, therefore, more sensitive (~7 db more sensitive). (However, long pulse can also induce more dealiasing failures.)

If dust storms are strong enough so that particulates are lofted into the atmosphere, a significant echo return in the velocity field may appear. Blowing snow is often confined to a shallow depth close to the ground and, therefore, will not likely be revealed in the velocity field except for close to the radar.

Some lofted particulates associated with fires and smoke are rather easily detected and strong winds are commonly associated with large fires. Therefore, monitoring fire-related windstorms (when terrain produces only limited blockage) is a significant capability. In fact, the early detection of fire related particulates within smoke (and/or debris) may be the first indication of significant fire (or explosion) (Figure 4-56). The R, DR, V, DV, and the VWP products are the primary products of choice.

4.14 Low-Level Jets. The low-level jet is the axis of a band of wind flowing at a faster rate than the overall environmental wind within the planetary boundary layer. It may be induced by orographic features, synoptic fronts, mesoscale, and even strong convective storm systems, or it may result from the horizontal temperature gradient created by the diurnal heating and cooling cycle. Low-level jets also act as conveyor belts for feeding moisture into weather systems and their associated rain/snow or convective storms. Severe thunderstorms have been observed to develop within, or at the nose of and downstream of, the low-level jet.

4.14.1 Recognition of Low-Level Jets. The low-level jet may be observed in velocity fields as a couplet of strong values surrounded by weaker winds above and below, upstream and downstream, of the radar (Figure 4-57). While not shown here, it is readily evident in the VWP where the time history and changes in height can be observed.

4.14.2 Considerations. At further distances from the radar, the sensitivity is decreased and the beam intercepts the atmosphere at progressively greater heights. As a result, the low-level jet may not be depicted well, or at all, depending on scatterers in the lower elevation scans of V products and beam height. Often, the low-level jet may be in the range of 0.9 to 1.8 km (3,000 ft to 6,000 ft) AGL. However, somewhat higher elevation scans of the velocity product may depict core velocity regions better at close radial distances from the radar.

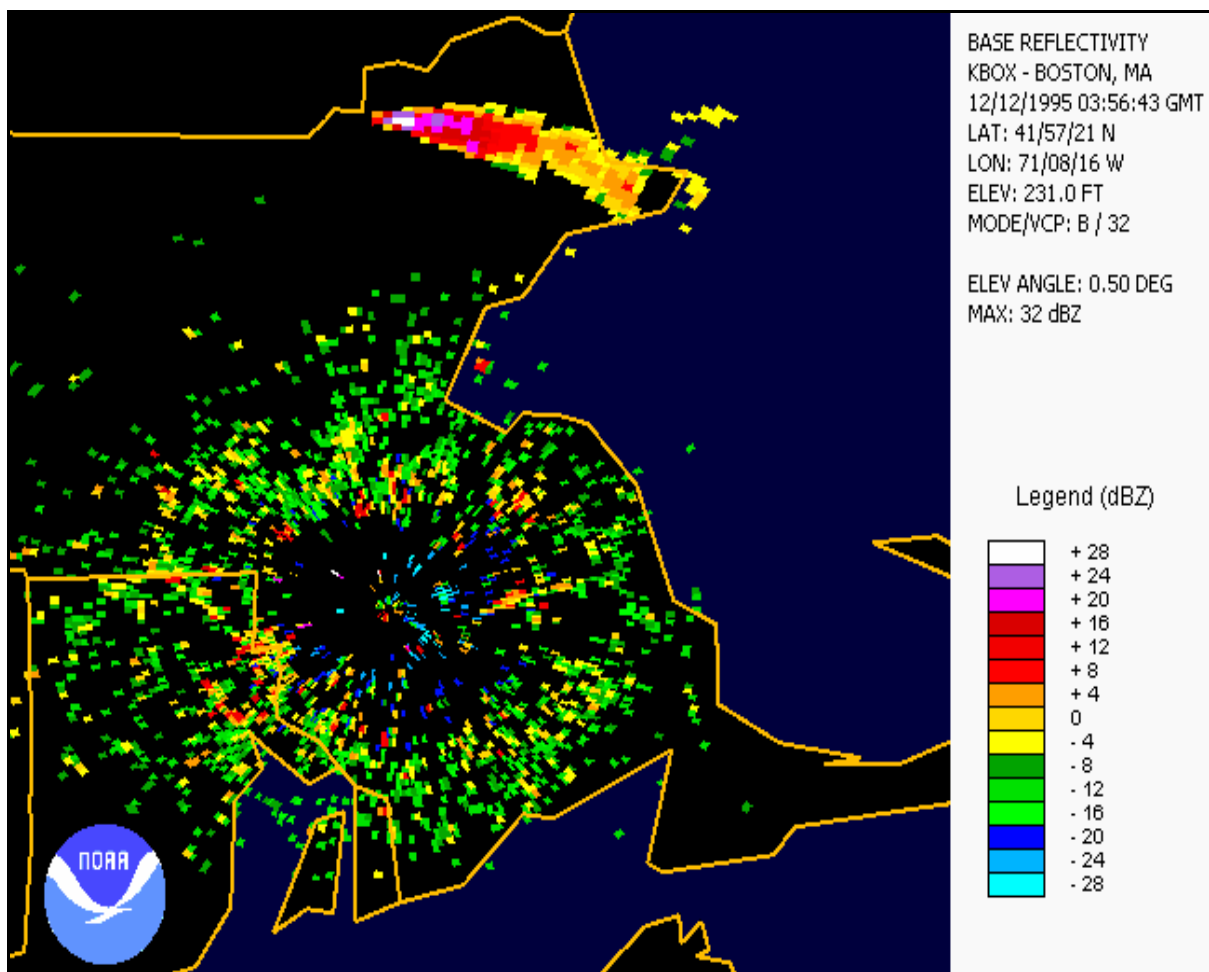


Figure 4-56
Smoke Plume Detected by Radar

A plume of smoke-borne particulates from a fire is detected in Clear Air Mode (top center of graphic) by the Boston, MA WSR-88D at 03:56 UTC on 12 December 1995 (NCDC NEXRAD Viewer graphic).

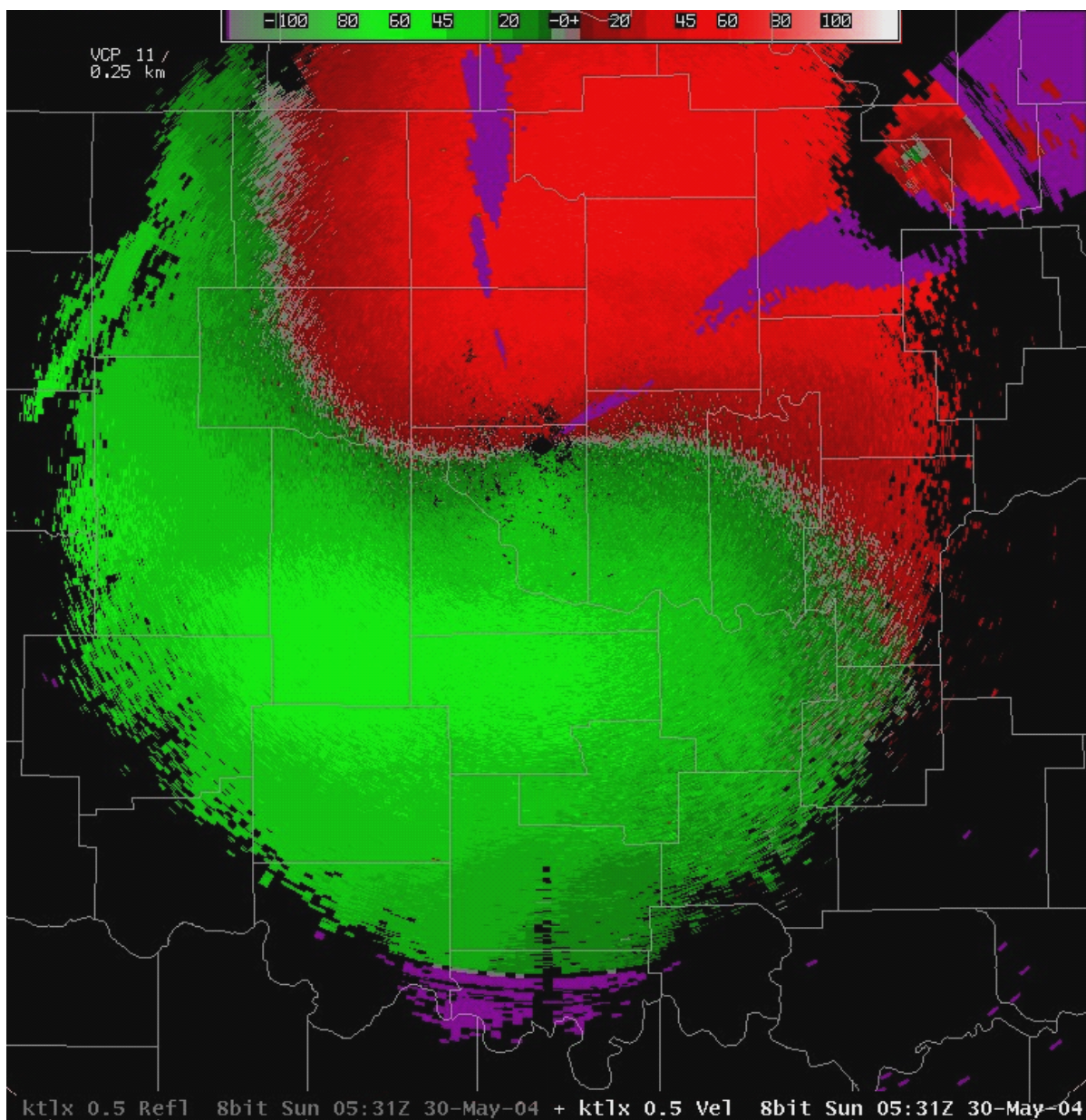


Figure 4-57
Base Velocity Data Array Product of a Low-Level Jet

Oklahoma City, OK WSR-88D Base Velocity Data Array product (DV) at 05:31 UTC on 30 May 2004 (AWIPS display). This image shows a south-southwesterly low-level jet with a maximum velocity from 191° at about 110 kmhr^{-1} (60 kts).

Normally, the VWP product is the primary product of choice. One radar, assuming adequate tracers, will depict the low-level jet over the radar. However, because of the limited width or horizontal extent of the amplified wind field, it may not be sampled by some regional radars. If the low-level jet is sufficiently large horizontally, then other adjacent radars may also sample the low-level jet or “sheet” of amplified winds.

4.15 Wind Shear. A major hazard to aviation is the presence of low-level wind shear. Wind shear may result from a variety of phenomena such as boundaries of all types, terrain, and strong inversions. Moreover, owing to the beam width at longer ranges (e.g., ~3.5 km at ~230 km) the normal occurrence of wind change with height will result in wind shear within the beam.

4.15.1 Recognition of Wind Shear. Wind shear along a boundary will appear as a discontinuity in the Doppler velocity field and is frequently associated with broadened velocity spectrum widths (Figures 4-58 and 4-59). Detection of wind shear and/or turbulence within the pulse volume is best accomplished via spectrum widths. Therefore, assuming sufficient tracers are present, frontal surfaces aloft or shear of the horizontal winds will be detected by enhanced areas, or layers, in the Spectrum Width product. Spectrum Width values of 5 ms^{-1} (8 kts), or higher, are usually associated with significant wind shear or turbulence, or both, within the beam.

Another method of inferring or observing wind shear is the observation of radial or azimuthal velocity gradients. This highlights local wind-shear phenomena in larger regions, as can the Combined Shear (CS) product. However, the CS product includes substantial smoothing which can actually prevent detection of some of the shear. In other words, some of the shear values are smoothed to the extent that some shear is actually eliminated. The VWP product can also be useful in detecting and monitoring significant wind speed and direction changes (wind shear) in the vertical within a limited radius of the radar. The default value for this radius is 29.6 km (16 nm), but that value is adaptable. However, if that shear is too large and contributes to a large asymmetry in calculation of the proper VAD sine wave value at any given height, then no data (“ND”) results in the VWP product for that height.

4.15.2 Considerations. In addition to significant smoothing, the CS tends to be “noisy” even when smoothed and, in the absence of larger and strong signatures, may be of little use. The product does not take vertical shear into account. For indications of shear in the vertical, the VWP or the VCS products may be useful.

4.16 Turbulence. Any disruption of ambient flow such as wind shear or flow deceleration (flow within downdraft regions or divergence at storm summit or the earth’s surface) results in turbulence.

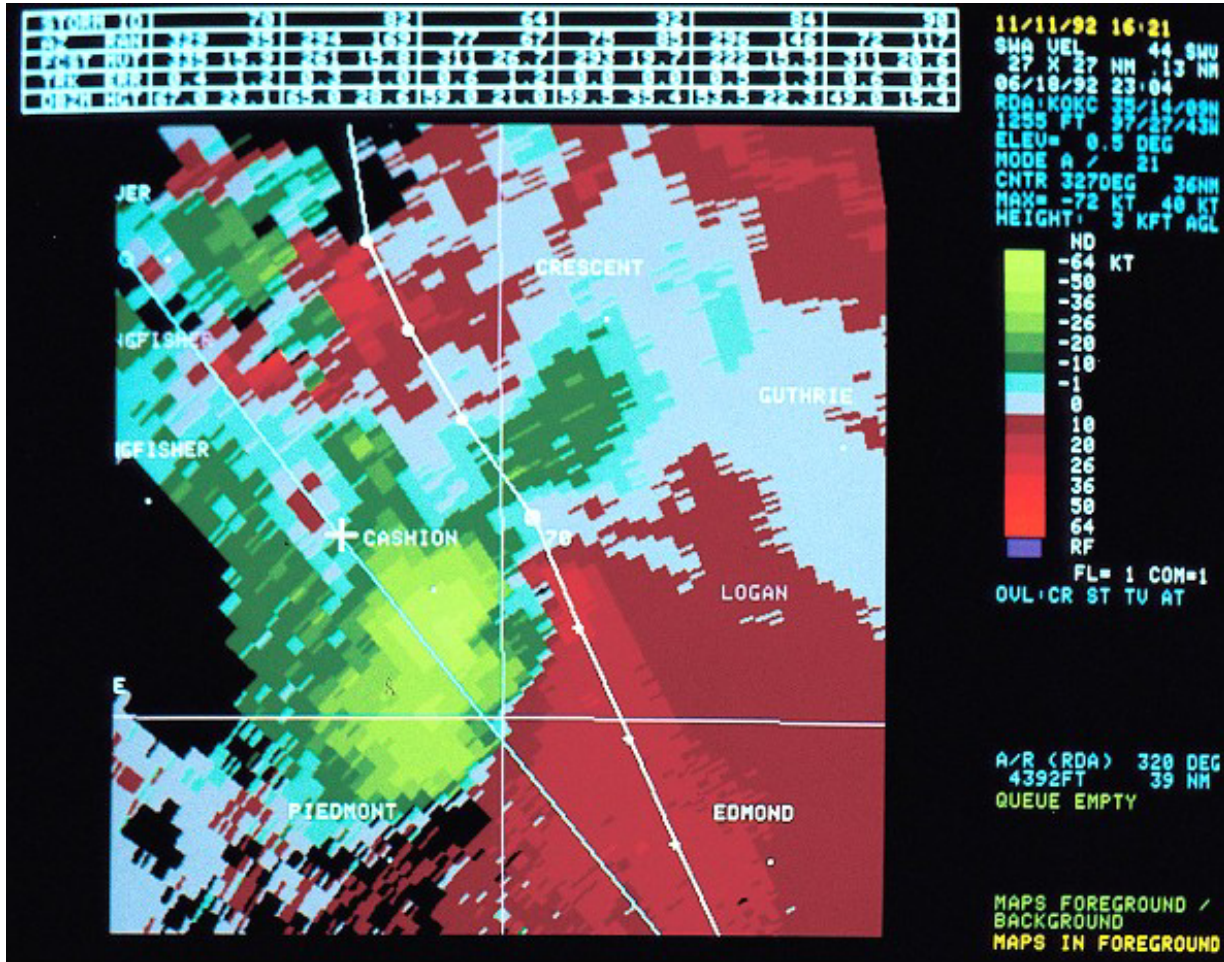


Figure 4-58
Severe Weather Analysis (Velocity) Product

Norman, OK WSR-88D Severe Weather Analysis (Velocity) product (SWV) at 23:04 UTC on 18 June 1992 (PUP display). The product shows a strong thunderstorm gust front where bright red abruptly changes to bright green.

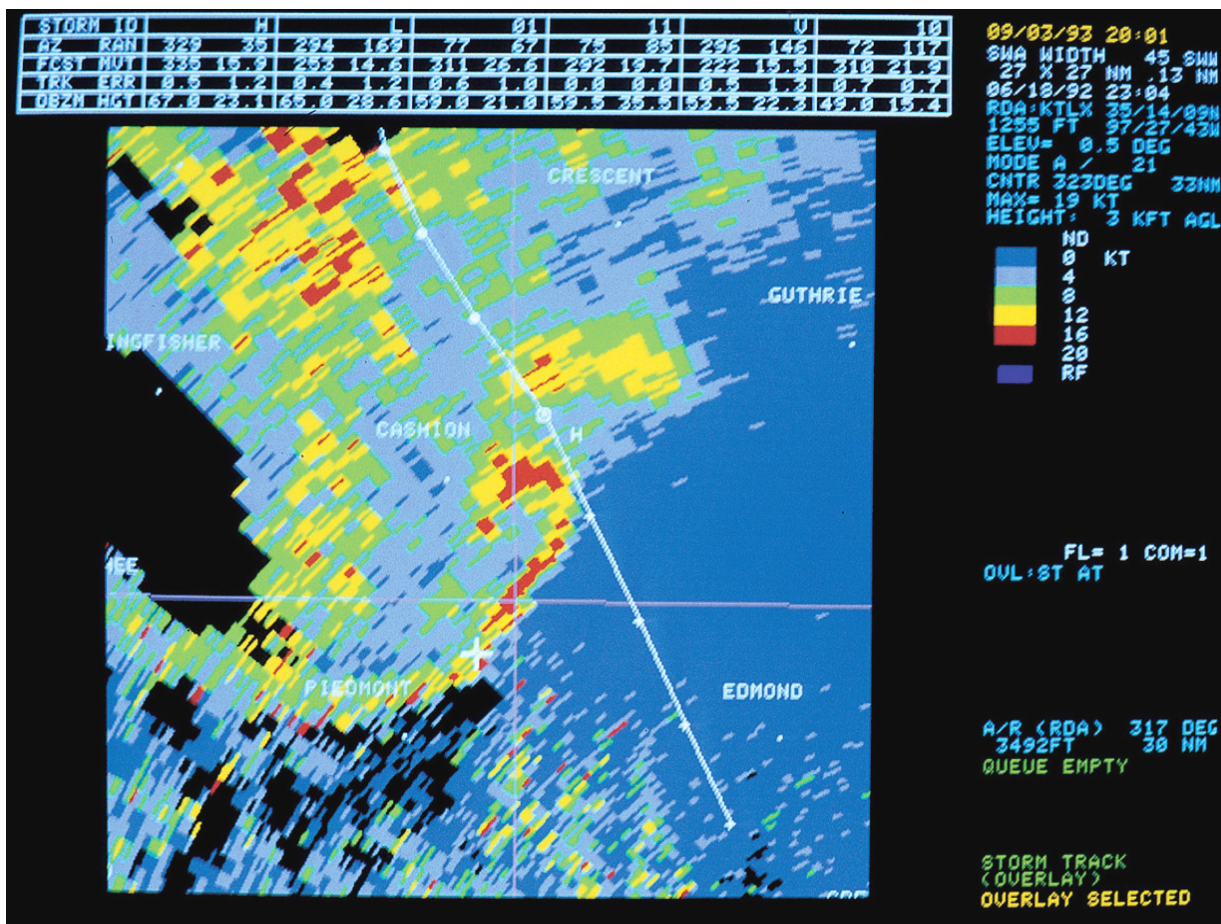


Figure 4-59
Severe Weather Analysis (Spectrum Width) Product

Oklahoma City, OK WSR-88D Severe Weather Analysis (spectrum width) product (SWW) at 23:04 UTC on 18 June 1992 (PUP display). This product is at the same time as Figure 4-58. Note the broadened spectrum width values in the area of the thunderstorm gust front (near the white cross hair).

4.16.1 Recognition of Turbulence. In the immediate vicinity of thunderstorms. for example, when the signal-to-noise ratio is good (~10 dB), spectrum width values of 8 knots or greater indicate turbulent areas. Higher spectrum width values will typically occur in regions of downdraft, low-level thunderstorm outflow and gust fronts (Figures 4-58 and 4-59), and in divergent areas at the top of storms.

Note that in Figure 4-58 the inflow to the storm (red velocities in the lower right) is rather smooth, while in Figure 4-59 the region of the gust front (sharp change from the red velocities to the bright green in Figure 4-58) is turbulent (note the broad spectrum widths in Figure 4-59). Note also in the upper left of Figure 4-58 where there is a mix of inbound and outbound velocities (shear), in the same area in Figure 4-59 denoted by broadened spectrum widths. This is a turbulent region as might be expected.

4.16.2 Considerations. The difference between turbulent areas and strong shear regions cannot be distinguished in the SW product because broadened SW values result from either shear or turbulence within the beam. Additionally, regions of wind shear typically break down with energy cascade downward into turbulence. Within a sample volume, spectrum width values may be higher due to shear, turbulence, or noise (low signal-to-noise ratio (SNR)). Spectrum broadening is secondarily caused by antenna rotation rate or the spread of scatterers' terminal fall velocities. These contributions are minor.

Spectrum width values widen significantly and Doppler velocities become erratic in areas with very low signal-to-noise ratios. In fact, the primary use of SW is now data quality. However, because of shear of the horizontal winds with height and increasing beam width with range, SW values broaden with increasing distance from the radar.

4.17 Microbursts. Microbursts occur when a rapidly subsiding column of air descends and spreads out at and near the surface. Frequently, this air is negatively buoyant, but there are exceptions when the air will overshoot its equilibrium level and continue to sink. There is no requirement that the divergence be axial symmetric, however, and it often is not. Microbursts may occur in the absence of precipitation when ice crystals or rain drops in virga evaporate aloft, cooling the air rapidly, creating negative buoyancy and accelerating the air toward the surface. Additionally, in thunderstorms, a high liquid water mass and heavy rainfall will also accelerate downdrafts, through precipitation drag, at times becoming microbursts. There also exists a “hybrid” class of microbursts that are created through both negative buoyancy and precipitation drag.

4.17.1 Recognition of Microbursts. Dry microbursts are detectable within WSR-88D velocity images due to atmospheric density gradients, insects, and particulate matter. For the “wet” microburst, the precipitation tracers are normally abundant. The microburst is identified by a significant velocity difference along a radial or group of radials with the radar-relative inbound velocity at a nearer radar range than the outbound value. To qualify as a “microburst,” the distance

between the velocity maxima in the signature must be less than 4 km apart. When the distance between these maxima are larger the signature qualifies as a “macroburst.”

Thus, a microburst will produce a unique signature detectable at low levels in the velocity field. A divergence couplet (i.e., a pattern of “strong” flow toward the radar, matched by an opposite pattern of “strong” flow away from the radar) will be seen on the display (Figure 4-60). A microburst is located in Figure 4-60 at the white cross where the velocity divergence is 23.7 ms^{-1} (46 kts), 10.3 ms^{-1} (20 kts) inbound, and 13.4 ms^{-1} (26 kts) outbound. Divergence of this magnitude is frequently damaging (Burgess and Lemon 1990). The strength of the signature is highly dependent on radar range to the microburst, as well as the angle of observations. The divergence signatures are often asymmetric. At times, apparent asymmetry can be created by storm motion superimposed on the microburst’s outflow. In this situation, either the velocity toward or away from the radar will be higher than its opposite. The strong downflow from a microburst descends very close to the ground before diverging. This divergence in the velocity field might also be detectable in VCS products if the signature is close enough to the radar (Figures 4-61 and 4-62). When descending air is also translating along the radial, the resulting divergence signature will most likely be asymmetric. But in many situations microburst signatures will not be symmetric in any case. Divergence maximizes from 2 to 4 minutes after initial development of the signature with a diameter of approximately 4 km (2.5 nm) or less and a velocity difference sometimes exceeding 51 ms^{-1} (100 kts). However, while divergence signatures of this strength are very rare, Burgess and Lemon (1990) found that a WSR-88D signature with a velocity difference of 18 ms^{-1} (35 kts) or more are generally damaging. The most intense velocity difference in the divergence signature is normally below about 300 m (~ 980 ft). For this reason, these local and sometimes damaging “outbursts” of wind are often below the radar horizon and, therefore, invisible to the radar unless the microburst is within ~ 40 km.

The products of choice for detecting and monitoring these signatures are R, DR, V, DV, and SWV, and the RCS and VCS. Note that these velocity products are ground-relative instead of storm-relative. Obviously, the damaging flow is ground-relative, thus these are appropriate products.

4.17.2 Considerations. As stated above, with the shallow vertical extent of the outflow from a microburst, this phenomenon will usually not be detected beyond the range of about 20 nm. In addition, because of the short-lived nature of the microburst phenomenon (typically 3 to 5 minutes) and the current scanning strategies used in the WSR-88D, Microbursts may be infrequently detected at their maximum divergent intensity. However, VCP 12 is the coverage pattern of choice because of the overlapping low-level beams in the vertical and the relatively rapid update rate (4.1 minutes).

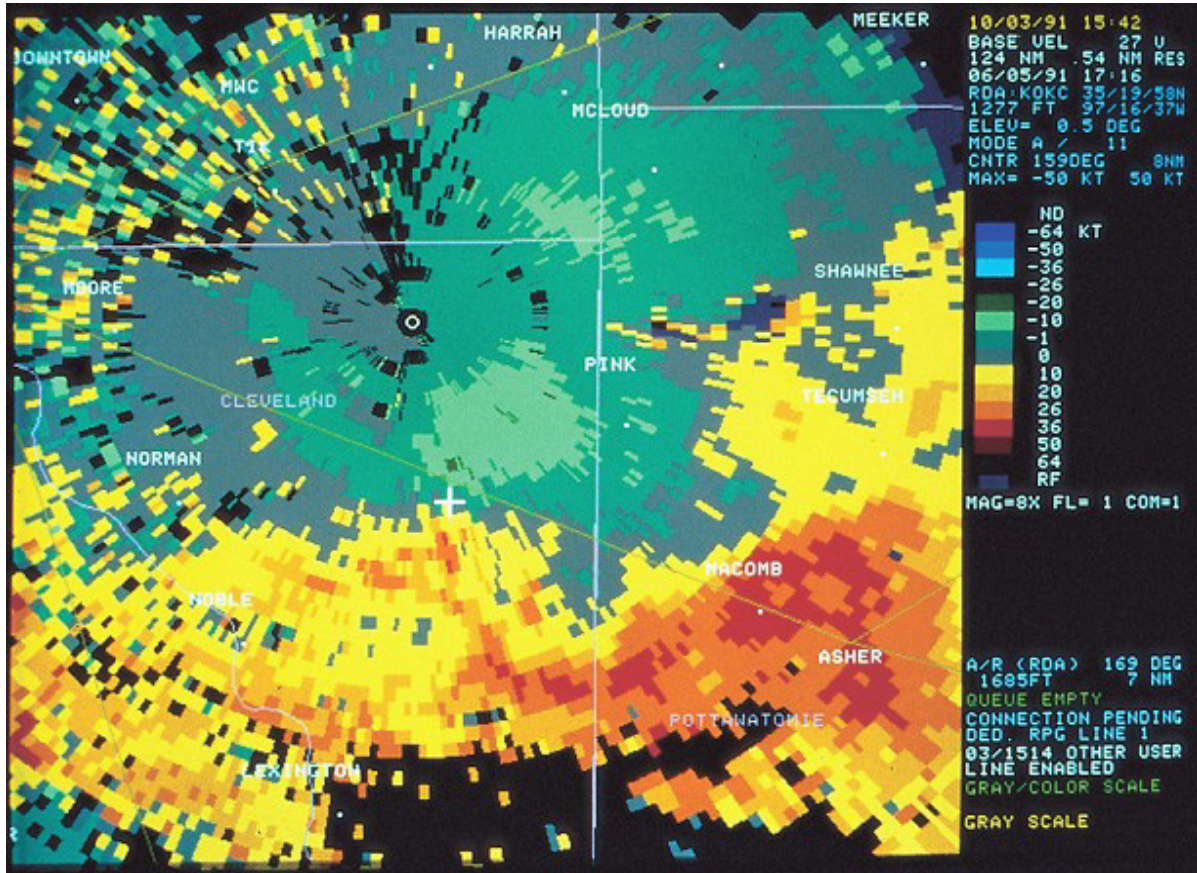


Figure 4-60
Microburst Detected on a Mean Radial Velocity Product

Oklahoma City, OK WSR-88D Mean Radial Velocity product at 17:16 UTC on 5 June 1991 (PUP display). A microburst is located at the white cross hair where the velocity divergence is 23.7 ms^{-1} (46 kts), 10.3 ms^{-1} (20 kts) inbound and 13.4 ms^{-1} (26 kts) outbound.

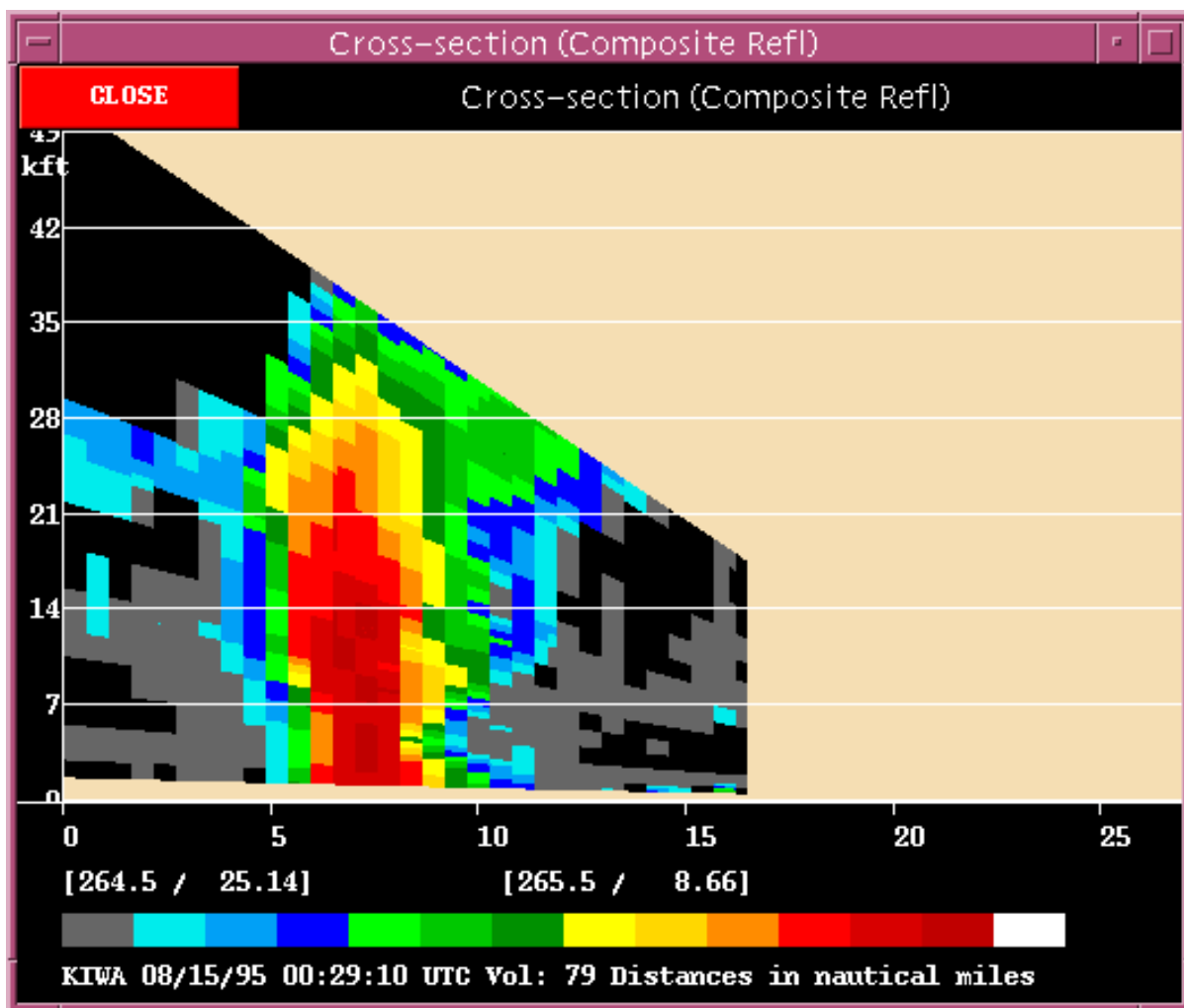
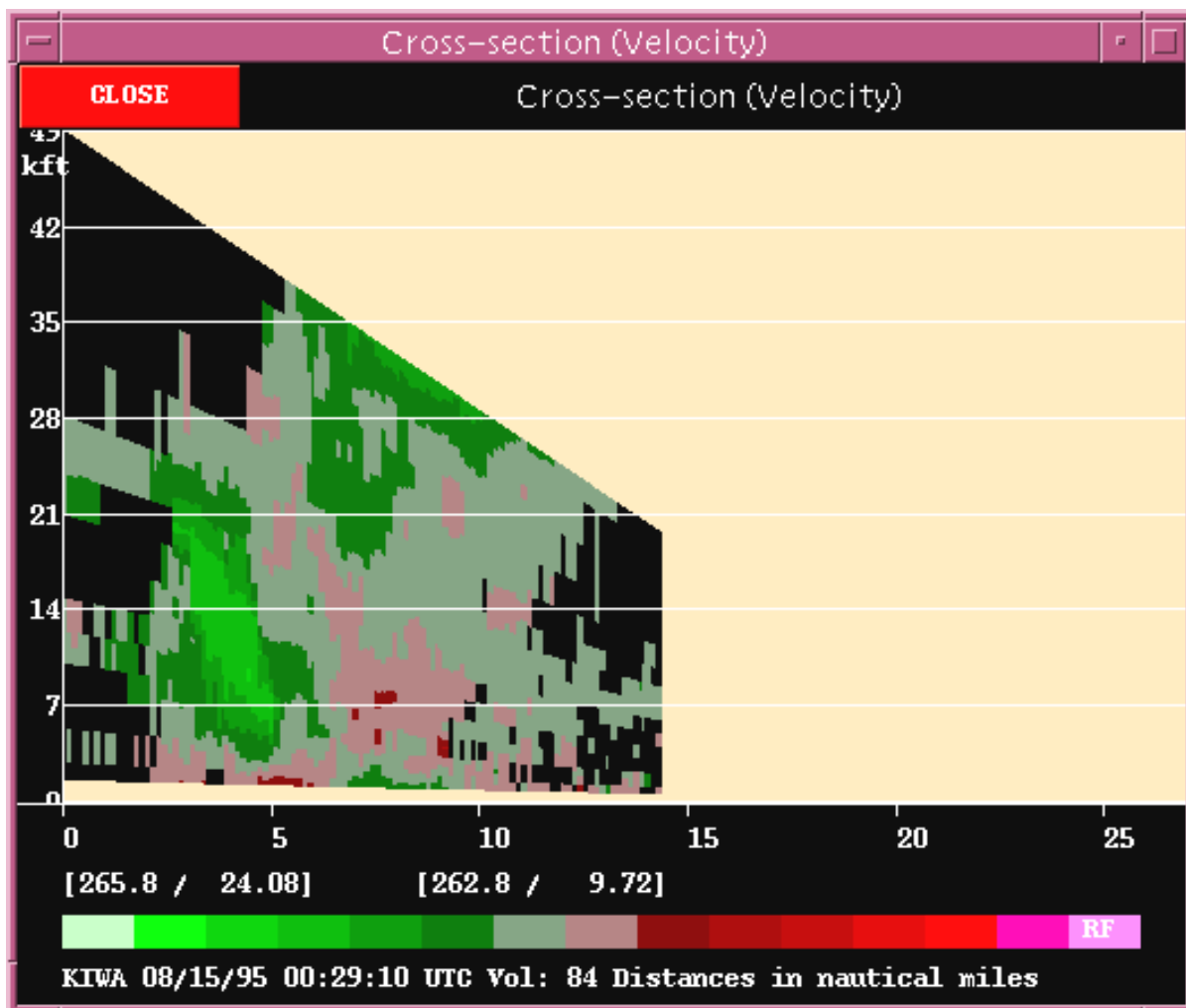


Figure 4-61
Reflectivity Cross Section of a Microburst-Producing Thunderstorm

Phoenix, AZ WSR-88D Reflectivity Cross Section product at 00:29 UTC on 15 August 1995 (AWIPS display). This product shows a microburst-producing thunderstorm shortly after the feature reached the surface.



As in Figure 4-61 except for a Velocity Cross Section product. Note the convergence aloft (~7,000 ft) into the reflectivity core and the divergence signature below extending just above the radar horizon.

At ranges nearer the radar (~ 40 km and less), the DV may prove most useful. At further distances from the radar, microbursts may be anticipated by monitoring high reflectivity cores at mid-levels 5 to 12 km (16,000 to 40,000 feet) as they descend and are often accompanied by flow convergence into these cores. Additionally, observations of the DCZ and the MARC regions are also indicative of both macrobursts and microbursts, but often the lead time for the MARC is generally on the order of two volume scans (Schomocker et al. 1996). Additionally, the false alarm rate may be high. Collapsing echo tops or rapidly diminishing VIL values may also indicate such an event. However, the collapse of some storms results in only weak outflow. Additionally, gaps in the VCPs may themselves create the apparent “collapse” (Howard et al. 1997; Maddox et al. 1999).

4.18 Considerations for Building a Routine Product Set. The following information is intended as guidance to users setting up RPS Lists and is subject to modification by agency-unique operational requirements. The data display systems typically provide the user with the capability to define several unique RPS Lists.

4.18.1 Initial Considerations. Each Associated User typically has the capability of creating and accessing numerous RPS lists depending on the type of weather situation. Every RPS List must be designed carefully in order to minimize the amount of editing of the “Current List.” Included here are some of the considerations for RPS List determination. These are guidelines only. The considerations below apply typically for 33.6 – 56 Kbps line speeds.

4.18.2 Some Local RPS List Considerations. Routine Product Set Lists must be designed with several things in mind. The object of the list is to provide the user with products needed most often in order to best sample the atmosphere and thereby interpret the current weather situation. Things which must be taken into consideration are:

1. Weather Mode/VCP Clear Air? Precipitation? Which VCP? You need to anticipate this information in order to know from what angles you have to choose.
2. Weather Situation Stratiform? How widespread will the precipitation be? Convective? Low Topped? Winter Weather? Clear Air Return? The user needs to know this to determine which products and what elevation angles will be utilized.
3. Range Where are the echoes located? Close to the RDA? Beyond 124 n mi? Both? This information will determine which of the current elevation angles will sample the precipitation at the appropriate height, considering the range to the echo and the anticipated vertical extent of the echoes being sampled.

4. Procedures Finally, the RPS List needs to be compatible with your display procedures. For example, when planning use of multi-panel displays, the proper products and product elevation angles must be on that list. Often, however, it will be the procedures which will be designed around the RPS Lists.

Associated Users with a 14.4 Kbps and 33.6 Kbps lines are limited to 50 products. Line quality may reduce the number of products available. Users with slower lines must also anticipate that the larger products such as SW or CR products also reduce the number of products received each volume scan.

4.18.3 Product Considerations. No predetermined RPS List, outside the National List, will always be appropriate, no matter how carefully thought out it is. Some overlap is necessary in order to keep real-time editing at a minimum. The user must always be prepared to change and fine tune the RPS List to ensure the products received are the products needed. Also, the user must keep in mind how these changes will affect the procedures used.

It is not always easy to decide which products to choose. Here are some considerations:

1. At least 4 elevations of reflectivity and velocity (Storm Relative) are needed *at a minimum* for proper storm structure evaluation. The elevations chosen will depend on the VCP, range, and the vertical extent of the anticipated echoes. For storm interrogation, products representing low, middle, and storm summit locations should be viewed as a minimum. As line speed permits, even more elevation cuts are desirable.
2. Additionally, the higher resolution base products such as DR and DV should always be considered, especially if severe weather is anticipated. Thus, the user should consider placing several slices of the high-resolution Velocity on the RPS List, as well as the matching DR products. This will be especially useful if features are small in scale or at a significant distance from the radar (i.e., being severely impacted by aspect ratio). It will also be beneficial with boundary detection or if echoes are of weak intensity. Also, the user will need this product if it is required to view the high resolution SRM display. The user must be aware that, for other than LAN-to-LAN connections, load shedding could be an issue. The same can be said for the high-resolution Reflectivity products.
3. Velocity products should never be obtained without a matching Reflectivity (or high resolution Reflectivity) product. Both types of base data are needed for proper interpretation.
4. The SRM and SRR subtracts the average motion of all detected storms (or storm for the region product) from the Base Velocity product so that flow relative to the

storms is presented. These products are best utilized when circulations are expected and storms are fast moving. The user must keep in mind that the SRM is inappropriate if ground-relative winds are of interest, like those associated with gust fronts and high wind events. The DV or DV products are more suited for ground-relative wind situations.

5. Some display systems may construct base velocity/and base reflectivity displays using the best resolution data that are available in the database. This is desirable. Therefore, if higher resolutions are present in these displays, they must be included on the RPS List. For example, if only a 4 km (2.2 nm) resolution CR product is required in the database, the product displayed will have only that resolution. If, however, both a 1 km (0.54 nm) and a 4 km (2.2 nm) resolution product are in the database, then the CR display will show a combination of both resolutions, using 1 km (0.54 nm) out to 230 km (124 nm), and 4 km (2.2 nm) from 230 to 460 km (124 to 248 nm).
6. MESOCYCLONE and TVS (M/MD, TVS) products should be included on all RPS Lists anytime convection is expected. They typically need to be checked every volume scan or displayed with other products (e.g., SRM) to prevent any unanticipated detections from being missed. When detections are indicated the user might consider adding the rapid update product versions (MRU and Tornado Vortex Signature Rapid Update (TRU)). However, note that TRU is selected on an elevation-by-elevation basis, so it can push the RPS List to its limitation on the number of entries. **Note:** The TVS and M/MD products should also be set for alerts for the same reason, keeping in mind that for RPG alerts, only the first (of many continuous) detections will be alerted until there is a volume scan free of either detection.
7. The STI product is useful out to 186 nm and may, therefore, be valuable on a Clear Air RPS List to monitor storms outside of 124 nm.
8. Precipitation algorithms will run while the radar is still in Clear Air Mode under certain conditions. Therefore, the user may choose to include precipitation products on the Clear Air RPS List.

4.18.4 National RPS List Requirements. To support the central collection and distribution of radar products via the RPCCDS, NOAAPORT, and the AWIPS Satellite Broadcast Network (SBN) Wide Area Network (WAN), a national set of products (list of products is at: <http://www.nws.noaa.gov/tg/rpccds.html>) is collected from 155 WSR-88D systems. For these sites, the National Product Set also includes Archive Level III products (Part A, Chapter 5, of this Handbook) and others identified for national collection.

Whenever a new RPS List is sent to the RPG, either automatically through a VCP mode change or manually through a request sent from the display system workstation (via the RPS List), the National Product Set is combined with the local user-defined RPS List and resent to the RPG. Even if the user needs to modify the “Current” RPS List or build a new list, it will be combined with the National Default List for the current operational mode. Duplicate products on the combined list will be dropped if a National product has a similar elevation angle (within 0.2 degrees) of the local office list and all other parameters are the same.

The site controlling the MSCF is responsible for modifying and copying the local user-specified RPS Lists to accommodate the changes brought about by the national central collection lists together with local needs. The differences in the various lists are, in general, due to the differences in clear air versus precipitation VCPs and those brought about by varying line speeds.

4.18.5 Clear Air Mode. Due to the slow scan rate, most of the products on the RPS List can be base products. The user may include a 16-level, low-elevation Clear Air Reflectivity product and an 8-level, long range Reflectivity product. Such derived products as the VWP and ET may also be added. Generally, there is time to handle OTRs for other products. Note that, in almost all cases, the VWP need not be requested every volume scan. In fact, in clear air conditions the rate of changes in the atmosphere may be slow enough that many of the products have request rates less often than every volume scan.

4.18.6 Precipitation Mode. Building RPS Lists for VCPs 11, 12, 121, and 21 can be complex. As explained above, conditions that influence the selection of products are the type, severity, range, and aerial extent of the precipitation. In addition, the support being provided to other offices, users, and WSR-88D sites may be a factor in building the RPS List.

With severe storms occurring at long range the RPS list should concentrate on low-elevation base products at the highest resolution. The STI product may be added. If storms are between 62 nm and 124 nm, velocity-derived products such as M, MRU, MD, and SRM may be included. Since the data compaction techniques are more efficient when the area of coverage is small, the RPS list can consist mainly of base products without inducing load shedding. One-time requests for such products as Cross Sections, SWA, and SRR may also be accomplished without inducing load shedding. (The use of VCP 121 and 21 will allow the user more time to make OTRs, as well as providing good resolution of base products.) The lowest five elevation scans for VCPs 11, 121, and 21 are identical in supporting the hydrology algorithms and will cover storms at long range. However, consideration should be given to VCP 12 use for longer ranges because of low-level overlapping beams.

An RPS List for convective precipitation at short to medium ranges should be built around VCPs 11 and 12. This will optimize algorithm performance and provide intermediate elevation scans for detailed analyses of storms using the SWA products and multi-panel base products. The RPS List should include one long range Reflectivity or Composite Reflectivity product and a few base products at intermediate elevation scans. About half the RPS List may consist of algorithm-derived

products. However, sufficient base products must be included to allow manual identification of severe storm circulations and structure and to allow the user to check algorithm output against base data. Again, products such as VWP need not be requested every volume scan.

If precipitation is widespread, base product size will be large and require longer transmission times. In this case, and if severe convection is not anticipated, the RPS List should be composed of fewer than one-half base products. The Precipitation Accumulation, ET, VWP, CR, and low-elevation angle R and V products may be included. Other base products may be needed to monitor middle and upper level atmospheric changes. But, in all cases, the user should rely on base data analysis.

4.19 Automated Alerts. With the WSR-88D, the user will be receiving large amounts of data for each volume scan. Since it is impossible to monitor all of these products at all times, it is sometimes helpful to be notified when certain predetermined meteorological criteria are met or exceeded within data from each volume scan. It is in this way that the alert process, which can be specified at many workstations, can help the user monitor this large volume of data and avoid overlooking critical data (Tables 4-1 and 4-2). The user can choose to set alerts using the appropriate equipment and procedures. Here we discuss, as an example only, one way this might be done within agency offices. Specific agencies or offices may choose to use the alerts in another fashion, or these agencies may have overriding concerns and directives.

As an example, widespread showers cover the screen but nothing severe is indicated. The user/forecaster will likely be devoting most of his/her time to other duties. If the user sets the reflectivity threshold at 50 dBZ, he/she will receive an alert when that criterion is first met or exceeded within the specified alert area or forecast to move into the area. This type of usage will supplement the users' monitoring of marginal weather. Or, while viewing a magnified display centered on an intense storm in one portion of the area, a mesocyclone is detected in another storm not currently on the display. The alert feature in this instance could notify the user of potentially severe storms not currently in view.

Once the user establishes what thresholds are critical for their area and mission for a given time of year, or for a particular weather scenario, he/she will be able to set alerts for these thresholds and determine in what part of the radar coverage area these thresholds will be monitored (office area of warning responsibility, for example).

4.19.1 Alert Use. Alerts in the WSR-88D are best utilized in two different ways: 1) During the transition from a "non-warning" or "monitor" type mode, to a "warning" situation, or 2) While in a warning situation, to highlight very significant weather that might be otherwise overlooked due to the high workload, or simply because this threat type was not anticipated. Thus, alerts can increase situation awareness. Alert use for marginal storms is not as valuable once widespread or frequent severe weather has begun. Below are some factors in the alert process design which affect their use in other instances.

1. The alert process will notify the user of an "alert condition." This means that once a phenomenon (in a particular alert area) has been alerted for, the user will not receive any additional alerts for that phenomenon until a volume scan passes in which that particular criteria is not met by any storm in the alert area. In other words, if one storm sets off the alert, the user will not get a new alert for that criterion when *any other* storm reaches the threshold, (even if the later storm is more severe) because the "alert condition" has not changed. In the case of TVS detection, for example, this means the user can not rely on the alert process to notify him/her of each TVS detection in the first volume scan where criteria are met, nor can the user expect any alerts for TVSs on subsequent volume scans if additional ones are detected. The user must look at each TVS/TRU product (and it's assumed the user would be) in order to observe detections at this point.
2. In general, if several storms in the same alert area contain algorithm-identified mesocyclones (for example), only the first one detected will be listed on the alert status screen.
3. The user will not get alerts for most features until after the entire volume scan is completed, since most features require the entire volume scan in order to be identified. This may be several minutes after the volume scan start time. The user may, however, get the alert itself before the product (which may display the alerted feature) is received into the user's database, since alerts have a higher priority than products. For example, a MESO alert could be sent to his/her workstation before the MESO product containing that feature arrives.

The net result of these characteristics makes relying on the alert process to notify the user of all severe storms a dangerous practice. Alerts are not designed for that purpose. Algorithm output and associated alerts should not replace the practice of monitoring base data and using this data for storm investigation/interrogation. The receipt of an alert should only serve to spur the user into further investigation and validation of the alerting feature. Furthermore, under no circumstances should the absence of an alert or algorithm-identified signature imply the absence of either severe weather or the existence of said signature. For this and other reasons, this document emphasizes reliance on base products.

4.19.2 Setting Alerts. Even though there are serious limitations to the alert process, an effective strategy can still make good use of this process. For example, VIL will trigger with a value of 50, TVS will trigger with the detection of a TVS, and MESO will trigger with the detection of a mesocyclone. One-Hour Precipitation and CR are also set. These alerts settings are being used in a "monitor" mode. But this does not alleviate the user of their responsibility to manually monitor and examine base data. Should this user get detection and shift gears into more of a warning mode, then the user might raise the threshold on VIL and CR, for example, to alert for the high-end detections as this user would no longer need notice of marginal thresholds. For each of these, "no" is the setting for alert-paired products in the example. Values assigned to the

threshold codes are fixed at the RPG and can only be altered with URC permission. The user's option is merely to select which of the established codes to choose for his/her use.

This strategy allows the user to be notified when marginal echoes develop, and then modify thresholds to get alerts for the most serious, and sometimes overlooked, features once warning operations begin. However, the user should also weigh the real need for alert use when the user is now applying their skill to storm interrogation through base data examination. The user must also keep in mind that if many alerts are set, the messages and/or audible alarms will probably become a nuisance, and will likely be ignored or turned off, thus defeating the purpose of the alerts and the alarm. On the other hand, the user does not want significant occurrences to go by undetected (excessive precipitation accumulation and flood potential during tornado occurrence, for example).

The user must remember the limitations of the Alert Process: there will not be new alerts for categories where "alert conditions" are still in effect until one volume scan has passed without that condition being detected anywhere in the alert area.

4.19.3 Alert Groups. Alert categories are divided into 3 alert groups, defined as follows:

GRID GROUP - Phenomena within this group meets or exceeds the thresholds in a specific Cartesian grid box. For example, a VIL value of 50 can be traced to a particular grid box.

VOLUME GROUP - Phenomena within this group meets or exceeds the thresholds for algorithm output assigned to a particular storm. For example, the MEHS refers to the storm as a whole, not necessarily to a specific grid box affected by the storm.

FORECAST GROUP - Phenomena within this group are currently associated with storms forecast to move into the established Alert Area. When the alert threshold is met and the "associated" storm is forecast (by the SCIT algorithm) to move into an Alert Area, a "forecast" alert is generated. Note - the forecast alert will be generated when a feature outside the alert area meets criteria and is forecast to move into the alert area. *However*, a forecast alert will also be generated if a feature *within* the alert area is forecast to remain within the alert area for at least one forecast period (15 minutes). This may thereby limit the usefulness of the forecast alerts once storms move within the alert area (assuming that the same criteria are already being alerted for within the alert area via the Grid or Volume alerts).

Additionally, the user must recognize that the alert algorithm does not actually anticipate development of a condition that does not already exist within the storm. The only thing actually "forecast" is storm movement, and that is done by the SCIT algorithm.

4.19.4 Alert Areas and Acknowledgments. Alert Areas are often set up to represent warning areas. One may overlap the other, be totally surrounded by another, or be totally

contained within another. In addition, a single alert area can be comprised of one area the size of the entire screen, or of several smaller areas which are non-contiguous. When alerts are received at a workstation, these alerts must be acknowledged. Otherwise, either/or audible and visual alarms will continue.

4.19.5 User Alert Message (UAM) Product. The UAM does not need to be on the RPS List in order to be received. Whenever alerts are set, the RPG will automatically produce this product every volume scan to indicate which new alerts were triggered during the *current* volume scan. The UAM is displayed on a text workstation along with the 3-letter radar mnemonic. Since this message contains only new alerts for the current volume scan, it is possible to have outstanding alerts in effect while the content of this product displays “No New Alerts This Scan.”

4.19.6 Alert-Paired Products. Some alerts may also result in products being sent to the user workstation. The user may choose to receive an RPG-specified product at the same time the alert is generated. These products are pre-assigned at the RPG and are also approved at the URC level of change authority. The user may only choose whether or not to receive these products. The product chosen to arrive with a particular alert may be specified so as to provide additional information about the phenomenon. The user may display the product from the menu just as any other products are displayed. It is, therefore, useful to know what the paired products are for various alerts in order to recognize them when they arrive. For example, a MESO Alert generated when a mesocyclone is detected may come with an SRR centered on the area where the mesocyclone was detected. Some example pairings for alerts which have proved effective are: For both the MESO and the TVS, the Storm Relative Region product, which will be generated at the slice and range of the feature triggering the alert. This reasoning is assuming that BOTH TVS and M are already on the RPS List. There is no advantage to receiving the “paired product” if that paired product is on your RPS List.

Alert-Paired Products are given the highest priority and will take up space in the queue and time on the transmission lines. If the user is having recurring problems with narrowband load shedding the way to help alleviate this problem is to decrease alerts or decrease or eliminate paired products at your workstation. However, alert-paired products are sent so rarely that this is insufficient to produce this problem. Other products may need to be deleted instead.

Table 4-1
Alert Types and Mnemonics (With the Assigned Order of Importance)

Alert Category	Alert Group	Alert Type	Mnemonic	Order of Importance
1	Grid	Velocity	GV	19
2	Grid	Composite Ref.	GR	13
3	Grid	Echo Tops	GT	16
4	Grid	Severe Wx Prob	GP	21
5	Grid	Not Used		
6	Grid	VIL	GL	7
7	Volume	VAD	VD	20
8	Volume	Max Hail Size	VZ	8
9	Volume	Mesocyclone	VM	3
10	Volume	TVS	VS	1
11	Volume	Max Storm Ref	VR	14
12	Volume	Prob of Hail	VH	10
13	Volume	Prob Svr Hail	VA	5
14	Volume	Storm Top	VT	17
15	Volume	Max 1-hr Precip	VP	12
16-24	Volume	Not Used		
25	Forecast	Max Hail Size	FZ	9
26	Forecast	Mesocyclone	FM	4
27	Forecast	TVS	FS	2
28	Forecast	Max Storm Ref	FR	15
29	Forecast	Prob of Hail	FH	11

Table 4-2
Alert Locations and Paired Window Product Centers

<u>CATEGORY CODE</u>	<u>ALERT AZ/RAN,SLICE LOCATION</u>
	<i>(as seen on S, AL screen)</i>
GRID GROUP	
1. Velocity	Lowest Elevation &/or AZ/Ran of alert box containing exceeding value.
2. Composite Reflectivity	" "
3. Echo Tops	" "
4. SWP	" "
5. -	
6. VIL	" "
VOLUME/FORECAST GROUPS	
7. VAD / VWP	Elevation computed from height and slant range of VAD AZ/Ran.
15. MAX 1-hr Rainfall	RDA
8, 25 HAIL	Storm Centroid AZ/Ran
9 MESO (Volume)	Meso: Feature Base elevation and AZ/Ran 2-D, 3-D Shear: Storm Centroid AZ/Ran and Lowest Elevation
25 MESO (Forecast)	MESO, 2-D, 3-D: Storm Centroid AZ/Ran and Lowest Elevation
10, 27 TVS	AZ/Ran and elevation of base
11, 28 MAX Storm Reflectivity	Elevation of MAX, Storm Centroid AZ/Ran
12, 29 MAX Storm Velocity	Elevation and AZ/Ran of lowest storm component.
13, 30 Storm Volume	Storm centroid AZ/Ran, and Lowest Elevation
14, 31 Storm Top	Storm centroid AZ/Ran, and Lowest Elevation

<u>PAIRED PRODUCT</u>	<u>ALERT PRODUCT CENTERS (and special conditions)</u>
SWA,SRR	Grid/Volume (Meso, TVS only): AZ/Ran, elevation of highest shear
	Grid/Volume (all others), and Forecast: AZ/Ran of Centroid, Lowest elevation.
RCS,VCS	AZ/Ran of Grid box, +/- 50km (generated along radar Azimuth)

Table 4-3
Application versus Product

<u>Application</u>	<u>Product</u>
Boundaries	R, SW, V, preferably at high resolution
Cloud/precip. Layers	R, RCS, V, VWP
Convection	CR, DSP, ET, HI, LRM, M, MRU, MD, OHP, R, RCS, SRM, SRR, SS, STI, STP, SWA, SW, THP, USP, TVS, TRU, V, VIL, Time-lapse of base R, High resolution for all products
Extratropical Cyclones	CR, DSP, ET, HI, OHP, R, RCS, STI, STP, SW, THP, USP, V, VCS, VWP, Time-lapse of base products.
Flash Floods	DSP, ET, LRM, OHP, R, STI, THP, STP, USP, VIL, VWP, time lapse of base R and OHP and STP products.
Hail	DSP, HI, OHP, R, RCS, SS, STI, STP, SRM, SRR, THP, V, VCS, VIL, High resolution products, Time-lapse of base R.
High Wind Events	V, VWP, R
Low-Level Jets	V, VWP
Melting Level	R, RCS, SW, VWP
Microbursts	CS, ET, SW, V, VCS, VIL, SRM, all high resolution products
Pre-Convective Development	R, SW, V, High resolution products, Time-lapse loops.
Tropical Cyclones	ET, M, OHP, R, SRM, STI, SW, THP, V, VCS, VIL, VWP, USP
Turbulence	V, SW, VCS
Wind Shear	CS, SW, V, VCS, VWP
Winter Storms	DSP, R, RCS, OSD, SSD, USD, STI, STP, SW, OSW, SSW, USW, V, VCS, Time-lapse of R and snowfall products

REFERENCES

- Amburn, S. and P. Wolf, 1997: VIL density as a hail indicator. *Wea. Forecasting*, **12**, 473-478.
- Atlas, D. (Ed), 1990: *Radar in Meteorology*. Amer. Meteor. Soc., Boston, MA, 323 pp.
- Battan, L. J., 1959: *Radar Meteorology*. University of Chicago Press, 161 pp.
- Blaes, J. L., C. S. Cerniglia Jr, and M. A. Caropolo, 1998: VIL density as an indicator of hail across eastern New York and western New England. *Eastern Region Technical Attachment*, No **98-8**, National Weather Service, NOAA, Department of Commerce, Bohemia, NY
- Brown, R. A., D. W. Burgess, and K. C. Crawford, 1973: Twin tornado cyclones within a severe thunderstorm: Single Doppler radar observations. *Weatherwise*, **26**, 63-69.
- Brown, R. A., L. R. Lemon, and D. W. Burgess, 1978: Tornado detection by pulsed Doppler radar. *Mon. Wea. Rev.*, **106**, 29-38.
- Browning, K. A., 1977: The structure and mechanism of hailstorms. Hail: A Review of Hail Science and Hail Suppression, *Meteor. Monogr.*, **16**, 1-43.
- Brooks, H. E., and J. P. Craven, 2002: Database proximity soundings for significant severe thunderstorms, 1957 – 1993. Preprints, *21st Conf. on Severe Local Storms*, San Antonio, TX, Amer. Meteor. Society, 639-642.
- Bruderer, B., 1977a: The study of bird migration by radar. Part I: The technical basis. *Naturwissen-schaften*, **84**, 1-8.
- Bruderer, B., 1977b: The study of bird migration by radar. Part II: Major achievements. *Naturwissen-schaften*, **84**, 45-54.
- Bruderer, B., 2000: Three decades of tracking radar studies on bird migration in Europe and the Middle East. Migrating Birds Know No Boundaries, International Seminar (and book) on Birds and Flight Safety in the Middle East, Israel, April 25-29, 1999, Ed. Yossi Leshem, Yale Mandelik, Judy Shamoun-Barnes. International Center for the Study of Bird Migration, Latrun, Israel, 107-141.
- Burgess, D. W., and L. R. Lemon, 1990: Severe thunderstorm detection by radar. *Radar in Meteorology* (D. Atlas, Ed.), Amer. Meteor. Soc., 619-647.
- Burgess, D. W., and M. A. Magsig, 1998: Recent observations of tornado development at near range to WSR-88D radars. Preprints, *19th Conf. on Severe Local Storms*, Minneapolis, MN, Amer. Meteor. Soc., 756-759.

- Burgess, D. W., M. A. Magsig, J. Wurman, D. C. Dowell and Y. Richardson, 2002: Radar observations of the 3 May 1999 Oklahoma City tornado. *Wea. Forecasting*, **17**, 456-471.
- Burgess, D. W., R. R. Lee, S. S. Parker, D. L. Floyd, and D. L. Andra, Jr, 1995: A study of mini-supercells observed by WSR-88D radars. Preprints, *27th Conf. on Radar Meteorology*, Vail, CO, Amer. Meteor. Soc., 4-6.
- Burgess, D. W., V. T. Wood, and R.A. Brown, 1982: Mesocyclone evolution statistics. Preprints, *12th Conf. on Severe Local Storms*, San Antonio, TX, Amer. Meteor. Soc., 422-424.
- Byers, H. R., and R. R. Braham, 1949: The Thunderstorm. U.S. Government Printing Office, Washington D.C., 287 pp.
- Carven, J. P., H. E. Brooks, and J. A. Hart, 2002: Baseline climatology of soundings derived parameters associated with deep, moist convection. Preprints, *21st Conf. on Severe Local Storms*, Amer. Meteor. Soc., San Antonio, TX, 643-646.
- Cerniglia, C. S., and W. R. Snyder, 2002: Development of warning criteria for severe pulse thunderstorm in the northeast United States using the WSR-88D. *Eastern Region Technical Attachment*, No **2002-03**, National Weather Service, NOAA, Department of Commerce, 14 pp., Bohemia, NY.
- Chisholm, A. J. and J. H. Renick, 1972: The kinematics of multicell and supercell Alberta hailstorms. Alberta Hail Studies, 1972, Research Council of Alberta Hail Studies Rep.No. 72-2, 24-31.
- COMET, Mesoscale Convective Systems: Squall lines and Bow Echoes, 1999, Cooperative Program for Operational Meteorology, Education and Training, Distance Learning Program. <http://www.meted.ucar.edu/convectn/mcs/>
- Doswell, C. A. III, 1985: The operational meteorology of convective weather, Vol. II: Storm scale analysis. NOAA Tech. Memo. ERL ESG-15, 240 pp.
- Doswell, C. A., III, and D. W. Burgess, 1993: Tornadoes and tornadic storms: A review of conceptual models. The Tornado: Its Structure, Dynamics, Prediction, and Hazards. (C. Church et al (Eds), Geophys. Monogr., Amer. Geophys. Union, 161-172.
- Doswell, C. A. III, Ed., 2001: Severe convective storms - An overview. *Meteor. Monogr.*, **50**, Ed. C. A. Doswell, Amer. Meteor. Soc., Boston, MA, pp. 1-26.
- Doviak, R. J. and D. S. Zrnic, 1984: *Doppler Radar and Weather Observations*. Academic Press, Inc., Orlando, FL, 458 pp.
- Edwards, R., and R. L. Thompson, 1998: Nationwide comparisons of hail size with WSR-88D vertically integrated liquid water and derived thermodynamic sounding data. *Wea. Forecasting*, **13**, 277-285.

- Fulton, R., J. Breidenbach, D. J. Seo, D. Miller and T. O'Bannon, 1998: The WSR-88D Rainfall Algorithm. *Wea. Forecasting*, **13**, 377-395
- Grant, B. N., R. Prentice, 1996: Mesocyclone characteristics of mini-supercell thunderstorms. Preprints, *15th Conf. on Weather and Forecasting*, Norfolk, VA Amer. Meteor. Soc., 362-365.
- Green, D. G. and R. A. Clark, 1972: Vertically integrated liquid water. A new analysis tool. *Mon. Wea. Rev.*, **100**: 548-797.
- Howard, K.W., J.J. Gourley, and R.A. Maddox, 1997: Uncertainties in WSR-88D measurements and their impacts on monitoring life cycles. *Wea. Forecasting*, **12**, 166-174.
- Kelly, T. A., R. Merritt, T. J. Donalds, and R. L. White, 2000: The avian hazard advisory system. Migrating Birds Know No Boundaries, International Seminar (and book) on Birds and Flight Safety in the Middle East, Israel, April 25-29, 1999, Ed. Yossi Leshem, Yale Mandelik, Judy Shamoun-Barnes. International Center for the Study of Bird Migration, Latrun, Israel, 101-105.
- Lee, B. D., and R. B. Wilhelmson, 1997: The numerical simulation of non-supercell tornadogenesis. Part I: Initiation and evolution of pretornadic mesocyclone circulations along a dry outflow boundary. *J. Atmos. Sci.*, **54**, 32-60.
- Lemon, L. R., R. J. Donaldson, Jr., D. W. Burgess, and R. A. Brown, 1977: Doppler radar application to severe thunderstorm study and potential real-time warning. *Bull. Amer. Meteor. Soc.*, **58**, 1187-1193.
- Lemon, L. R., 1978: On the use of storm structure for hail identification. Preprints, *18th Conf. on Radar Meteorology*, Boston, MA, Amer. Meteor. Soc., 203-206.
- Lemon, L. R., and C. A. Doswell III, 1979: Severe thunderstorm evolution and mesocyclone structure as related to tornadogenesis. *Mon. Wea. Rev.*, **107**, 1184-1197.
- Lemon, L. R., 1980: Severe thunderstorm radar identification techniques and warning criteria. NOAA Tech. Memo. NWS NSSFC-3, 60 pp.
- Lemon, L. R., and E. M. Quetone, 1994: Interpretation of the radar-centered "Donut" Signature. Postprints, First WSR-88D User's Conf., NOAA, Gov. Printing Office, Norman, OK, 102-111.
- Lemon, L. R., and S. Parker, 1996: The Lahoma storm deep convergence zone: Its characteristics and role in storm dynamics and severity. Preprints, *18th Conf. on Severe Local Storms*, Boston, MA, Amer. Meteor. Soc., 70-75.
- Lemon, L. R., 1998: The radar "three-body scatter spike": An operational large hail signature. *Wea. Forecasting*, **13**, 327-340.

- McCaul, Jr., E. W., 1987: Observations of the Hurricane "Danny" tornado outbreak of 16 August 1985. *Mon. Wea. Rev.*, **115**, 1206-1223.
- Maddox, R. A., Zaras, D. S., MacKeen, P. L., Gourley, J. J., Rabin, R., Howard, K. W., 1999: Echo height measurements with the WSR-88D: Use of Data from One Versus Two Radars, *Wea. Forecasting*, **14**, 455-460.
- Miller, D. J., and R. H. Johns, 2000: A detailed look at extreme wind damage in derecho events. Preprints, *20th Conf. on Severe Local Storms*, Orlando, FL, Amer. Meteor. Soc., 52-55.
- Miller, D. J., Andra, D. L., Evans, J. S., and R. H. Johns, 2002: Observations of the 27 May 2001 high-end derecho event in Oklahoma. Preprints, *21st Conf. on Severe Local Storms*, San Antonio, TX, Amer. Meteor. Soc., 13-16.
- Moller, A. R., C. A. Doswell, and R. W. Przybylinski, 1990: High precipitation supercells: a conceptual model and documentation. Preprints, *16th Conf. on Severe Local Storms*, Kananaskis Park, Alberta, AB, Amer. Meteor. Soc., 52-57.
- Moller, A. R., 2001: Severe local storms forecasting. Chapter 11, *Severe Convective Storms*, *Meteor. Monogr 50*, Ed, C. A. Doswell, III, Amer. Meteor. Soc., Boston, MA. pp 433-480.
- Moore, J. T. and M. A. Kaster, 1993: Physical processes organizing wintertime frozen precipitation events in the Midwest. Preprints, *13th Conf. on Weather Analysis and Forecasting*, Vienna, VA, AMS, 512-515.
- Petersen, W. A., L. D. Carey, S. A. Rutledge, J. C. Knivel, N. J. Doesken, R. H. Johnson, T. B. McKee, T. Von der Haar, J. F. Weaver, 1999: Mesoscale and radar observations of the Fort Collins flash flood of 28 July 1997. *Bull. Amer. Meteor. Soc.*, **80**, 191-216.
- Przybylinski, R. W., and W. J. Gery, 1983: The reliability of the bow echo as an important severe weather signature. Preprints, *13th Conf. on Severe Local Storms*, Tulsa, OK, Amer. Meteor. Soc., 270-273.
- Przybylinski, R. W., 1995: The bow echo: Observations, numerical simulations, and severe weather detection methods. *Wea. Forecasting*, **10**, 203-218.
- Przybylinski, R. W., G. K. Schmocker, and Y. J. Lin, 2000: A study of storm and vortex morphology during the 'intensifying stage' of severe wind mesoscale convective systems. Preprints, *20th Conf. on Severe Local Storms*, Orlando, FL, Amer. Meteor. Soc., 173-176.
- Quoetone, E. M., K. Huckabee, 1995: Anatomy of an effective warning: Event anticipation, data integration, feature recognition. Preprints, *14th Conf. On Weather Analysis and Forecasting*, Amer. Meteor. Soc., Dallas, TX, 420-425.

- Shields, M.T., R.M. Rauber, and M. K. Ramamurthy, 1991: Dynamical forcing and mesoscale organization of precipitation bands in a Midwest winter cyclonic storm. *Mon. Wea. Rev.*, **119**, 936- 964.
- Schmocker, G. K., R. W. Przybylinski, and Y. J. Lin, 1996: Forecasting the initial onset of damaging downburst winds associated with a Mesoscale Convective System (MCS) using the Mid-Altitude Radial Convergence (MARC) signature. Preprints, *15th Conf. on Weather Analysis and Forecasting*, Norfolk, VA, Amer. Meteor. Soc., 306–311.
- Spratt, S. M., D. W. Sharp, P. Welsh, A. C. Sandrik, F. Alsheimer and C. Paxton, 1997: A WSR-88D assessment of tropical cyclone outer rainband tornadoes. *Wea. Forecasting*, **12**, 479-501.
- Trapp, R. J., E. D. Mitchell, G.A. Tipton, D. W. Effertz, A. I. Watson, D. L. Andra, and M. A. Magsig, 1999: Descending and non-descending tornadic vortex signatures detected by WSR-88Ds. *Wea. Forecasting*, **14**, 625-639.
- Trapp, R. J., G. J. Stumpf, and K. L. Manross 2005: A reassessment of the percentage of tornadic mesocyclones. *Wea. Forecasting*, **20**, 680-687.
- Wakimoto, R. M., C. Huaqing, and H. V. Murphey, 2004: The superior, Nebraska supercell during BAMEX. *Bull. Amer. Meteor. Soc.*, **85**, 1095-1106.
- Willoughby, H. E., F. D. Marks, and R. J. Feinberg, 1984: Stationary and moving convective bands in hurricanes. *J. Atmos. Sci.*, **22**, 3189-3211.
- Wilson, J. W. and D. Reum, 1986: "The hail spike": reflectivity and velocity signature. *Preprints, 23rd Conf. on Radar Meteorology*. Snowmass, CO, Amer. Meteor. Soc., 62-65.
- Wilson, J. W. and D. Reum, 1988: The flare echo: Reflectivity and velocity signature. *J. Atmos. Oceanic Technol.*, **5**, 197-205.
- Witt, A., and S. P. Nelson, 1991: The use of single-Doppler radar for estimating maximum hailstone size. *J. Appl. Meteor.*, **30**, 425- 431.
- Witt, A., M. D. Eilts, G. J. Stumpf, J. T. Johnson, E. D. Mitchell, and K. W. Thomas, 1998: An enhanced hail detection algorithm for the WSR-88D. *Wea. Forecasting*, **13**, 286-303.
- Zrnica, D. S., 1987: Three-body scattering produces precipitation signature of special diagnostic value. *Radio Sci.*, **22**, 76-86.

